

**Chair of Hydrological Modeling and Water Resources**

Albert-Ludwigs-University of Freiburg

Mirjam Sulamith Scheller

# Evaluation of karst vulnerability methods by tracer tests and modeling



MSc-Thesis under the guidance of JProf. Dr. Andreas Hartmann

Freiburg i. Br., May 2020







**Chair of Hydrological Modeling and Water Resources**

Albert-Ludwigs-University of Freiburg

Mirjam Sulamith Scheller

# Evaluation of karst vulnerability methods by tracer tests and modeling

Examiner: JProf. Dr. Andreas Hartmann

Co-Examiner: Dr. Natalie Orlowski

MSc-Thesis under the guidance of JProf. Dr. Andreas Hartmann

Freiburg i. Br., May 2020

## Declaration of Authorship

I, Mirjam S. Scheller, hereby declare that this thesis is entirely the result of my own original work, if not indicated otherwise. Any use of the works of other authors, in any form, is properly acknowledged and referred at the point of use. Furthermore I declare, that this work has not been submitted for credits elsewhere.

Freiburg, 18<sup>th</sup> of May 2020

Mirjam S. Scheller

*“Water is fluid, soft, and yielding. But water will wear away rock, which is rigid and cannot yield.  
As a rule, whatever is fluid, soft, and yielding will overcome whatever is rigid and hard.  
This is another paradox: what is soft is strong.”*

— Lao Tzu

## Acknowledgements

I would like to gratefully thank the following people for their support during my master thesis:

- First of all my supervisor JProf. Dr. Andreas Hartmann for providing an interesting topic and for his support throughout my working progress.
- Dr. Natalie Orłowski for being willingly included as Co-Examiner.
- I also want to offer a special thanks to Assit. Prof. Dr. Nataša Ravbar and her team for showing me the study site, for introducing me to the classical Karst of Slovenia and for supporting me. I really enjoyed the trip to Slovenia and I am thankful for all the advices and help they gave me.
- Dr. Yan Liu for helping me improve my matlab programming skills and my understanding of the VarKarst model.
- The whole HydMod team for their support and the nice company during lunch breaks.
- My family for their moral support throughout my entire life. I wouldn't be where I am without them.
- Last but not least I want to thank my friends Marie Gärtner and Jasper Opdenhoff for giving me great professional and moral advices regarding my thesis.



## Table of content

Declaration of Authorship .....	i
Acknowledgements .....	iv
List of Figures .....	vii
List of Tables .....	ix
List of Abbreviations .....	x
Abstract .....	xii
Zusammenfassung .....	xiii
1. Introduction .....	1
1.1. State of the art .....	2
1.1.1. Karst hydrological processes .....	2
1.1.2. Karst vulnerability methods .....	3
1.1.3. Research gaps .....	9
1.2. Research objectives .....	9
2. Study site .....	10
2.1. Tracer tests .....	14
2.2. Preliminary conceptual model .....	20
2.3. Data preparation .....	23
3. Methodology .....	24
3.1. The VarKarst model .....	25
3.1.1. Mathematical description .....	26
3.1.2. Model development .....	28
3.1.3. Model evaluation .....	31
4. Results .....	33
4.1. Developments of VarKarst model .....	33
4.2. Simulations of discharge and tracer breakthrough curves .....	35
4.3. Model predictions .....	39
4.3.1. Parameter sensitivities .....	39
4.3.2. Predicted time series .....	41
4.3.3. Tracer advection .....	43
4.3.4. Selection of model compartment for tracer injection .....	46
4.4. Vulnerability .....	47

---

5. Discussion.....	49
5.1. Observation data.....	49
5.2. Model evaluation.....	50
5.2.1. Simulations of discharge and tracer breakthrough curves.....	50
5.2.2. Current limitations of tracer breakthrough curve predictions .....	52
5.2.3. Model precision and accuracy .....	54
5.3. Improvements of the conceptual model .....	57
5.4. Classification as vulnerability method.....	58
6. Conclusion and Outlook.....	59
List of References.....	60
Appendix .....	65
A. Figures.....	65
B. Equations .....	72

## List of Figures

Figure 1.1: Comparison of the percentage of carbonate outcrops and the contribution of karst water to the total water supply	1
Figure 1.2: Conceptual model of a karst aquifer and its groundwater flows	3
Figure 2.1: Map showing the location of the study site	10
Figure 2.2: Hydrogeological map of the catchment of the Unica springs	11
Figure 2.3: Map of soil depths of the catchment of the Unica springs	11
Figure 2.4: Relative coverage of each soil texture type of the catchment of the Unica springs	12
Figure 2.5: Long-term mean monthly precipitation, discharge and temperature value	13
Figure 2.6: Boxplots of the discharge for each hydrological year with additional mean discharge values	13
Figure 2.7: Injection points and points of measurements of the tracer tests applied in the catchment of the Unica springs.	14
Figure 2.8: Part 1: Time series plots of all tracer tests including discharge and precipitation data	18
Figure 2.9: Part 2: Time series plots of all tracer tests including discharge and precipitation data	19
Figure 2.10: Flow directions under low and high flow conditions (modified after Ravbar (2013))	20
Figure 2.11: Preliminary conceptual model of the catchment of the Unica springs	22
Figure 3.1: Steps of the modeling workflow	24
Figure 3.2: Structure of the VarKarst model	25
Figure 3.3: Schematically flow ways of the water and the solute through one of the model compartments	29
Figure 3.4: Separation of discharge and tracer test data into warm up, calibration and validation period	32
Figure 4.1: Water balance of the catchment of the Unica springs over the simulated time period	33
Figure 4.2: Soil storage capacity of each model compartment and its distribution function	34
Figure 4.3: Discharge time series of a dry and wet hydrological year of the calibration period (left). Simulated discharge values of these time series plotted over their respective observed discharge values (right).	35
Figure 4.4: The best 5% of simulated tracer breakthrough curves of each tracer test	36
Figure 4.5: Boxplots of parameters for each simulated time series	37
Figure 4.6: Dotty plots and histograms of 63 parameter sets selected by the calibration	40
Figure 4.7: Cumulative parameter distributions	41
Figure 4.8: Predicted discharge time series of a dry and wet hydrological year of the validation period.	41
Figure 4.9: Predicted break through curve of the tracer test T9	42
Figure 4.10: Dotty plots of the 63 parameter sets and their KGE regarding the discharge of the validation period (2010-2017) and the tracer test T9	42

Figure 4.11: Characteristic tracer breakthrough curve times of the observed tracer breakthrough curves compared with the lags of the cross correlation of the simulated tracer tests	43
Figure 4.12: Dominant velocities of all tracer tests plotted over the leaner distance and $Q_{\text{mean10d}}$	44
Figure 4.13: Detailed plot of dominant velocities of all tracer tests plotted over the leaner distance and $Q_{\text{mean10d}}$ . Tracer test are divided into tests with the same hydrological conditions and tests with constant linear distances	45
Figure 4.14: Ratios of concentrated and diffuse recharge differentiated for each tracer test	47
Figure 4.15: Ratios of concentrated and diffuse recharge. Combination of all tracer tests of Figure 4.14.	48
Figure 5.1: Comparison of selected parameter ranges and values of best model performances by different approaches	54
Figure A.1: Sketch of flow directions at low and high flow conditions	65
Figure A.2: Pictures of the injection point of tracer test T4 (Oil collector)	65
Figure A.3: Input data of the VarKarst model subdivided into warm up, calibration and validation periods.	66
Figure A.4: Calculated potential evapotranspiration for the warm up, calibration and validation periods.	66
Figure A.5: Dotty plots of all simulations. Maximum KGE colored in blue (Part 1)	67
Figure A.6: Dotty plots of all simulations. Maximum KGE colored in blue (Part 2)	68
Figure A.7: Comparison of simulated and observed tracer concentrations	69
Figure A.8: Maximum and dominant velocities and velocity of 50% of racer recovered of all tracer tests plotted over the leaner distance and $Q_{\text{mean10d}}$	70
Figure A.9: Detailed plot of maximum and dominant velocities and velocity of 50% of racer recovered of all tracer tests plotted over the leaner distance and $Q_{\text{mean10d}}$	71

## List of Tables

<b>Table 1.1: Overview of the most common karst vulnerability methods in Europe.</b>	<b>5</b>
<b>Table 2.1: Effective porosities and their relative coverage of the catchment of the Unica springs</b>	<b>12</b>
<b>Table 2.2: Summary of all tracer tests carried out in the catchment of the Unica springs</b>	<b>15</b>
<b>Table 3.1 Overview of the VarKarst model parameters</b>	<b>25</b>
<b>Table 3.2: Overview of the VarKarst model parameters and their set ranges</b>	<b>32</b>
<b>Table 4.1: Percentage coverage of each soil depth of the catchment of the Unica springs</b>	<b>34</b>
<b>Table 4.2: KGEs of the discharge (calibration time period) and of all tracer tests</b>	<b>35</b>
<b>Table 4.3: KGEs of different compartments selected for tracer injection</b>	<b>46</b>
<b>Table 4.4: 95<sup>th</sup> percentile of the KGE of the simulations of each tracer test</b>	<b>48</b>
<b>Table A.1: Comparison between different numbers of varying parameters</b>	<b>69</b>
<b>Table A.2: Comparison of different numbers of parameter sets</b>	<b>69</b>

## List of Abbreviations

### Abbreviations

Am.	Amidorhodamin g
cal	Calibration
DOC	Dissolved organic carbon
DIN	Dissolved inorganic nitrogen
GIS	Geographic Information Systems
KGE	Kling-Gupta efficiency
Max.	maximum
m.s.a.l.	Meters above sea level
Na.	Naphthionate
Quan.	Quantile
S1	Malenščica spring
S2	Unica spring
T	Tracer test
Ur.	Uranine
val	Validation

### Chemical formulae

$\text{CaCO}_3$	Mineral calcite
$\text{CaMg}(\text{CO}_3)_2$	Mineral dolomite
Cl	Chlorine
$\text{CO}_2$	Carbon dioxide
$\text{Ca}^{2+}$	Calcium
$\text{HCO}_3^{2-}$	Bicarbonate
$\text{NO}_3$	Nitrate
$\text{SO}_4$	Sulfate

### Symbols

$A$	Recharge area	[km <sup>2</sup> ]
$\alpha$	Variability	[variable]
$\alpha_{fsep}$	Distribution coefficient of diffuse and concentrated recharge	[-]
$\alpha_{GW}$	Groundwater variability constant	[-]
$\alpha_{SE}$	Distribution coefficient of soil/epikarst depth variability constant	[-]
$B$	Bias	[variable]
$\Delta t$	Modeling time step	[d]
$c_{epi,tracer}$	Concentration of tracer in the epikarst	[mg mm <sup>-1</sup> ]
$c_{spring,tracer}$	Concentration of tracer at the spring	[mg m <sup>-3</sup> ]
$C_v$	Vulnerability concentration	[mg m <sup>-3</sup> ]
$E_{act}$	Actual evapotranspiration	[mm]
$E_{pot}$	Potential evapotranspiration	[mm]
$f_c$	Separation factor	[-]
$i$	Number of model compartment	[-]
$K_c$	Conduit storage coefficient	[d]
$K_{GW}$	Groundwater storage coefficient	[d]
$K_{max,epi}$	Maximum epikarst storage coefficient	[d]
$K_{epi}$	Mean epikarst storage coefficient	[d]
$m_{conc,tracer}$	Mass of tracer in concentrated recharge	[mg]
$m_{diff,tracer}$	Mass of tracer in diffuse recharge	[mg]
$m_{epi,tracer}$	Mass of tracer in epikarst storage	[mg]

---

$m_{GW,tracer}$	Mass of the tracer in the groundwater	[mg]
$m_{tracerIn}$	Total mass of injected tracer	[mg]
$N$	Number of total model compartments	[-]
$\sigma$	Standard deviation	[variable]
$P$	Precipitation	[mm]
$Q_{epi}$	Epikarst outflow	[mm d <sup>-1</sup> ]
$Q_{GW}$	Groundwater contribution	[mm]
$Q_{main}$	Spring discharge	[m <sup>3</sup> s <sup>-1</sup> ]
$Q_{mean10d}$	Mean discharge 10 d before tracer injection	[m <sup>3</sup> s <sup>-1</sup> ]
$Q_{surf}$	Surface runoff	[mm]
$r$	Linear correlation coefficient	[-]
$R_{conc}$	Concentrated groundwater recharge	[mm]
$R_{diff}$	Diffuse groundwater recharge	[mm]
$R_{epi}$	Recharge from the soil to the epikarst	[mm]
$t_{tracerIn}$	Time of tracer injection	[d]
$t_{V50}$	Time at which fifty percent of the tracer was recovered at the springs	[d]
$t_{Vdom}$	Time till the peak of the tracer breakthrough curve	[d]
$t_{Vmax}$	Time till the first tracer concentration was measured at the springs	[d]
$\mu$	Mean	[variable]
$V_e$	Mean epikarst storage capacity	[mm]
$V_{epi}$	Amount of water stored in the epikarst layer	[mm]
$v_{50}$	Velocity at which fifty percent of the tracer was recovered at the springs	[km d <sup>-1</sup> ]
$v_{dom}$	Velocity of the peak of the tracer breakthrough curve	[km d <sup>-1</sup> ]
$v_{max}$	Velocity of the first tracer occurring at the spring	[km d <sup>-1</sup> ]
$V_{GW,i}$	Amount of water stored in the ground water layer	[mm]
$VI$	Vulnerability index	[-]
$V_{max,e}$	Maximum epikarst storage capacity	[mm]
$V_{max,S}$	Maximum soil storage capacity	[mm]
$V_S$	Mean soil storage capacity	[mm]
$V_{soil}$	Amount of water stored in the soil layer	[mm]

## Abstract

Water from karst aquifers is among the most important source for drinking water supplies. Consequently, appropriate protection and sustainable management of these aquifers are essential. Several karst vulnerability methods were developed in the past decades. Due to the hydrologic complexity and variability of karst systems, predicting potential contaminations and aquifers' responses to changes in climate conditions, still remains challenging. In this study, the dynamics of potential solute contaminant transport in the Unica springs catchment, located in the southwest of Slovenia, are characterized and simulated with a semi-distributed karst model. The catchment of the Unica springs encompasses autogenic and allogenic recharge across an area of about 820 km<sup>2</sup>. The major part of the catchment shows high degrees of karstification. In order to take the temporal and spatial characteristics of the catchment into account, the model is linked to spatial resolved soil information. Several tracer tests at different injection points and different hydrological conditions were applied. The shapes of the tracer breakthrough curves at the springs could be simulated very well. The description of advection processes by the model will require some further research. Nevertheless, the approach improved the understanding of potential contaminants' transport and recharge behavior in a large complex karst system and justified the consideration of spatiotemporal hydrologic variability in solute transport forecasting. It proposes a first step towards a better evaluation, management and protection of water resources in karst areas.

**Keywords:** Karst vulnerability, numerical modeling, tracer breakthrough curves, hydrological variabilities, spatiotemporal variation, Unica, Slovenia.



## Zusammenfassung

Wasser aus Karstgrundwasserleitern ist eine der wichtigsten Quellen der Trinkwasserversorgung. Folglich sind ein angemessener Schutz und ein nachhaltiges Management dieser Grundwasserleiter unerlässlich. In den vergangenen Jahrzehnten wurden mehrere Methoden der Karstvulnerabilität entwickelt. Die Vorhersage potenzieller Kontaminationen und Reaktionen der Grundwasserleiter auf Veränderungen der Klimabedingungen bleibt jedoch aufgrund der hydrologischen Komplexität und Variabilität von Karstsystemen eine Herausforderung. In dieser Studie wird die Dynamik des Transports potentiell gelöster Schadstoffe im Einzugsgebiet der Unica-Quellen im Südwesten Sloweniens charakterisiert und mit einem semi-distribuierten Karstmodell simuliert. Das Einzugsgebiet der Unica-Quellen umfasst autogene und allogene Grundwasserneubildungen auf einer Fläche von etwa 820 km<sup>2</sup>. Der zentrale Teil des Einzugsgebietes weist einen hohen Verkarstungsgrad auf. Um die zeitlichen und räumlichen Eigenschaften des Einzugsgebietes zu berücksichtigen, ist das Modell mit räumlich aufgelösten Bodeninformationen verknüpft. Es wurden mehrere Tracerversuche an verschiedenen Injektionspunkten und unter verschiedenen hydrologischen Bedingungen durchgeführt. Die Formen der Tracer- Durchgangskurven an den Quellen konnten sehr gut simuliert werden. Die Beschreibung der Advektionsprozesse durch das Modell erfordert noch weitere Untersuchungen. Nichtsdestotrotz konnte das Verständnis über Transporte potentieller Schadstoffe und Grundwasserneubildungen in einem komplexen Karstsystem verbessert und die Berücksichtigung der raum-zeitlichen hydrologischen Variabilität bei der Vorhersage des Transports gelöster Stoffe gerechtfertigt werden. Die Studie stellt den ersten Schritt in Richtung einer besseren Bewertung, eines nachhaltigeren Managements und zielgerichteten Schutzes der Wasserressourcen in Karstgebieten dar.

**Schlüsselwörter:** Karstvulnerabilität, numerische Modellierung, Tracer-Durchgangskurven, hydrologische Variabilität, raum-zeitliche Variation, Unica, Slowenien.



# 1. Introduction

Water resources are essential for the future wellbeing of the humankind and the entire ecosystem. In order to assure a certain quality and quantity of these resources, protecting groundwater aquifers is inevitable. Around 35% of Europe's land surface is covered by carbonate rocks (Cooperation in Science and Technology, 1995). Therefore water from karst aquifers is among the most important drinking water supplies. As shown in Figure 1.1 the carbonate outcrops in countries like Slovenia cover an area of 42%. About 50% of the total water supply in Slovenia is covered by water from carbonate aquifers and some regions in Slovenia are completely dependent on water from karst aquifers.

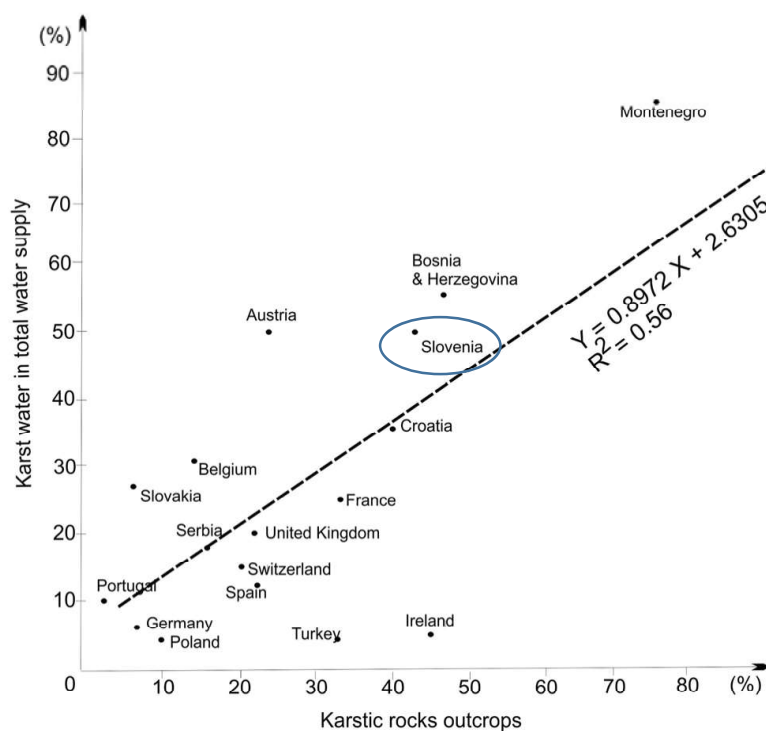


Figure 1.1: Comparison of the percentage of carbonate outcrops in the total country area and the contribution of karst water to the total water supply for selected countries in Europe (results of Cooperation in Science and Technology (1995) and Hartmann et al. (2014a), published in Stevanović (2019), modified).

Karst systems are known for their high degree of heterogeneity, permeability and anisotropy. These properties result in a slow flowing fraction of recharge through the matrix and a fast flowing fraction of recharge through the conduits of the system. Springs in these systems are known to have a high variation of response to precipitation events. As karst systems are highly complex and variable systems, predicting their responses to potential sources of contaminations and changes in climate, remains challenging. Several Karst vulnerability methods have been developed in the last decades in order to define protection strategies in karst regions. In the following chapters a detailed literature review will be given about the special processes in karst regions and their vulnerability. Furthermore, existing methods which describe karst vulnerability will be presented.

## 1.1. State of the art

### 1.1.1. Karst hydrological processes

In hydrogeology the term karst refers to surface and subsurface formations in carbonate rocks, which are mainly formed by dissolution of the soluble rocks. Carbonate rocks, which are most relevant for water resource managements, are limestone (consisting of the mineral calcite,  $CaCO_3$ ) and dolomite rock or dolostone (consisting of the mineral dolomite,  $CaMg(CO_3)_2$ ) (Hartmann et al., 2014a). Rainwater, which flows toward the carbonate bedrock, takes up carbon dioxide ( $CO_2$ ) from the atmosphere, the vegetation and from microbial processes in the soil. A dissolution of the carbonate rock, regarding the following equation, is taking place:



The products of this reaction are dissolved calcium ( $Ca^{2+}$ ) and bicarbonate( $HCO_3^{2-}$ ). The degree of carbonate rock dissolution depends on several aspects like lithological factors (chemical and mineralogical purity of the rock), physicochemical factors (temperature and  $CO_2$  partial pressure) and the  $CO_2$  concentration in the water (originated from the atmosphere and from biological processes in the soil) (Hartmann et al., 2014a).

In the following, the processes of karstification in karst aquifers will be explained. Karstification processes are the formation of karst aquifers by dissolution kinetics. In Figure 1.2 the basic concepts of karst aquifers are illustrated. For most karst regions a rather thin soil layer is characteristic, through which rainwater can flow rapidly. In some regions the rock is not covered by any soil at all. Beneath the soil layer the upper carbonate rock layer, which is called epikarst, is located. It lies within the unsaturated zone. This layer is known to be highly karstified due to the high amount of  $CO_2$  present in the percolating water. Karstification processes of carbonate rock outcrops lead to the formation of landforms such as karren, dolines, swallow holes and poljes. Karren are formations due to karstification varying in size depending on slope and structure of the carbonate rock surface (Hartmann et al., 2014a). They can be an indicator for zones of intense epikarst development (Goldscheider and Drew, 2007). Dolines are closed, sub-circular natural depressions or holes in the ground caused by collapses of the surface layer (Hartmann et al., 2014a; Goldscheider and Drew, 2007). Swallow holes or ponors are places where water drains to the subsurface in a carbonate rock area. This stream of water which is draining towards the subsurface is called sinking stream (Hartmann et al., 2014a). Poljes are large, flat, plain and closed formations in karst regions with water mostly drained by swallow holes. Deposits tend to accumulate in poljes. Thus, they show a relative thick soil layer (Hartmann et al., 2014a). In the subsurface networks of open fractures, karst conduits and caves are formed. These networks often drain towards a large karst spring. In this system caves are able to store some of the downward flowing water during low flow conditions (Williams, 2008). Solids potentially get accumulated and eventually washed out by heavy rainfall events (Williams, 1983). Because of the high permeability of the rock, only few surface water can be found in karstic regions during low flow conditions (Ravbar, 2013). Entire rivers from neighboring or overlying nonkarstic rocks can sink into swallow holes and drain into the karst aquifer (Hartmann et al., 2014a). This recharge is called allogenic recharge. Water is entering the system by dolines, shafts or swallow holes and therefore creates point recharge to the system. Autogenic recharge contains the precipitation which directly falls on the karstic area (Hartmann et al., 2014a). Furthermore, recharge in karst can be split into a fast flow component, with a low storage capacity in the conduit (concentrated flow), and a slow flow component, with a high storage capacity in the matrix of the karst system (diffuse flow). An exchange between those components is possible. Consequently, karst regions show a duality, a high heterogeneity and an anisotropy of hydrological processes (Ravbar, 2013).

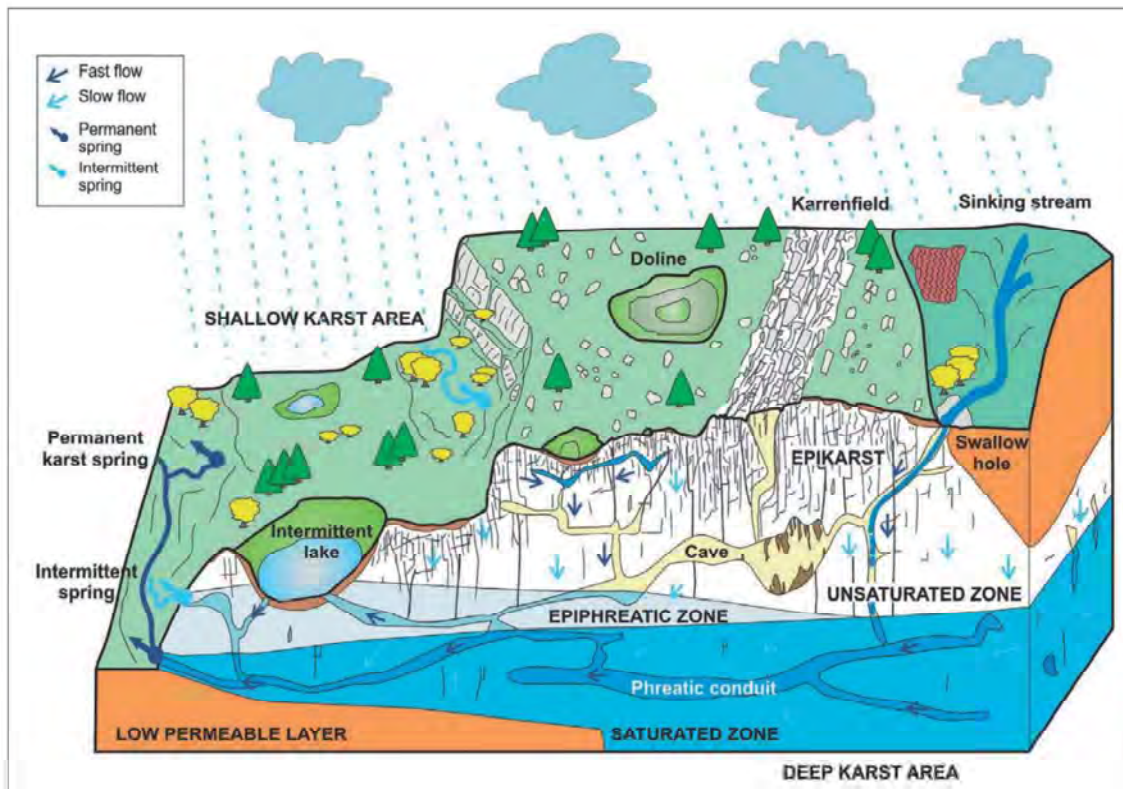


Figure 1.2: Conceptual model of a karst aquifer and its groundwater flows by Ravbar (2013)

In well-developed karst systems the residence times of contaminants are often short and contaminants are not attenuated sufficiently (Goldscheider, 2005). Only a small portion of the total aquifer containing a well-developed conduit system, can be sufficient enough to have a major impact on the hydraulic behavior and the contamination of the system (Ravbar, 2013). These characteristics are tried to be quantified with the help of natural and artificial tracer tests. Though, artificial tracer tests can only describe the hydrological characteristics at one point and one hydrological condition. Because of the high sensitivity of karst aquifers an effective and accurate protection strategy needs to be defined. Therefore, karst vulnerability methods had been developed. The most common will be presented in the following chapter.

### 1.1.2. Karst vulnerability methods

To clarify the term vulnerability, Vrba and Zaporozec (1994) have described it as a qualitative, relative, non-measurable and dimensionless property. Goldscheider (2005) pointed out that a high vulnerability is caused by a low natural protection. Though, there is no universal definition of the term yet. Considering the, in Chapter 1.1.1 mentioned properties of karst aquifers, defining areas of low natural protection in karst regions is quite complex. For porous aquifers (e.g. sandstone aquifers) zones of high vulnerability are specified by isochrones (lines of same travel times). Depending on the European country the values for the travel time lines, in which special protection should be provided, can vary from ten up to 100 days. The usage of this approach for karst aquifers would lead to huge zones of high vulnerability, resulting in conflicting interests regarding land-use (Goldscheider et al., 2000). However, as it is important to protect fresh water sources and resources, approaches had been made to describe those areas within a karstic catchment that are especially vulnerable for contaminations. In Table 1.1 the most common karst vulnerability methods, regarding European countries, are listed.

They can be divided into qualitative, semi- quantitative and quantitative methods. While qualitative and semi-quantitative methods rely on parametric system models, quantitative methods use process-based simulation models or statistical methods to receive karst vulnerability. In 1996 the first vulnerability method especially for karst regions, called EPIK, had been invented by Doerfliger (1996). Fundamental regarding the further development of karst vulnerability methods was the COST Action 620 (European Cooperation in the Field of Scientific and Technological Research). It started in 1997 and ended in 2002. The Action, entitled “Vulnerability and Risk Mapping for the Protection of Carbonate (Karst) Aquifers”, was set up by the European Commission in order to develop an improved and consistent European approach for the protection of karst groundwater. It aimed to define and clarify the basic concepts of vulnerability focused on karst aquifers. Furthermore, detailed alternatives for vulnerability, risk and hazard mapping assessments were presented. By Sinreich et al. (2014) risk, in context of this study, is defined as “the probability of harmful groundwater contamination with respect to a combination of (intrinsic or specific) vulnerability, hazard potential and adverse consequences on groundwater’s social and economic value”. The basic concept for most of the methods of the COST Action 620 is the origin-pathway-target model (Cooperation in Science and Technology, 1995). This model leads to three factors of aquifers vulnerability: the potential pollution (origin), the transport way (pathway) and the contaminated resources (target). The terms “intrinsic” and “specific” vulnerabilities have been defined within the Cost Action 620. Intrinsic vulnerability is taking the geological, hydrological and hydrogeological characteristics of an area into account. However, it is independent of the nature of the contaminant and the contamination scenario. Specific vulnerability is considering the properties of a particular contaminant or group of contaminants additional to the intrinsic vulnerability of the area. Vulnerability can also be distinguished into resource and source vulnerability in dependence of the aimed target. For resource vulnerability assessments only the vertical route of the potential contaminant through the unsaturated zone is considered. Source vulnerability assessments consider the vertical as well as the lateral movement of contaminants through the unsaturated zone. According to which, resource vulnerability describes the vulnerability of the groundwater table and can be used for the delineation of resource protection zones, and source vulnerability approaches define the vulnerability of a certain source or well. Thus, maps for spring or well protection zoning can be provided by source vulnerabilities (Goldscheider, 2002).

In the following, qualitative and semi-quantitative methods for karst vulnerability assessments will be described collectively. The main procedures, innovations, advantages and disadvantages are going to be discussed. An overview of the methods can be found in Table 1.1. As previously mentioned, qualitative and semi-quantitative methods are based on parametric system models. They result in a map of the catchment with different classifications of vulnerability. In order to obtain this map, several parameters of the medium are selected and described by spatial resolved layers of the catchment area. These layers depict parameters like properties of the bedrock, soil cover, precipitation, concentration of flow, karst network development, infiltration condition, degrees of karstification, topography, recharge rates and many more. Each parameter is classified into defined categories or discrete intervals, which reflects the relative degree of vulnerability to contaminations (Goldscheider, 2002). According to the way the scores of each layer are combined (cumulatively with weights or multiplicatively), Matrix Systems, Point Count System Models and Rating Systems can be differentiated (Iván and Mádl-Szőnyi, 2017). The demand of data needed for vulnerability methods highly depends on the method used. While the Simplified Method (Matrix System) was especially evolved for regions with data scarcity and therefore has a low demand of input information, methods like the Slovene Approach (Rating System) require a high amount of input data. Though, minimizing the data input may lead to an oversimplification of the method and to major inaccuracies (Iván and Mádl-Szőnyi, 2017).

Table 1.1: Overview of the most common karst vulnerability methods in Europe. *X* stays for yes, -for no and *S* for scenarios. The table is adapted from Iván and Mádl-Szőnyi (2017).

Assessment approach	Data demand	Results	Validation	Methods	Intrinsic	Specific	Resource	Source	Spatial res.	Temporal res.	Publications		
Qualitative	Low	Classified map	Limited possibilities	Simplified Method	X	-	X	(X)	-	X	Nguyet and Goldscheider (2006)		
Semi-quantitative				Parametric system model	Rating system	PI	X	-	X	(X)	-	X	Goldscheider et al. (2000)
						REKS	X	-	-	X	-	X	Malik and Jaromir (1999)
						COP, COP + K	X	-	X	X	-	X	Vias et al. (2006), Andreo et al. (2009)
					Point count system	Slovene approach	X	-	X	X	-	X	Ravbar and Goldscheider (2007)
						EPIK	X	-	-	X	-	X	Doerfliger (1996)
						RISKE	X	-	(X)	(-)	-	X	Kattaa et al. (2010)
						KARSTIC	X	-	-	X	-	X	Davis (2002)
						VURAAS	X	-	-	X	-	X	Laimer (2005)
						Pan-European Approach	X	X	X	X	S	X	Andreo et al. (2006), Daly et al. (2002)
Quantitative	Process-based simulation model	High	Possible	Transit time, concentration, pathways or transport of contaminant	PaPRIKA	X	-	X	X	S	X	Plagnes et al. (2010)	
					PRESK	X	-	X	-	-	X	Koutsis and Stourmaras (2011)	
					DRISTPI	X	-	X	-	-	X	Jiménez-Madrid et al. (2012)	
					Time-Input method	X	-	X	-	-	X	Kralik and Keimel (2003)	
Process-based simulation model	High	Possible	Transit time, concentration, pathways or transport of contaminant	VULK	X	X	X	X	-	X	Filipponi et al. (2009), Sinreich et al. (2014)		
				<i>IT</i> and <i>C<sub>V</sub></i>	X	X	-	X	(X)	X	Butscher and Huggenberger (2008), Butscher and Huggenberger (2009a)		

The Pan-European Approach is the only of these methods which is accounting for the properties of contaminants and is able to describe specific vulnerability. All qualitative and semi-quantitative methods can describe the intrinsic vulnerability. Six of the thirteen methods provide resource and source vulnerability maps, the other seven either account for resource or source vulnerability. Some methods like COP/COP+K and Pan-European Approach can differentiate between allogenic and autogenic recharge contributions. Temporal variability of vulnerabilities by applying different scenarios can only be considered by the methods Pan-European Approach and PaPrika. For example, the Pan-European Approach is addressing different scenarios according to its precipitation-factor. The scenarios are differentiated in humid climate with extreme events, humid climate without extreme events, dry climate with extreme events and dry climate without extreme events. Thereby, vulnerability depending on different conditions regarding precipitation can be described. In order to be able to define the vulnerability of study sites with highly different characteristics, different methods were invented. Hence, the VURAAS Method considers the special properties of karst alpine regions and the PRESK Method was designed to be applied in karstified Mediterranean regions. For all qualitative and semi-quantitative methods validation can only be realized to a limited possibility. Applied validations are based on hydrogeological data, tracer tests, spring hydrographs and comparison with other vulnerability methods. In summary, classified maps provide a perfect linkage between decision makers (e.g. in politics) and hydrologist. Because of their layer structure and their applicability in Geographic Information Systems (GIS) they are easy to be used. However, doubts have arose in relation to their applicability, accuracy and reliability. Iván and Mádl-Szőnyi (2017) pointed out that different methods applied at the same study site have led to different or even contradictory results. At the same time comparing the methods, is one of the few validation possibilities. According to Daly et al. (2002) this “is showing the need for more flexible and physically based methods”. Daly et al. (2002) also pointed out, that a general validation of the results should be performed by data not being included for the vulnerability assessment. Additional, Iván and Mádl-Szőnyi (2017) asserted that some of the methods do not have been tested sufficiently yet (REKS, RISKE, PRESK, VURAAS) and only a few of the methods are enabled to consider temporal variability.

Because of the doubts regarding qualitative and semi-quantitative vulnerability methods a shift towards physically reasonable and comprehensive approaches had been made in the past years (Iván and Mádl-Szőnyi, 2017). Daly et al. (2002), Sinreich et al. (2014), Butscher and Huggenberger (2009b) and others recommended to focus on the development of physically based or process-based approaches. Hence, quantitative methods, like the Time-Input method, the VULK method and the  $VI$  and  $C_v$  method, have been evolved. These quantitative methods relay on process-based simulation models or statistical methods. As statistical methods are not of interest for this thesis, they will no further be discussed. Quantitative methods, which relay on process-based simulation models, either simulate or evaluate physical and chemical processes of the movement and transport of water and contaminants in the environment (Focazio, 2002). As risks can also be defined by key physical parameters like transit time, attenuation (relative concentration) or recovery, quantitative methods often result in transit time, concentration, pathways or transport of contaminants (Sinreich et al., 2014).



In the following, the mentioned quantitative methods will be presented in detail. The Time-Input method was developed by Kralik and Keimel (2003) for mountainous areas. The main factors of this approach are travel time from surface to groundwater and input of groundwater recharge. Groundwater recharge is described by a simple water balance equation. The travel time from the surface to the groundwater is calculated by dividing the thickness of layers of the unsaturated zone by their hydraulic conductivity. Locations of faults are considered as well as karst features and the inclination of bedding planes. Only vertical infiltration processes are taken into account, by which resource vulnerability is described. The assumption, that “potential contaminants behave similarity to an ideal tracer and move more or less like the infiltrating water” (Kralik and Keimel, 2003) was set. Therefore, only intrinsic vulnerability is described by this method. The method is able to be adapted to different hydrogeological environments and climatic zones. As a result the vulnerability is expressed in real time and not classified by dimensionless numbers. Thereby, the plausibility of results are easier to verify and the evaluation is more transparent. The main factors of the method can be evaluated by techniques including investigations of the discharge and dynamics (hydrographs) of springs or wells, analysis of isotope or natural tracers, water balance calculations, tracer tests and model calculations. However, Iván and Mádl-Szőnyi (2017) pointed out that “the final travel time values are not exact mean values, rather relative numbers, but (that) they indicate tendencies”. This statement is weaken the point of the good evaluation of the method. The method is considering the mean bad condition to obtain travel times. Neither extreme events nor temporal variability are considered.

The VULK method, developed by Jeannin et al. (2001), was the first quantitative, process-based, numerical approach. Its main objective is to assess intrinsic and specific vulnerability (Sinreich et al., 2014). It can calculate one dimensional advection-dispersion-reaction and retardation and degradation processes. Whereby, retardation and degradation processes account for contamination-specific processes. The latest version of the model is linked to a GIS-database, which enables to model breakthrough curves for any point or polygon on a catchment that has been characterized in terms of input parameters (Sinreich et al., 2014). Solving one-dimensional transports of contaminants, the dual porosity of karst aquifers is considered. Four different layers are required to describe resource vulnerability: topsoil, subsoil, non-karstic bedrock and unsaturated karst layer. The output of one layer is the input of the next one. Considering source vulnerability the saturated karst layer is added. Layer properties are uniform and time-independent. Taking dual porosity into account, the model can have up to seventeen parameters to be determined. The model visualizes breakthrough curves for each sub-system (different layers and mobile/immobile phases). The received breakthrough curves provide values for key physical parameters, which assist in the compilation of resource or source protection maps (Sinreich et al., 2014). The resulting output data are transit time, maximum concentration and duration of a contamination. A VULK–vulnerability map can be obtained by means of coupling the transport model with GIS. So far vulnerability maps have only been described by values like transit time and attenuation (Iván and Mádl-Szőnyi, 2017). Thus, there is no categorization in high and low vulnerabilities. A validation of the method can be provided by tracer tests in the field and in the laboratory. A disadvantage of the VULK method is, that the functions of the protective layers are only described by model parameters and not by rainfall and runoff phenomena. A steady-state flow and transient transport are assumed. Thus, breakthrough curves for only one hydrological condition can be simulated. A change of the hydrological condition is not considered. Another disadvantage of the methods is that for every injection point of contamination input parameters of the model have to be determined.

Butscher and Huggenberger (2008) combined a vulnerability map and time series to provide a quantitative basis for drinking water management and regional planning. The vulnerability map is provided by the semi-quantitative EPIK method. This map can only address on hydrological condition and therefore is not temporal resolved. In order to account for temporal variations, time series of the vulnerability index  $VI$  and vulnerability concentration  $C_v$  are simulated for several springs within the catchment (Butscher and Huggenberger, 2009a).  $VI$  is based on the ratio of spring discharge originating from the conduit system (concentrated recharge) and from the matrix system (diffuse recharge).  $C_v$  represents the modeled concentration of a standard contaminant in the spring water. These time series are calculated by the lumped numerical model AQUASIM, in which karst flow systems are represented by mixed reactor models. Hence, recharge vulnerability of the area is provided by EPIK and spring protection classes from the numerical model AQUASIM. Because of the lumped characteristic of the statistical model, it is not possible to address the concentration of contamination at the spring to different parts of the recharge area. But it can be shown, how precipitation and evaporation effect the contamination at the spring, regarding time of first appearance, maximum concentration and time of maximum concentration. A validation of the method has not been discussed in the publications of Butscher and Huggenberger (2007), Butscher and Huggenberger (2008), Butscher and Huggenberger (2009a) or Butscher and Huggenberger (2009b). It was only suggested to use a calibrated numerical model to validate vulnerability maps. Iván and Mádl-Szőnyi (2017) pointed out that a validation of the source vulnerability (numerical model) is possible. In summary, the validation of quantitative methods for karst vulnerability assessments is feasible. Mostly data from tracer tests are used for the validation. Quantitative karst vulnerability methods can provide temporal resolved vulnerabilities to some extent. Though, they are very complex and have a high demand of input data (Iván and Mádl-Szőnyi, 2017).

In the past few years the semi-distributed lumped process-based karst simulation model VarKarst, firstly published by Hartmann et al. (2012), has been developed further and combined with other methods. Thereby, the model might be able to account for spatiotemporal vulnerability. The structure of the VarKarst model will be precisely explained in Chapter 3.1. In order to consider spatiotemporal variability of recharge rates Hartmann et al. (2014b) combined a GIS based recharge estimation method (APLIS) with the numerical VarKarst model. By this combination temporal and spatial resolved recharge rates are provided without the need of adding additional model parameters. Regarding the recharge rate, the method indirectly can describe intrinsic and resource vulnerability. Though, no transit time distributions or categorization of vulnerabilities have yet been defined for this method. In the study of Mudarra et al. (2019) solute transport processes have been implemented to the process of the VarKarst model for the first time. Tracer test data were used to improve the reliability of the model. Though, the tracer test and its transit time distribution were not able to be predicted yet. However, by Hartmann et al. (2012), Hartmann et al. (2013a) and Hartmann et al. (2014b) it has been shown that taking not only discharge data but discharge data and hydrochemical data or data from tracer tests into account can be useful for the calibration and evaluation of the VarKarst model. In Hartmann et al. (2014b) and Hartmann et al. (2015) better model results for the validation period were achieved, considering discharge and hydrochemical data. Using additional data improves the sensitive of the model parameters and enables the model to consider all important karst processes without provoking an overparametrization. Overparametrization of a model occurs, if to many model parameters are set. Different combinations of those parameters can result in similar model performances, known as equifinality. Parameters lose their identifiability and the uncertainty of the model increases (Hartmann et al., 2014a). Adding additional information to the model, can improve the consideration of all important karst processes without decreasing the sensitivity of the model parameters. This has the advantage, of the model able to be applied at any karst site (Hartmann et al., 2013c).

### 1.1.3. Research gaps

Considering the presented literature, there is a lack of karst vulnerability methods considering different hydrological conditions. Vulnerability is not only depending on recharge conditions like surface and subsurface structure of the ground, but also on precipitation and evapotranspiration patterns (Butscher and Huggenberger, 2009b). As these recharge conditions variate both over time and space, methods which aim to assess karst vulnerabilities should consider spatiotemporal variations. Butscher and Huggenberger (2009b) pointed out, that especially in a changing climate future karst vulnerability methods have to be temporal resolved in order to be able to describe the effects of those changes in climate. Yet, only a few studies have quantified the impact of climate change on karst water resources (Hartmann et al., 2014a). One reason could be the high demand of data or the overparametrization of numerical models, if they are resolved temporal and spatial (Hartmann et al., 2015). A linkage between spatial and temporal resolved methods is needed in order to be able to address areas of high potential risks of reducing the quality of the water of the recharge and discharge. Additionally, a lack of methods which can be validated was observed for the presented karst vulnerability methods. In order to achieve precise and accurate model results a validation is inevitable.

## 1.2. Research objectives

The goal of this study is to enable the simulation and prediction of transit time distributions of virtual tracer tests carried out in a karst catchment. The particular influence, of potential contaminations for each point of the catchment, on the quality of the spring is intended to be characterized for any hydrological condition. Therefore, the VarKarst model will be used with certain modifications. According the following hypotheses a simulation of spatiotemporal karst vulnerabilities is possible:

- 1.) By the linkage of spatial distributed soil information and the semi-distributed VarKarst model spatial and temporal variabilities are considered for the results of the model.
- 2.) Tracer breakthrough curves can be simulated and predicted with the VarKarst model by:
  - a. Considering solute transport in the structure of the VarKarst model, using the assumption of complete and instantaneous mixing within every model step.
  - b. Using observations of carried out tracer tests and discharge data to calibrate the model.
  - c. Accounting for advection processes by the linear distance between the injection point and the spring or by the hydrological initial conditions of the tracer tests.
- 3.) The possibility of overparametrization of the VarKarst model and equifinality of the model parameters is avoided by adding soil information data and thereby reducing the number of model parameters.
- 4.) Using not only discharge but discharge and tracer test information for the calibration of the model is decreasing the uncertainties of the model.
- 5.) Karst vulnerability can be described with the help of the ratio of concentrated and diffuse recharge
- 6.) The combination of experimental and modeling approaches leads to an improved understanding of potential contaminants' transport and the quantification of the study sites' complex recharge behaviors.

If transit time distributions are able to be predicted, information about the vulnerability of the catchment regarding climate changes could be provided. Thus, adequate water management could be proposed in order to sustain good water qualities for springs in karst regions.

## 2. Study site

Aiming to describe spatiotemporal karst vulnerability by the prediction of transit time distributions of virtual tracer tests, the catchment of the Unica springs was used as study site. The catchment is located in the southwest of Slovenia in the Dinaric Karst region. The Dinaric Karst region is the carbonate part of the Dinaric Mountains between the Adriatic Sea and the Pannonian Basin. It is known for its characteristic relief forms of numerous poljes elongated in NW-SE direction, which is also called “Dinaric” direction. This area is designated as “classical” karst. It shows karst typical characteristics like: high karst plateaus, leveled surfaces, dolines, large and deep caves, sinking rivers and abundant springs (Zupan Hajna, 2019). Thus, the catchment of the Unica springs is featuring all this karst characteristics. It is covering an area of 820 km<sup>2</sup> with elevations varying between 446 and 1312 m.a.s.l. The system drains through the permanent karst springs, Malenščica (S1) and Unica (S2) towards the Unica river. Those springs are located at the southern border of the Planinska polje. The Unica river flows into the Ljubljana river, which joins the river Sava. The spring S1 is used for drinking water supply.

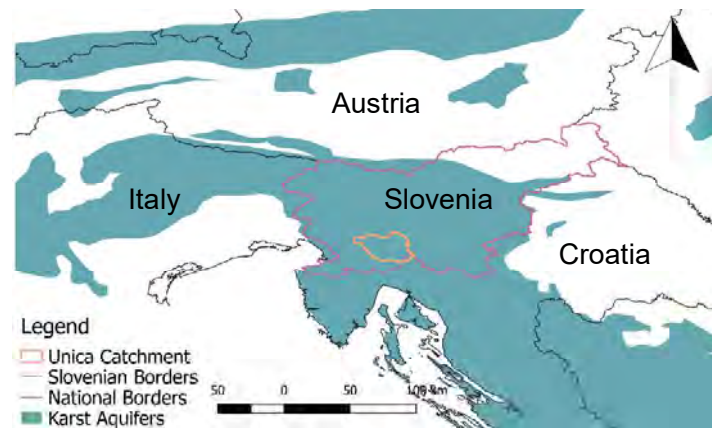


Figure 2.1: Map showing the location of the study site (Data source of karst aquifers: Chen et al. (2017)).

In Figure 2.2 the hydrogeology characteristics of the catchment are shown. The data was provided by the Karst Research Institute ZRC SAZU. The Jarvoniki karst massif forms the central part of the catchment. This karst aquifer is highly karstified and therefore shows karst characteristics like a high permeability, anisotropy, heterogeneity, poljes, dolines, sinking rivers and others. On the southeastern side in the direction of the Snežnik thrust fold the Pivka river flows. Along this river alluvial deposits, which form intergranular aquifers with lower permeability, and flysch rocks occur. On the western side of the Pivka basin there are flysch rocks, which feature a low permeability as well. On the northwest side of the Jarvoniki karst massif along the Idrija fault zone a series of poljes were formed. They are orientated in the “Dinaric” direction. At the bottom of these Poljes alluvial deposits are accumulated. Thus, low permeability prevails at the poljes. Outflows from the series of poljes flow towards the Rak sinking stream. Northeast of the Idrija fault zone the Bloke plateau is located. It consists of Triassic Dolomite (fissured carbonate rock) and consequently is attributed with a medium permeability. Typical for a karst region the bedrock is covered by a rather thin soil layer. Within the catchment of the Unica springs the depths of the soil variate between 0 and 200 cm (see Figure 2.3). The soil depth data, which was provided by the Karst Research Institute ZRC SAZU, was determined by several assumptions; e.g. by the distance to a swallow hole or polje. The soil depths haven’t been measured directly.

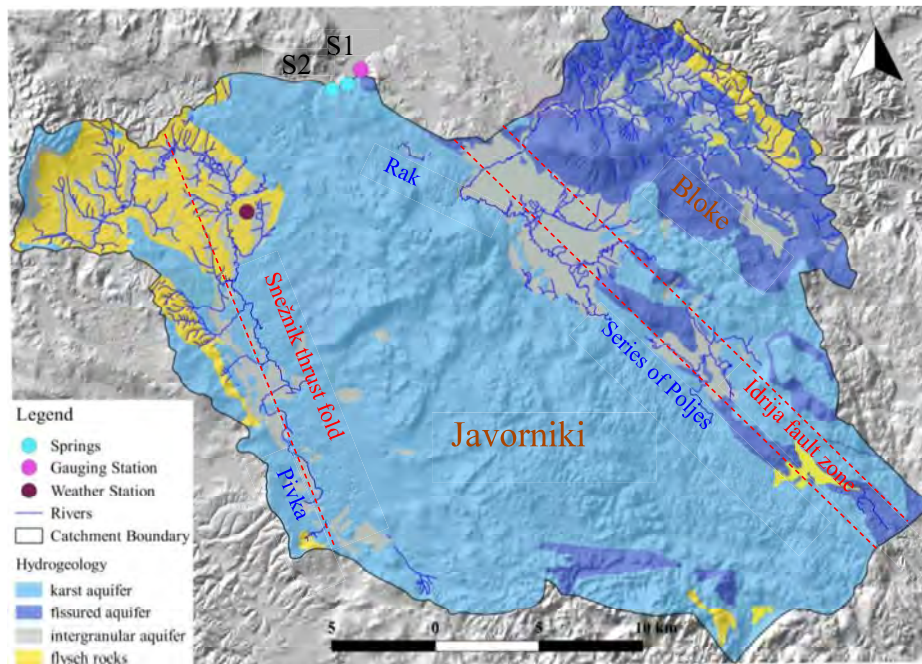


Figure 2.2: Hydrogeological map of the catchment of the Unica springs

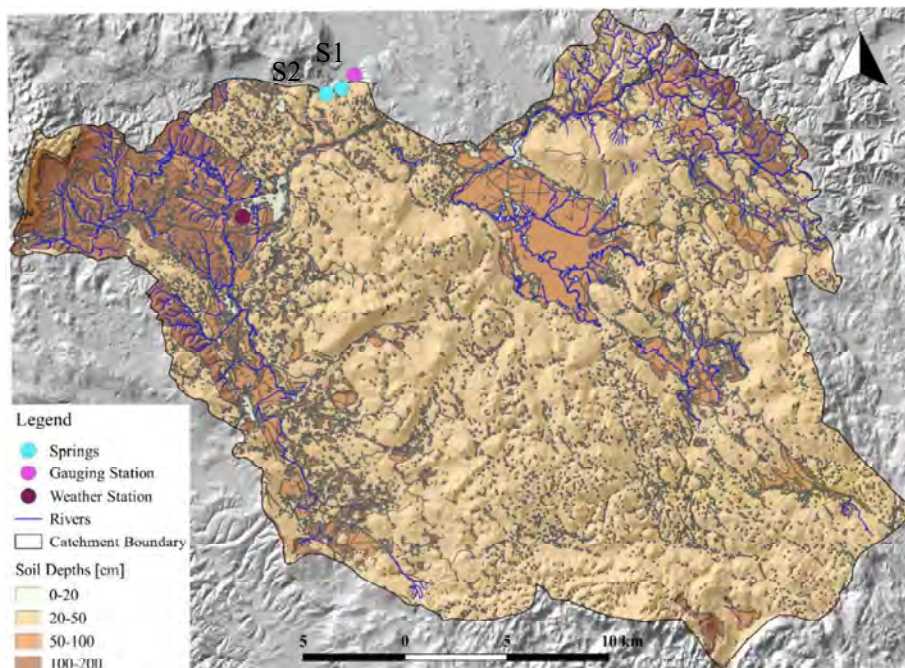


Figure 2.3: Map of soil depths of the catchment of the Unica springs

Though, it is conspicuous that soil depths are higher for areas, which are not located on the carbonate rocks of the karst aquifer. Thicker soil layers are found along the Pivka river basin, at the poljes and the Bloke mountain. Figure 2.4 is showing the relative coverage of soil textures of the catchment of the Unica springs. The information of the soil texture is obtained from the European Soil Data Centre (Ballabio et al., 2016). According to this data the most common soil textures of the catchment are loam and silt.



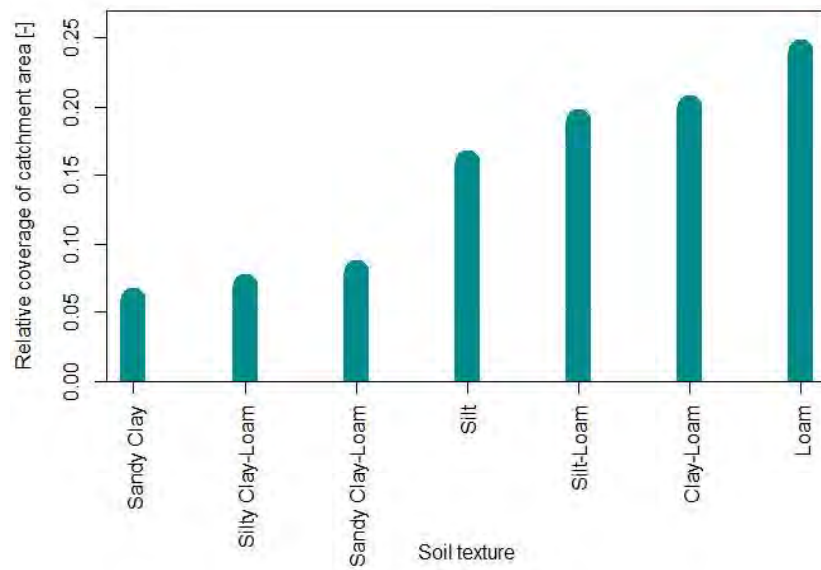


Figure 2.4: Relative coverage of each soil texture type regarding the area of the catchment of the Unica springs (Data source: Ballabio et al. (2016))

The effective porosities of each soil type regarding to Rawls et al. (1983) are listed in Table 2.1. According to this the mean effective porosity, weighted by the relative coverage, of the catchment of the Unica springs is 0.42.

Table 2.1: Effective porosities and their relative coverage of the catchment of the Unica springs regarding soil types

Soil Type	Silty Clay-Loam	Sandy Clay	Sandy Clay-Loam	Clay-Loam	Silt	Silt-Loam	Loam
Effective porosity [ $\text{cm}^3 \text{cm}^{-3}$ ] (Rawls et al., 1983)	0.448	0.328	0.330667	0.384	0.45425	0.49375	0.4475

The discharge of the catchment is measured at the gauging station Unica Hasberg. The station is located at the Unica river after the junction of the two springs S1 and S2, see Figure 2.2. In this study the discharge measured at this gauging station is set to be the discharge of the Unica springs. Meteorological data is collected at the weather station in Postojna at an elevation of 533 m.a.s.l. Daily time series of discharge, precipitation and temperature are provided by the Ministry of the Environment and Spatial Planning of the Slovenian Environment Agency. At the study site Ocean climate, featuring warm temperatures, fully humid and warm summers, prevails. The long-term monthly average precipitation of the time period 1991 till 2017 is showing maximum values of  $6 \text{ mm d}^{-1}$  in September and November. In the summer months mean values around  $3 \text{ mm d}^{-1}$  are present. Two peaks of discharge can be discovered throughout a hydrological year. The global peak is reached in December ( $36 \text{ m}^3 \text{s}^{-1}$ ) while a second minor peak is occurring in April. The minimum mean discharge value of  $5 \text{ m}^3 \text{s}^{-1}$  is reached in August. Mean monthly temperatures variate from  $0.4^\circ\text{C}$  in January and  $19.4^\circ\text{C}$  in August.

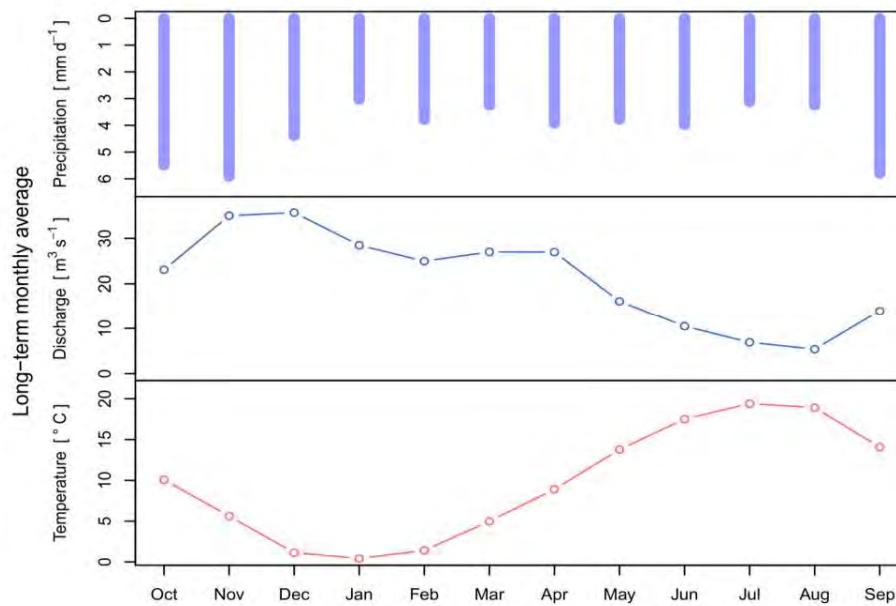


Figure 2.5: Long-term mean monthly precipitation, discharge and temperature value regarding the time period 1991-2017

With values of one to  $90 \text{ m}^3\text{s}^{-1}$ , the discharge at the gauging station Unica Hasberg is highly variable. In Figure 2.6 the variability of discharge values throughout the hydrological years 1992 till 2017 are presented. While in the driest hydrological year (2012) of the entire time period the mean discharge value was only  $8 \text{ m}^3\text{s}^{-1}$ , the mean values in the two following years were with values of 33 and  $35 \text{ m}^3\text{s}^{-1}$  more than four times bigger than the mean value of the driest year. Thus, the discharge can highly variate from one year to another. Especially wet years (e.g. 2001, 2013, and 2014) are showing a high variability of discharge values. Though high discharge values were reached, small values could still be measured. The discharge of the catchment of the Unica springs can be describe as highly fluctuating, which is a typically feature for the discharge of karst catchments.

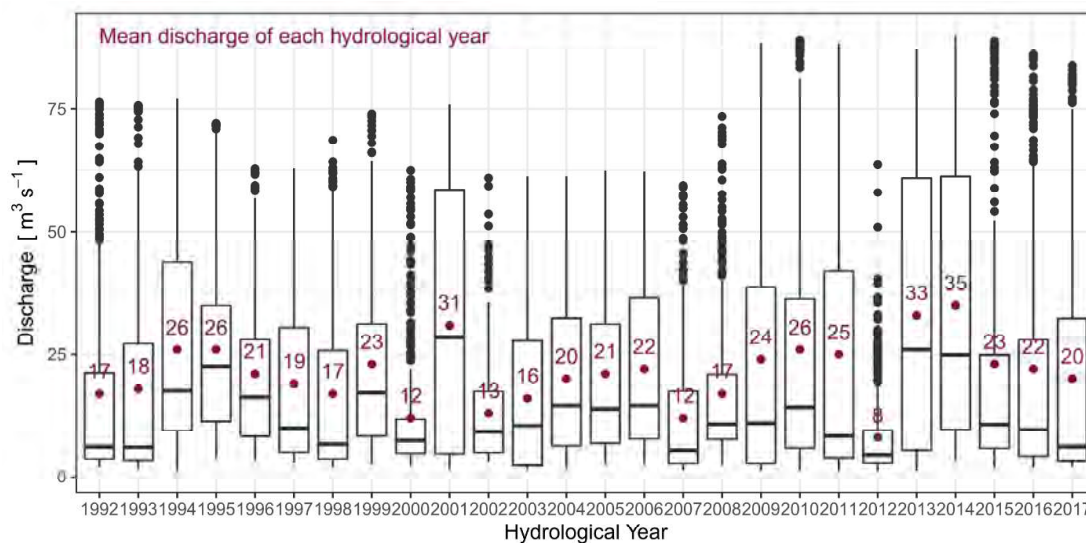


Figure 2.6: Boxplots of the discharge for each hydrological year with additional mean discharge values potted. All Boxplots of this thesis are showing the median as a horizontal line; the box representing the 25th and 75th percentile; the whiskers extend to 1.5 times the interquartile range.

## 2.1. Tracer tests

It's a common approach in karst regions to execute artificial tracer tests in order to improve the schematic understanding of the hydrological system. Flow path ways and travel time durations can be identified by tracer tests. The Karst Research Institute ZRC SAZU provided data of nine tracer tests, executed at the catchment of the Unica springs. These tests were carried out at different locations and during different hydrological conditions. Dye tracers (Uranine, Amidorhodamin g and Naphthionate) were applied to the system in different amounts. As those dye tracers are considered to be conservative, it is assumed that they behave in a similar way like the water of the system. In the map of Figure 2.7 the location of the injection point for each tracer test is marked. Tracer tests were mainly carried out within in a radius of 10 km distance from the springs S1 and S2. Only one test (T9) was exceeding these 10 km radius. Its linear distance to the springs was almost 20 km. The tracers of the tests T3, T5 and T8 were all injected at the same point during different hydrological conditions. At the two springs S1 and S2 water was sampled manually and automatically. Tracer concentrations were determined by measuring the fluorescence of the water samples at different wavelengths. For some tests fluorescence was also measured *in situ*. Discharge values were observed at both springs. Figure 2.7 is showing the groundwater travel times for high flow conditions. The travel times were estimated by the Karst Research Institute ZRC SAZU, taking artificial tracer tests, geological, speleological and natural tracer data into account (Ravbar and Goldscheider, 2007). The travel times can range from smaller than one day up to bigger than ten days at high flow conditions. The majority of the tests were carried out at regions of groundwater travel times smaller than ten days at high flow conditions.

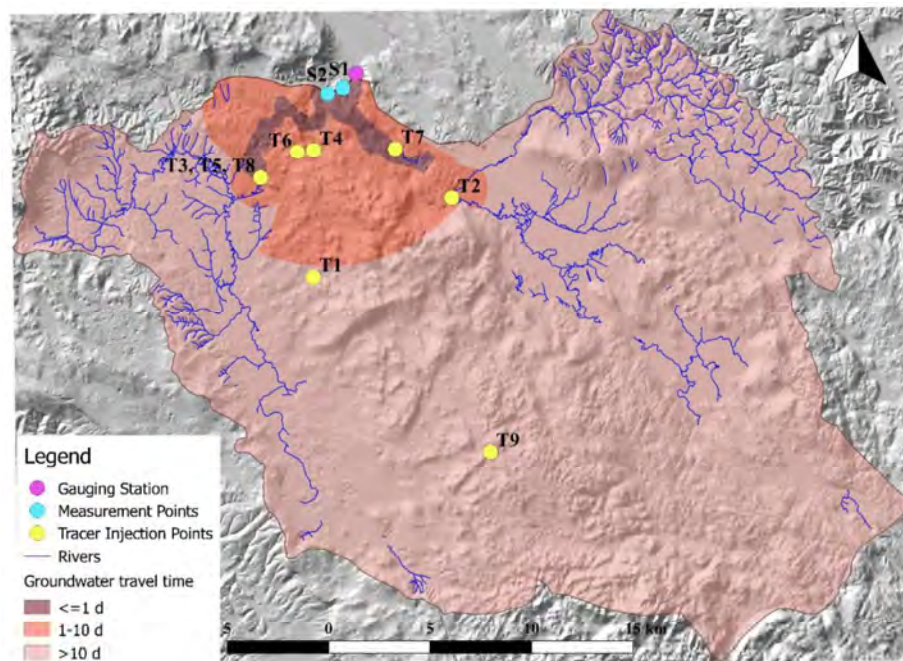


Figure 2.7: Injection points and points of measurements of the tracer tests applied in the catchment of the Unica springs.

The characteristics of all tracer tests are summarized in Table 2.2. Seven of the nine tracers were injected into sinking streams, shaft, dolines or ponors. The injection points of the tracer tests T4 and T6 were the outlet of an oil collector and a karren field. The oil collector is an artificial construction, which collects and retains water from the highway. All the points of injection of these tests suggest the assumption that no significant interactions between the tracer and the soil can be assumed.



Table 2.2: Summary of all tracer tests carried out in the catchment of the Unica springs (Abbreviations: Uranine = Ur.; Amidorhodamin g = Am., Naphthionate = Na.)

N° tracer test	T1	T2	T3	T4	T5	T6	T7	T8	T9
Date of injection	10.06.1997	15.05.2008		13.11.2008			29.05.2009		01.12.2014
Hydrological condition	Low flow	Precipitation event, increasing discharge (medium flow)		High flow, recession period			At the beginning of recession period, followed by a discharge peak (low flow)		High flow, recession period (high flow)
Description of injection point	Doline (at Poček military training area)	Ponor (Mala Karlovica)	Sinking stream (Pivka river at Postonska Jama)	Outlet of oil collector (at Ravbar-komanda)	Sinking stream (Pivka river at Postonska Jama)	Karren field (on the karst surface)	Sinking stream (Rak river)	Sinking stream (Pivka river at Postonska Jama)	27-meter-deep shaft/doline (Blatna Dolina)
Tracer	Ur.	Ur.	Am.	Ur.	Am.	Ur.	Am.	Na.	Ur.
Mass injected [kg]	4	2.85	2.82	1	1	0.5	0.5	2	38
Mass recovered [kg]	2.49	2.93	1.59	2.29	3.66	0.17	1.05	1.49	5.43
Springs tracers were detected	S1	S1	S2	S1	S2	S2	S1	S2	S1
Elevation at injection point [m.a.s.l.]	583	549	512	598	512	582	501	512	1014
Linear distance between injection and observation points [km]	9.3	7.8	5.6	3.2	5.6	3.6	4.2	5.6	19.5
Travel time high flow [d]	> 10	1-10	≤1	1-10	≤1	1-10	≤1	≤1	> 10
Maximum flow velocity by data source [km d <sup>-1</sup> ]	0.60	5.76	3.36	1.68	0.86	0.11	0.77	0.16	0.59
Time [d] (calculated) till:									
First tracer appears	9.5	5.3	6.0	5.5	5.5	17.5	9.3	32.0	33.8
Maximum tracer conc.	23.0	8.5	7.0	18.0	10.8	44.5	32.0	42.0	39.0
50% tracer recovered	159.7	8.5	7.0	19.0	19.8	44.5	34.3	43.0	47.3
Data source	Kogovšek et al.(1999)	Gabrovšek et al. (2010)	Gabrovšek et al. (2010)	Gabrovšek et al. (2010)	Gabrovšek et al. (2010)	Ravbar et al. (2012)	Ravbar et al. (2012)	Ravbar et al. (2012)	Petrič et al. (2018)

In Figure 2.8 and Figure 2.9 the tracer breakthrough curves and the discharge of the Unica springs and the precipitation of the weather station are shown. Note that the ranges of the y-axis are not of the same magnitude for all tracer concentrations. The tracer concentrations were calculated by the measured concentrations at the springs S1 and S2 and weighted by their respective discharge values. Afterwards six hourly data were generated for the tracer, discharge and precipitation data. Masses of recovered tracers were calculated. The durations till the first appearance of the tracer, the maximum tracer concentration and 50% of the tracer being recovered are estimated. The calculations will be explained in more detail in Chapter 2.3. Tracers were injected at five different times. Thus, at three of those times multi-tracer tests were carried out with up to three different kind of tracers injected at different points at the catchment simultaneously. In the following, each tracer test will be describe in detail.

In June 1997 Uranine was injected into a doline 9.3 km apart from the springs. During the measurement period two main peaks and several smaller ones regarding rainfall have been recorded with values up to 26 mm in 6h. As an initial condition the catchment can be assumed to be rather unsaturated, as there was not much rainfall occurring in the previous months before the tracer was injected. The first two peaks of discharge did not exceed values of  $30 \text{ m}^3\text{s}^{-1}$ . Thereafter, discharge values were rather small for the time period from August till December. From December on they rose up till  $69 \text{ m}^3\text{s}^{-1}$ . The tracer was detected at both springs. 2.49 of the 4 kg injected tracer was recovered over a time period of about 7 months. The tracer could first be detected 9.5 d after the injection and reached its maximum concentration of  $0.068 \text{ mg m}^{-3}$  after 23.0 d, while it took 159.7 d to measure half of the recovered tracer mass at the springs. This times do not contradict the assumption of the travel times of Figure 2.7, where ground water travel times at this injection point were set to be higher than 10 d for high flow conditions. The time period of measurement was by far the longest for this tracer test.

The tracers Uranine and Amidorhodamin g were injected at two different locations during a rainfall event in May 2008. 2.85 kg of Uranine were injected into a ponor and 2.82 kg of Amidorhodamin g were injected into a sinking stream during a precipitation event and increasing discharge values. Only one day before the injection rain started to fall, before there were seven days without precipitation. With discharge values up to  $21 \text{ m}^3\text{s}^{-1}$  and precipitation values of maximum 4.4 mm in 6h, maximum tracer concentrations were measured only after 8.5 d in case of tracer test T2 and 7 d in case of tracer test T3 after the injection. The tracer breakthrough curves of both tests show one significant and narrow peak. Though similar amounts of tracers were applied for both tests, maximum concentrations of tracer test T2 reached up to  $1.99 \text{ mg m}^{-3}$  while the maximum concentration of the tracer tests T3 was  $0.85 \text{ mg m}^{-3}$ . In case of tracer test T3 tracer concentrations were only measured at S2 and not all injected tracer could be recovered at the spring. The injected tracer of tracer test T2 could be completely recovered and were measured at both springs. The fast response of the springs to the injection of the tracer must be explained by the hydrological condition as several other tracer tests which also were carried at the injection point of tracer test T3 show a much slower reaction of the springs. The peak of tracer test T3 is 1.5 d earlier than the one of tracer test T2. This goes along with the fact, that the injection point of tracer test T3 is closer to the springs (linear distance: 5.6 km) than the injection point of tracer test T2 (linear distance: 7.8 km).

The tracer tests T4 and T5 were carried out in November 2008. The tracers Uranine and Amidorhodamin g were injected during a discharge recession, followed by heavy rainfall and a rise in discharge up to  $88.6 \text{ m}^3\text{s}^{-1}$ . With such high discharge values the initial hydrological condition can assumed to be high flow. The first appearance of both tracers were detected simultaneously after 5.5 days. Although the linear distance between the injection point and the springs of tracer test T5 is longer, the peak of the breakthrough curve of tracer test T5 was reached first. A maximum concentration of  $0.54 \text{ mg m}^{-3}$  was measured.

For these two tests the distances do not seem to be as significant as the characteristics of the particular injection point. The tracer of the test T5 was injected into a sinking stream, from where it was transported rather quickly towards S2. In case of tracer test T4 the tracer was added into the outlet of an oil collector. Thus, the tracer might not been immediately fed to the springs S1 and S2. For the tracer test T4 a maximum concentration of  $0.17 \text{ mg m}^{-3}$  was measured. The breakthrough curves of both tests do not show a clear peak like the tracer tests T2 and T3. It is of interest, that for both tests more tracer was recovered than injected. The following possible explanations were given by the Karst Research Institute ZRC SAZU. They raised the possibility that the reason for the high recovery rates were the very high discharge values in December 2008. Although measured concentrations for this time period were less than  $0.1 \text{ mg m}^{-3}$ , the calculated recovery was very high due to very high discharge values. In addition, the measured concentrations might be a result of washed out pollutants, which were accumulated in the aquifer during low flow conditions. Those pollutants can increase the fluorescence signal, without any tracers being present.

In June 2009 three different tracers (Uranine, Amidorhodamin g and Naphthionate) were applied to the karst aquifer. For these tests the maximum discharge value throughout the observation period was  $12.86 \text{ m}^3\text{s}^{-1}$ . Thus, it's the lowest maximum discharge value of all tests. The precipitation reached values up to 10.4 mm per 6h, which are higher than the precipitation values for the time period of tracer tests T2 and T3. The hydrological initial condition in June 2009 can be assumed to be low flow. Although the tracers of tracer tests T7 and T8 both were injected into a sinking river, they show very different recoveries of the tracers at the springs. The tracer, which was injected into the Pivka sinking stream (T8), took 32 d to firstly be recorded at the spring. The tracer could only be detected at spring S2. Three-quarter of the injected mass were recovered. By the time of 32 d the maximum of the tracer concentration  $0.46 \text{ mg m}^{-3}$  of the tracer injected into the Rak sinking stream (T7) has already been reached. For tracer test T7 twice as much tracer was recovered at spring S1 as injected. According to the tracer tests T7 and T8 the following assumption for low flow conditions can be done: water from the Pivka river drains toward spring S2 and water from the Rak river drains toward spring S1. Although the tracer of tracer test T6 was applied on a karren field the tracer concentration at the springs increased surprisingly fast. The maximum tracer concentration of tracer test T6 ( $0.10 \text{ mg m}^{-3}$ ) was reached only 2.5 d after the maximum of tracer test T8 ( $0.92 \text{ mg m}^{-3}$ ), which appeared after 42 d. The tracers of tracer tests T6 was only detected at spring S2. Around one third of the tracer of tracer test T6 was recovered. One explanation for the almost same duration till the maximum tracer concentration of tracer tests T6 and T8 could be the shorter linear distance from the injection point to the springs of tracer test T6. The linear distance from the injection point of tracer test T6 was 2 km shorter than the one from tracer test T8. Though, the response of the spring to the tracer test T7 was the fastest. The linear distance between injection point and springs of tracer test T7 lay between the distances of the other to tracer tests. All of the three tracer breakthrough curves do not show one but several peaks.

The final tracer test was carried out in the center of the karst aquifer during high flow conditions. Uranine was injected into a 27 m deep shaft (doline) and flushed with water. With almost 20 km to the sampling points, it has the longest linear distance. This distance is visible in the measured tracer concentration at the springs in form of a shift of the tracer breakthrough curve of several weeks. The discharge during the tracer injection was  $87.0 \text{ m}^3\text{s}^{-1}$ , while it was decreasing afterwards. Two peaks are visible in this tracer breakthrough curve, but there is no such pattern in the precipitation or in the discharge measurements. This leads to the assumptions, that the tracer was transported through different ways and processes through the karst aquifer to the springs. The tracer could be detected at both springs. The maximum tracer concentration of  $0.49 \text{ mg m}^{-3}$  was detected after 39 d. After five month only 5.43 kg of the injected 38 kg were recovered at the springs.

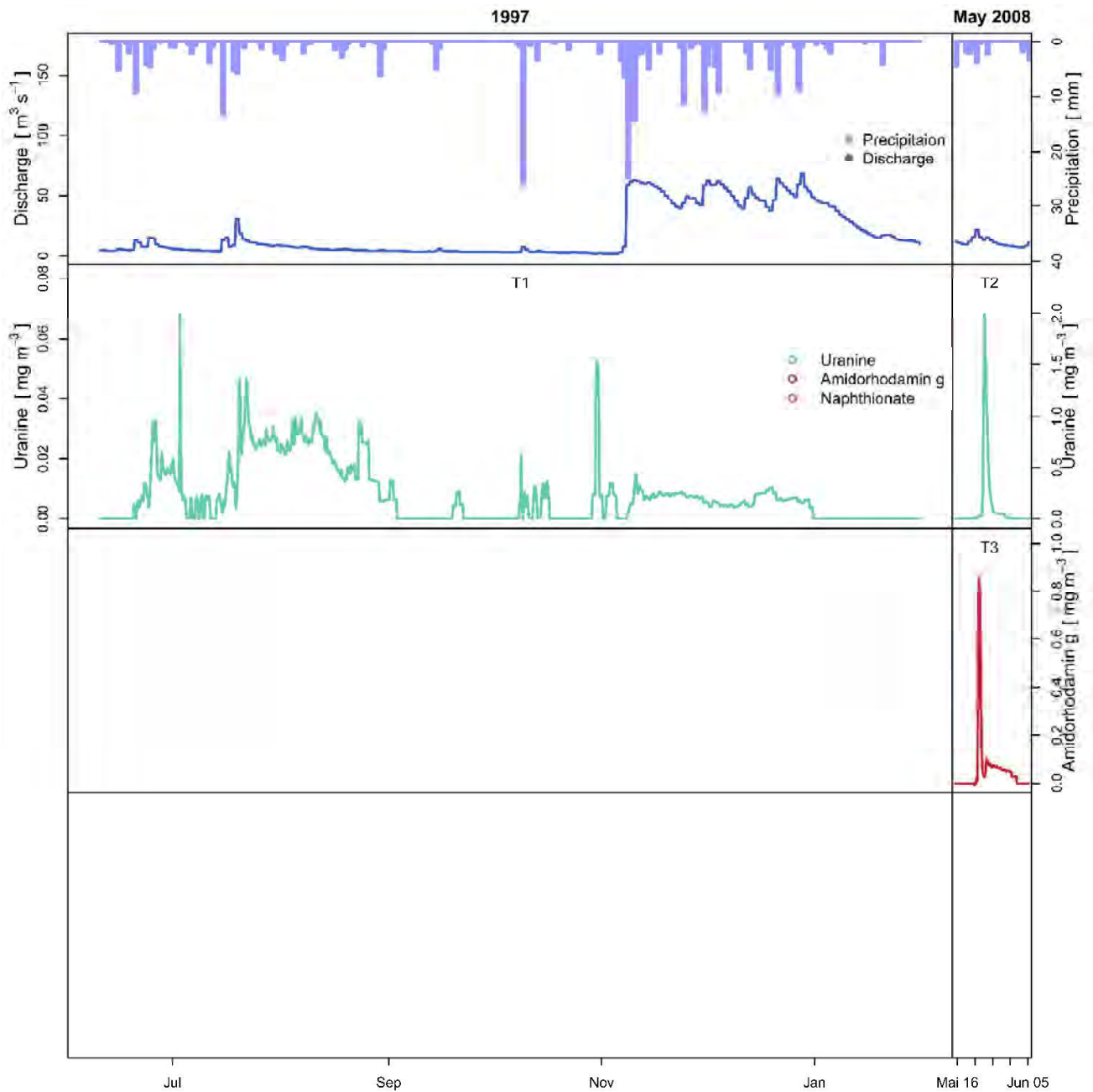


Figure 2.8: Part 1: Time series plots of all tracer tests including discharge and precipitation data. Note that the axes for the tracer concentrations differ.

As mentioned before, the tracers of the tracer tests T3, T5 and T8 were all injected at the same point, the Pivka sinking stream. Thus, the differences between the three tracer breakthrough curves are only caused by different hydrological conditions. The lowest flow condition was during the tracer test T8 in June 2009. The longest time (32 d) till the first appearance of the tracer at the springs was recorded. During tracer test T5, which started in November 2008, the highest discharge and precipitation values of the three tests have been measured.

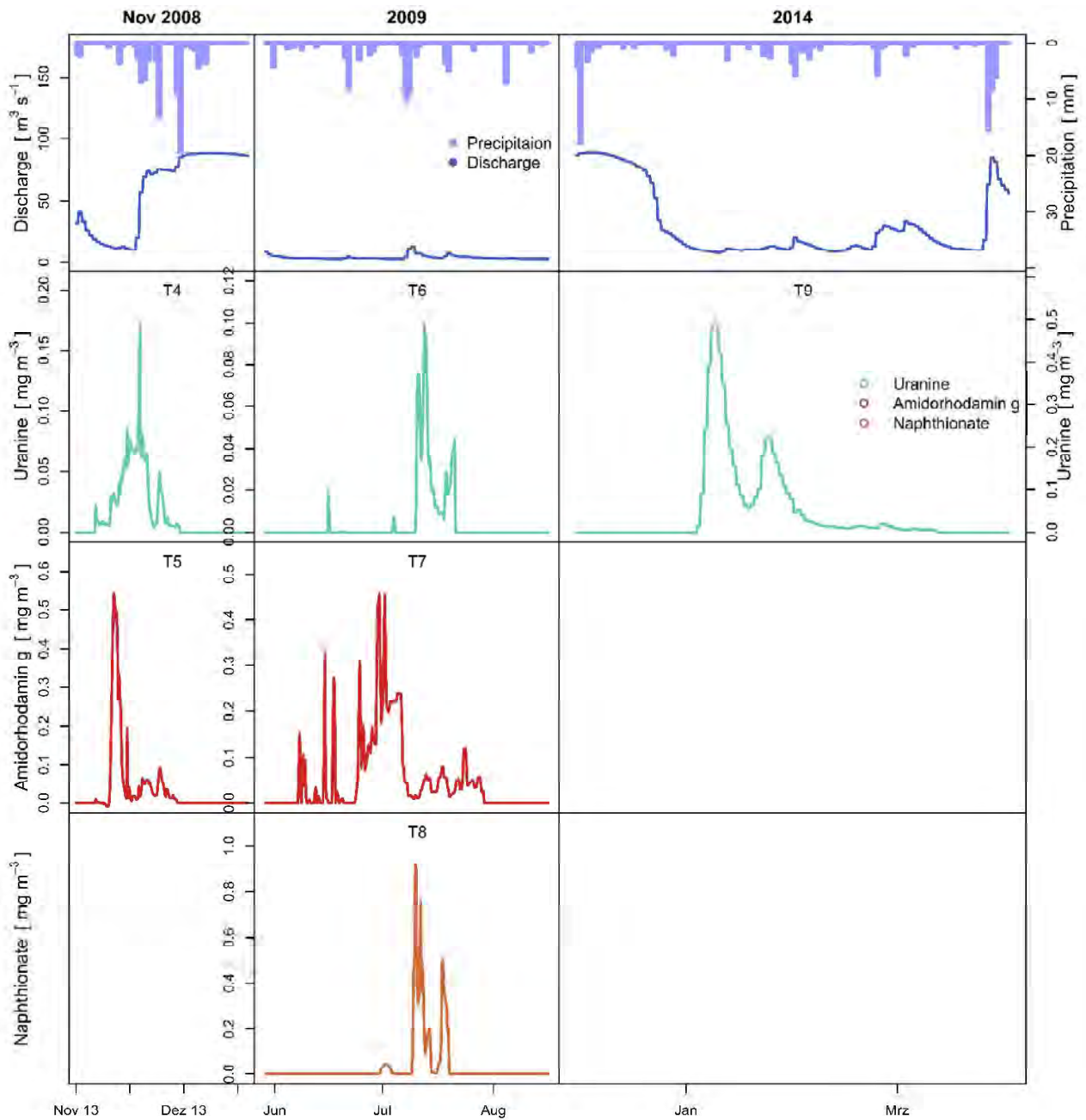


Figure 2.9: Part 2: Time series plots of all tracer tests including discharge and precipitation data. Note that the axes for the tracer concentrations differ.

Regardless this fact, the tracer of the test T3 (May 2008) were detected at the springs almost after the same amount of time (5.3 d) than the tracer of tracer test T5 (5.5 d). One possible explanation could be, that the saturation of the karst aquifer was still high in the case of tracer test T3. The tracer was applied in May in which the system could still be saturated because of high precipitation value in the winter months.

In order to enable the comparison of all nine tracer tests, the maximum flow velocities (velocities of the first tracers appearing at the springs) of the tracer tests provided by literature are compared. Please consider that in case of the tracer tests T1, T2, T4 and T9, tracers were detected at both springs. If velocities for both springs were given by literature, the mean was calculated. The maximum velocities can later be compared to the estimated values by this study. The tracer tests T2 and T3 have by far the highest maximum flow velocities of all tracer tests. Velocities of  $5.76$  and  $3.36 \text{ m s}^{-1}$  were reached. With a value of  $1.68 \text{ m s}^{-1}$  the tracer test T4 is showing a rather high velocity as well. The tracer tests T1, T5, T7 and T9 show velocities between  $0.5$  and  $1 \text{ m s}^{-1}$ . Tracer tests T6 and T8 resulted in maximum velocities smaller  $0.5 \text{ m s}^{-1}$ . Not all tracer tests applied at the same hydrological condition describe similar velocities. According to the velocities found by literature, velocities do not only depending on the hydrological condition but also the point of tracer injection.

## 2.2. Preliminary conceptual model

With the help of the presented data and information of literatures, assumptions in order to describe a preliminary conceptual model of the catchment of the Unica springs can be made. In a conceptual model the schematic understandings of the system are tried to be explained.

The catchment of the Unica springs can be divided into the following three subcatchments (west to east):

- 1.) Pivka sinking river (allogenic recharge)
- 2.) Javorniki karst aquifer (autogenic recharge)
- 3.) Rak sinking river and series of poljes (allogenic recharge)

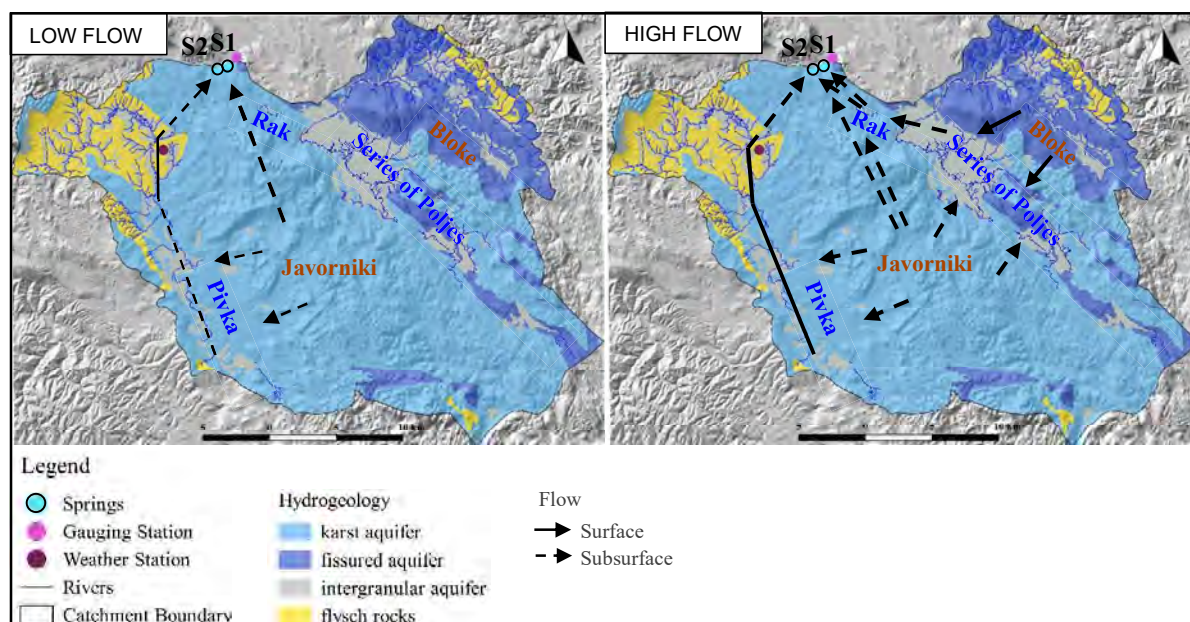


Figure 2.10: Flow directions under low and high flow conditions (modified after Ravbar (2013))

The contributions of those subcatchments to the springs highly depends on the hydrological condition. The flow directions during low and high flow conditions are summarized in Figure 2.10. The center of the catchment the Jarvoniki karst massif functions as a karst aquifer with dominant groundwater flow (Metka Petrič, 2005). The water from precipitation events directly infiltrates and autogenic recharge is formed. During low flow the main flow from the Javorniki karst aquifer faces towards the spring S1.

The Pivka river is also fed by the Javorniki karst aquifer. The water of this river flows along a well-developed system of karst channels and emerges at spring S2. The Pivka river in general accounts the biggest portion of the discharge of the spring S2 (Ravbar et al., 2012). The Rak sinking river and the series of poljes are not contributing water to the springs during low flow. This changes for high flow conditions. Then all three subcatchments are contributing to the discharge of the springs. After a rain event several intermittent springs along the border of the Javorniki karst massif get activated. This leads to an exposure of the Pivka river to the surface at the southwest border and ponding of water at the Poljes at the northeastern border of the karst massif. Additionally, the poljes are fed by surface water from Bloke mountain. By the tracer test T2 it is proven that the Rak river is compound of water from the Javorniki karst aquifer and runoff water from the Bloke mountain (Petrič et al., 2018). The two river branches Rak and Pivka confluence in a subterranean cave and flow towards the spring S2. A certain amount of water from the Rak river is progressively flowing towards the spring S1. Additionally, the spring is fed by recharge from the series of poljes and the Javorniki karst aquifer. Tracer tests T3, T5 and T8 have proven that there is no direct connection between the spring S1 with the ponor of the Pivka River at any hydrological condition. Spring S1 is recharged through a diffuse system of fissures with limited outflow capacity. This leads to a limited discharge at spring S1 (Gregor Kovačič, 2010). As there is an additional input to the discharge from Bloke mountain during high flow conditions, the part from Bloke mountain gains more importance at the discharge of spring S1 and pushes the flow of Javorniki karst aquifer towards the spring S2 in case of high flow conditions. Thus, maximum discharge values are constrained to spring S2, because of the underground well-developed conduits towards this spring.

In order to have a better understanding of the driving processes of the catchment, a preliminary conceptual model and the flow during high flow conditions are presented in Figure 2.11. The preliminary conceptual model is described by two cross sections of the catchment. The top of Figure 2.11 is showing the cross section of the catchment from northwest to southeast, presenting the Javorniki karst aquifer, which drains towards the springs S1 and S2. If rainfall occurs at the Javorniki mountain it partially evaporates. The remaining water is flowing through a thin soil layer towards the unsaturated zone of the epikarst. In the epikarst layer the water can either flow along smaller or bigger conduits or through the matrix system. This results in different flow velocities. Exchanges between water in the conduit and the matrix system are likely to occur. The water from the epikarst flows towards the epiphreatic zone. The epiphreatic zone is known to be regularly flooded and to have a significant porosity. The conduits of the unsaturated zone are mostly formed vertically, which results in a fast flow of water from the surface towards the epiphreatic zone. Thus, the water level of the epiphreatic zone can rise quickly after a rainfall event. From the epiphreatic zone the water is contributed to the saturated zone and the springs. Groundwater recharge and discharge are created. In the epiphreatic and saturated zones conduits are formed mainly in a horizontal direction, due to the horizontal flow of groundwater (Clemens et al., 1999; Kogovšek et al., 1999).

The bottom cross section of Figure 2.11 is describing the catchment from southwest to northeast, showing the flows from the Javorniki karst aquifer towards the Pivka river and the series of poljes. Due to the Snežnik thrust fold a shallow karst zone at the region of the Pivka river basin southwest of the Javorniki karst massive with Flysch and Sandstone was formed. As Flysch and Sandstone show a lower permeability than the surrounding Karst, they act like a hydrogeological barrier and intermittent karst springs, which flow into Pivka river, occur (Petrič and Kogovšek, 2005). Beneath this relative thin layer of Flysch and Sandstone subsurface flows towards a spring outside the boundaries of the catchment of the Unica springs have been identified (Metka Petrič, 2005; Kogovšek et al., 1999).



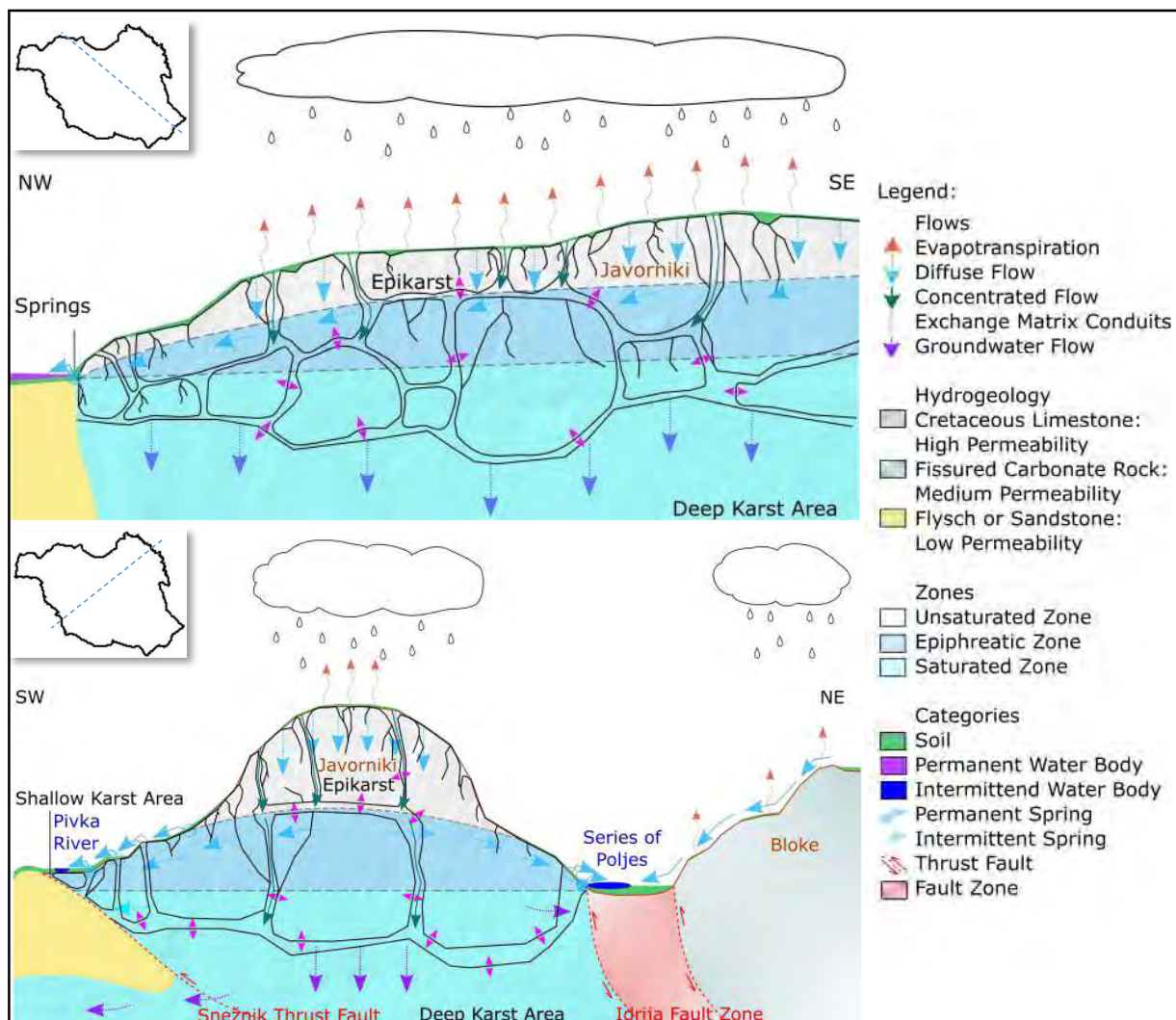


Figure 2.11: Preliminary conceptual model of the catchment of the Unica springs during high flow conditions. Top: Cross section northwest to southeast. Bottom: Cross section southwest to northeast.

The water of the Javorniki karst aquifer also flows towards a series of poljes at the northeastern border of the karst massive. These poljes are formed along the Idrija fault zone. They are also fed by recharge from the Bloke mountains. This mountain consists of Triassic dolomite (fissured carbonate rock), thereby only a small amount of the rainwater infiltrates. A big amount of the rainfall is generated into surface runoff (Gabrovšek et al., 2010; Prelovšek, 2014). During low flow conditions no water can be detected at the surface of the Pivka river basin or the poljes. This changes after a rainfall event. If the level of the epiphreatic zone rises, water will be drained towards the Pivka river and the poljes. After a certain water level, water will be visible at the surfaces.

The information and conclusion from the preliminary conceptual model should be kept in mind when describing the study site with a numerical model, as those can improve the reliability of the numerical model. Additional, an adjustment of the preliminary conceptual model with the help of the results of the numerical model can improve the knowledge of processes and characteristics of the studied karst aquifer (Mudarra et al., 2019).



### 2.3. Data preparation

Aiming to simulate discharge as well as tracer concentrations at the spring with a numerical model, some preparations of the presented data need to be done. The temporal resolution of all available time series are rescaled to a six hourly resolution. Daily precipitation values are divided by four in order to receive six hourly values. Daily discharge and temperature values are repeated four times. The potential evapotranspiration is calculated with the help of the Thornthwaite's equation (see Attachment B, Thornthwaite (1948)). For the calculation a time series of daily temperature data is needed as well as the latitude of the study site. Afterwards the daily evapotranspiration is converted into six hourly data by dividing the daily value through four. The measurement intervals of the tracer test are not uniform, they vary between hourly to daily resolutions. Therefore, the smallest time difference, e.g. one hour, is used to create a time series for each tracer test with uniform time intervals. If no new measurement took place, the previous concentration or discharge value is repeated. Tracer concentrations and discharge were measured at the springs S1 and S2. In order to provide one time series of tracer concentrations at the gauging station, the by discharge of the two springs weighted mean of the two tracer concentrations is used. Afterwards six hourly intervals are calculated by the mean of the concentration values. The mass of the tracer at each time step is calculated by multiplying the tracer concentration and the discharge values. The mass of recovered tracer is the sum of these tracer masses. The velocity of the first tracer occurring at the spring  $v_{max}$  is defined by the linear distance from the injection point to the springs divided by the duration of time till the first tracer concentration was measured at the springs  $t_{Vmax}$ . The velocity of the main peak  $v_{dom}$  is affected by the time the peak of the tracer breakthrough curve  $t_{Vdom}$  is reached. If several peaks are recorded, the time of the maximum tracer concentration is chosen. The velocity  $v_{50}$  is described by the time  $t_{V50}$  at which fifty percent of the recovered tracer was measured at the springs. These values are additionally multiplied by varying aquifer porosities in order to consider the variability of the injection points. For the aquifer porosity the effective porosity is considered.

The water balance of the system is calculated for the entire time period of the model input data time series, in order to see if the catchment itself is a closed system and if the precipitation data is appropriately representing the entire catchment. Therefore, the effective precipitation is calculated by subtracting the potential evapotranspiration from the precipitation. Using the recharge area of the catchment, the unit of the discharge is modified to enable the calculation of the storage by subtracting the discharge values from the effective precipitation values.

### 3. Methodology

In this chapter the methodology used to simulate discharge and tracer test breakthrough curves is described. The workflow which was followed by this thesis regarding modeling is presented in Figure 3.1.

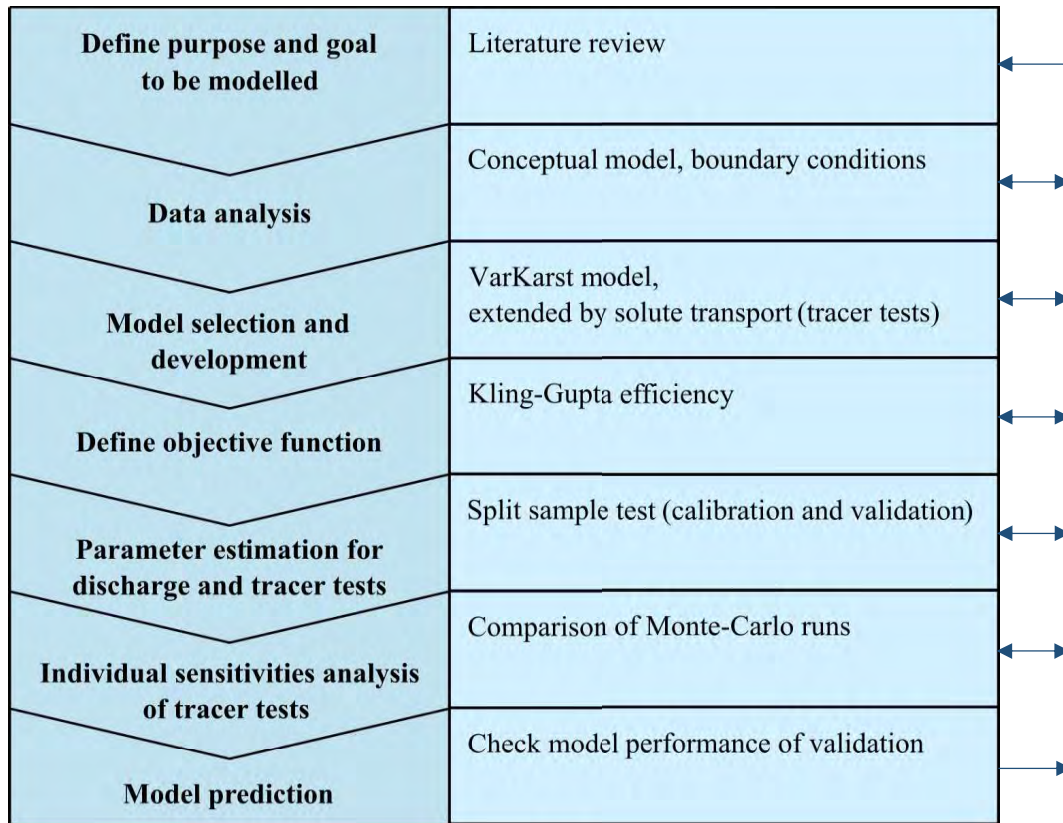


Figure 3.1: Steps of the modeling workflow (modified after Beven (2006))

As a first step the goal and purposes of the modeling part needs to be defined. This can be achieved with the help of a literature review and the determination of the resulting research gap (see Chapter 1.1). In this case it is of interest to enable simulating virtual tracer breakthrough curves at any hydrological condition. After analyzing the data of the study site, assumptions for a conceptual model can be made and boundary conditions can be set (see Chapter 2). All the now following model steps will be presented in more detail in the subchapters of the current chapter. With the help of the results from the data analysis the appropriate model type can be selected. In this case the VarKarst, with an extension of solute transport modeling, is chosen. The VarKarst model is set up in the programming language Matlab. The Kling-Gupta efficiency KGE is used as an objective function to evaluate the model results. The parameter estimation for modeling discharge and tracer breakthrough curves was done by a split sample test. The sensitivity of the parameters is specified with the help of several Monte-Carlo runs. In order to consider model productiveness the performance of the model validation is tested. Depending on the results after each step the workflow has to be (partially) repeated. All pre- and postprocessing are done with the software R.

### 3.1. The VarKarst model

In the following the concepts of the semi-distributed, process based VarKarst model, will be elucidated. It was firstly introduced by Hartmann et al. (2012). The VarKarst model was chosen for this study, as it is able to describe the heterogeneity of recharge processes, which is typically for karst regions. The heterogeneity is applied by model compartments, which contribute different amounts of concentrated and diffuse recharge towards the groundwater. By distributing the recharge area into different model compartments, the model is also able to take the spatial variability of parameters, which are driving physical processes, into account. Describing the variability of the model parameters along the model compartments by distribution functions, the model has the advantage of considering spatial variabilities without requiring much more input data or model parameters. The required data sets of the model are time series of precipitation and potential evapotranspiration data. The model parameters, which are listed in Table 3.1, have to be set. The parameters will be discussed in detail in Chapter 3.1.1.

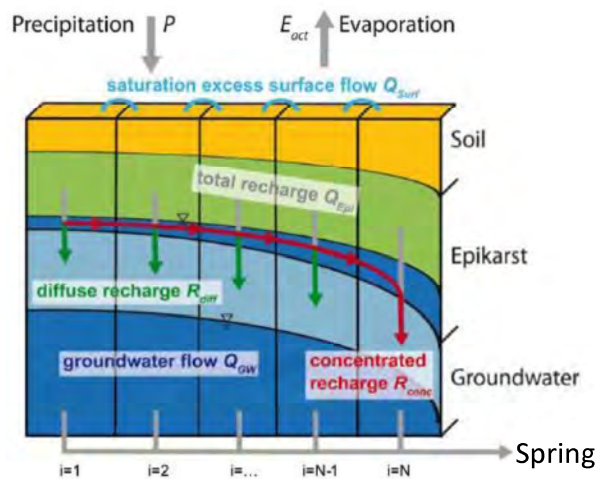


Figure 3.2: Structure of the VarKarst model (modified after Hartmann et al. (2014b))

Table 3.1 Overview of the VarKarst model parameters

Parameter	Unit	Description
$\alpha_{SE}$	-	Soil/epikarst depth variability constant
$K_{ept}$	d	Mean epikarst storage coefficient
$V_s$	mm	Mean soil storage capacity
$V_e$	mm	Mean epikarst storage capacity
$\alpha_{fsep}$	-	Recharge separation variability constant
$\alpha_{GW}$	-	Groundwater variability constant
$A$	$km^2$	Catchment area
$K_c$	d	Conduit storage coefficient

In Figure 3.2 the structure of the VarKarst model is shown. The model is not only divided into different compartments, but also into different layers (soil, epikarst and groundwater). Effective precipitation, in this case precipitation subtracted by the actual evapotranspiration, is added to the soil layer from where it is flowing towards the epikarst layer. If the soil of one compartment is saturated the excesses water flows on the surface towards the next compartment. Saturation excess surface flow occurs. From the epikarst layer the water is divided into concentrated and diffuse recharge. The concentrated recharge of all compartments is flowing towards the groundwater layer of the last compartment of the model. The diffuse recharge drains towards the groundwater layer of each compartment. The sum of the exiting water from the groundwater layer of all compartments forms the discharge at the spring. Hartmann et al. (2012) set the number of model compartments to 15. With this number of compartments the model can provide stable mean values and coefficients of variation.

### 3.1.1. Mathematical description

Hereafter, the mathematical formulations of the VarKarst model, following the flow of water from the top of the soil through the different layers towards the discharge of the spring, will be presented. The mathematical descriptions of the model are based on Mudarra et al. (2019) and Hartmann et al. (2013a). Starting with the characteristics of the soil layer, the variability of soil thickness across the 15 model compartments is described by the parameter  $V_S$  (mean soil storage capacity in mm) and the distribution coefficient  $\alpha_{SE}$ . The soil storage capacity for each compartment  $i$  is determined by the following equation:

$$V_{S,i} = V_{max,S} \left( \frac{i}{N} \right)^{\alpha_{SE}} \quad (2)$$

$V_{S,i}$ : Soil storage capacity at each compartment [mm]

$V_{max,S}$ : Maximum soil storage capacity [mm]

$N$ : Number of model compartments [-]

$\alpha_{SE}$ : Distribution coefficient (Soil/epikarst depth variability constant) [-]

$V_{max,S}$  can be derived from the mean soil storage capacity  $V_S$  [mm]. Here  $i_{1/2}$  defines the compartment, where the volume of the soil on the left equals the volume on the right.

$$\int_0^{i_{1/2}} V_{max,S} \left( \frac{x}{N} \right)^{\alpha_{SE}} dx = \frac{\int_0^N V_{max,S} \left( \frac{x}{N} \right)^{\alpha_{SE}} dx}{2}; \quad V_S = V_{max,S} \left( \frac{i_{1/2}}{N} \right)^{\alpha_{SE}} \quad (3)$$

$$\Downarrow$$

$$V_{max,S} = V_S * 2^{\left( \frac{\alpha_{SE}}{1+\alpha_{SE}} \right)}$$

$E_{act,i}$ , the actual evapotranspiration of each compartment [mm], can be calculated with the help of the amount of water stored in the soil layer of each compartment  $V_{soil,i}$  [mm].  $Q_{surf,i}$  is the excess water from compartment  $i-1$  (see Equation 10).

$$E_{act,i}(t) = E_{pot}(t) \frac{\min[V_{soil,i}(t) + P(t) + Q_{surf,i}(t), V_{S,i}]}{V_{S,i}} \quad (4)$$

$E_{pot}$ : Potential evapotranspiration [mm]

$P$ : Precipitation [mm]

$Q_{surf,i}$ : Surface runoff of each compartment [mm]

In order to define the distribution of the storage capacity of the epikarst the same parameter ( $\alpha_{SE}$ ) like for the soil layer is used.

$$V_{e,i} = V_{max,e} \left( \frac{i}{N} \right)^{\alpha_{SE}} \quad (5)$$

$V_{e,i}$ : Epikarst storage capacity for each compartment [mm]

The derivation of  $V_{max,e}$  is likewise the procedure of  $V_{max,S}$ .

Recharge from the soil to the epikarst  $R_{epi,i}$  is defined by:

$$R_{epi,i}(t) = \max[V_{soil,i}(t) + P(t) + Q_{surfsoil,i}(t) - E_{act,i}(t) - V_{s,i}, 0] \quad (6)$$

With the epikarst storage coefficient of each compartment  $K_{epi,i}$  [d] the epikarst outflow of each compartment  $Q_{epi,i}$  [mm d<sup>-1</sup>] can be generated.

$$Q_{epi,i} = \frac{\min[V_{epi,i}(t) + R_{epi,i}(t), V_{e,i}]}{K_{epi,i}} \quad (7)$$

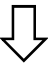
$V_{epi,i}$ : Amount of water stored in the epikarst layer [mm]

The distribution of  $K_{epi,i}$  can also be described by the distribution coefficient  $\alpha_{SE}$ .

$$K_{epi,i} = K_{max,epi} * \left(\frac{N-i+1}{N}\right)^{\alpha_{SE}} \quad (8)$$

The maximum epikarst storage coefficient  $K_{max,epi}$  [d] is described by the mean epikarst storage coefficient  $K_{epi}$  [d] and the distribution coefficient  $\alpha_{SE}$ .

$$N * K_{epi} = \int_0^N K_{max,epi} \left(\frac{x}{N}\right)^{\alpha_{SE}} dx$$



$$K_{max,epi} = K_{epi} * (\alpha_{SE} + 1) \quad (9)$$

As mentioned earlier, lateral surface runoff occurs, if maximum soil and epikarst storage capacities are exceeded by the stored water volume.

$$Q_{surf,i+1}(t) = \max[V_{epi,i}(t) + R_{epi,i}(t) - V_{epi,i}, 0] \quad (10)$$

Diffuse and concentrated groundwater recharge ( $R_{diff,i}$  [mm] and  $R_{conc,i}$  [mm]) are found by splitting the outflow from the epikarst, with the help of a variable separation factor  $f_{C,i}$  [-] and the distribution coefficient  $\alpha_{fsep}$  [-].

$$R_{conc,i}(t) = f_{C,i} * Q_{epi,i}(t) \quad (11)$$

$$R_{diff,i}(t) = (1 - f_{C,i}) * Q_{epi,i}(t) \quad (12)$$

$$f_{C,i} = \left(\frac{i}{N}\right)^{\alpha_{fsep}} \quad (13)$$

Diffuse recharge is generated from model compartments  $i = 1$  till  $i = N - 1$ . Concentrated recharge flows laterally to the ground water compartment  $i = N$ , which presents the conduit system. Thus, groundwater contributions to the discharge  $Q_{GW,i}$  [mm] of the model compartments  $i = 1 \dots N - 1$ , make up the matrix system. They are defined by:

$$Q_{GW,i}(t) = \frac{V_{GW,i}(t) + R_{diff,i}(t)}{K_{GW,i}}; \quad i = 1 \dots N - 1 \quad (14)$$

$V_{GW,i}$ : Amount of water stored in the ground water layer [mm]

The groundwater storage coefficient  $K_{GW,i}$  [d], is calculated by a conduit storage coefficient  $K_C$  [d] and a groundwater variability constant  $\alpha_{GW}$  [-].

$$K_{GW,i} = K_C * \left(\frac{i}{N}\right)^{-\alpha_{GW}} \quad (15)$$

Groundwater contribution of the model compartment  $i = N$  to the discharge reflects the characteristics of the conduit system.

$$Q_{GW,i}(t) = \frac{V_{GW,N}(t) + \sum_{i=1}^N R_{conc,i}(t)}{K_C}; \quad i = N \quad (16)$$

$V_{GW,i}$  is described by:

$$V_{GW,i}(t) = V_{GW,i}(t-1) + R_{diff,i}(t) - Q_{GW,i}(t); \quad i = 1 \dots N-1 \quad (17)$$

and

$$V_{GW,i}(t) = V_{GW,i}(t-1) + \sum_{i=1}^N R_{conc,i}(t) - Q_{GW,i}(t); \quad i = N \quad (18)$$

Calculating the sum of the groundwater contributions to the discharge of all compartments, generates the discharge of the spring  $Q_{main}$ . By dividing the discharge with the recharge area  $A$  [km<sup>2</sup>], it gets rescaled to  $m^3 s^{-1}$ .

$$Q_{main}(t) = \frac{A}{N} * \sum_{i=1}^N Q_{GW,i}(t) \quad (19)$$

### 3.1.2. Model development

In the course of this thesis the VarKarst model is modified in order to avoid overparameterization and to be able to implement tracer tests. Firstly, the model needed to be set to six hourly temporal resolution in order to enable the simulation of narrow tracer breakthrough curves. Though, parameters and other values will be presented in daily units in order to provide a comparison with values from literature. Parameters like  $K_{epi}$  and  $K_C$  with daily units are set to be converted into units of 6h within the model.

Secondly, the sensitivity of the parameters of the VarKarst model is meant to be improved by reducing the number of model parameters as the problematic of overparameterization of hydrological models have been described by many researchers (e.g. Schoups et al. (2008), Schoups et al. (2010) and Whittaker et al. (2010)). Overparameterization of a model leads to parameter nonuniqueness and equifinality. Thus, the parameter of the catchment area is set to a fixed value, provided by the Karst Research Institute ZRC SAZU. The parameters  $V_s$  and  $\alpha_{SE}$  are replaced by fixed values, using spatial soil information of the catchment side. In case of the parameter  $V_s$ , the parameter is omitted by setting a fixed value for each soil storage capacity of each compartment. In order to provide the storage capacity, soil depths are multiplied by the mean effective porosity of the catchment. The mean effective porosity is calculated by the relative coverage of the different soil types of the catchment. Soil storage capacities for the 15 model compartments are obtained by the distribution of the calculated soil storage capacities into 15 different ranges. They are addressed to each model compartment, using the lowest capacity for the first compartment ( $i=1$ ) and the highest for the last compartment ( $i=15$ ). With the help of the root mean square error the  $\alpha_{SE}$  -value with the best fit to the soil storage capacity distribution is detected.

The procedure of linking spatial distributed information to the semi-distributed structure of the model, is based on the results of a study done by Hartmann et al. (2014b). In this study it was successfully tested weather spatial results of a GIS-based approach in combination with the VarKarst model can provide spatiotemporal information. Consequently, the assumption was made, that input data of the GIS-based approach like soil depths can create a linkage between spatial and temporal information as well. Knowing the distribution of the soil storage capacity, a fixed value for  $\alpha_{SE}$  can be defined. By Hartmann et al. (2013a) it was shown, that one coefficient ( $\alpha_{SE}$ ) was sufficient to describe the distribution of the soil storage capacity, the epikarst storage capacity and the epikarst storage coefficient along the model compartments. Thus, the fixed value of  $\alpha_{SE}$  can additionally be applied to describe the distribution of the epikarst storage capacity and the epikarst storage coefficient.

Finally, the model is enhanced to take solute transport into account, in order to enable the VarKarst model to simulate tracer breakthrough curves. The assumption of complete and instantaneous mixing for every model compartment is set for the VarKarst model like in Mudarra et al. (2019). Therefore, the mass of tracer, which enters the epikarst or groundwater storage of a model compartment, mixes completely and instantaneous with the water and the stored tracer within the storage. Figure 3.3 is showing the schematically flow ways of the water and the injected tracer through one of the model compartments. All tracer information are marked in pink. The tracers are assumed to be conservative. Thus, any degradation processes or reactions are not considered by the model. The characteristics of the tracers reflect the ones of the water.

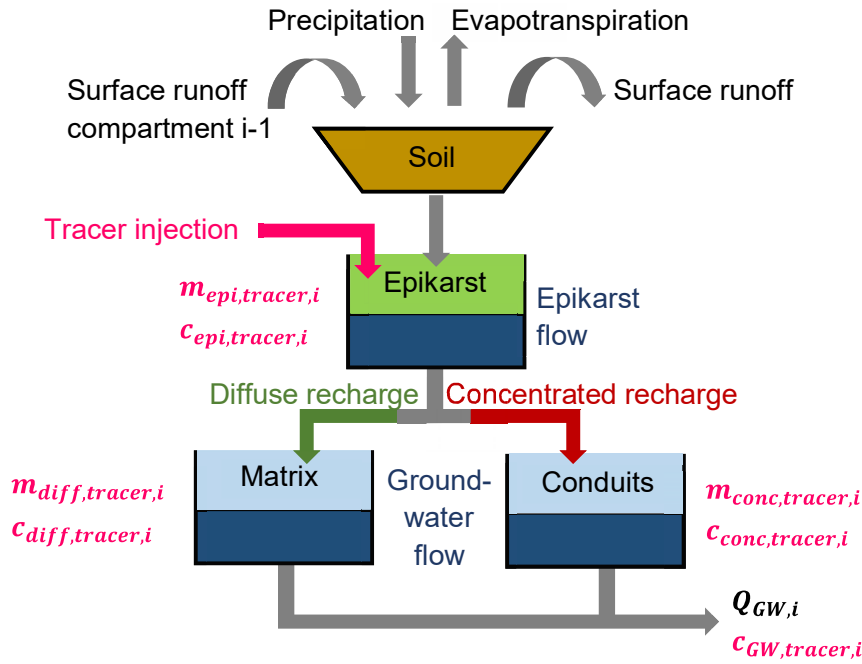


Figure 3.3: Schematically flow ways of the water and the solute through one of the model compartments. Tracer information is marked in pink.

For this study, the injection of the mass into fast flow ways was preferred. By a try and error method the mass of the tracer is set to be injected completely into model compartment  $i=15$ . Thereby, the rapid flow of the conduit system is emphasized.

$$m_{tracerIn,i} = m_{tracerIn} ; \quad i = N \quad (20)$$

$$m_{tracerIn,i} = 0 ; \quad i = 1 \dots N - 1 \quad (21)$$

$m_{tracerIn}$ : Total mass of injected tracer [mg]

$m_{tracerIn,i}$ : Mass of injected tracer for each compartment [mg]

As the tracer of all tracer tests was injected at carbonate outcrops, the soil layer can be omitted and tracers can directly be injected into the epikarst layer of the VarKarst model. As the VarKarst model is not able to simulate tracer losses the recovered mass of the tracer test is applied as injection mass to the model. The initial condition for the injection is set if the time  $t$  equals  $t_{tracerIn}$ . Then the mass of the tracer in the epikarst of model compartment  $i=15$  shows the total mass of the injected tracer.

$$m_{epi,tracer,i}(t = t_{tracerIn}) = m_{tracerIn,i} \quad (22)$$

$t_{tracerIn}$ : Time of tracer injection [d]

$m_{epi,tracer,i}$ : Mass of tracer in epikarst storage for each compartment [mg]

The mass of tracer in the epikarst storage after the injection is defined by:

$$m_{epi,tracer,i}(t) = \max[m_{epi,tracer,i}(t-1) - m_{diff,tracer,i}(t-1) - m_{conc,tracer,i}(t-1), 0]; \quad t > t_{tracerIn} \quad (23)$$

$m_{diff,tracer,i}$ : Mass of tracer in diffuse recharge [mg]

$m_{conc,tracer,i}$ : Mass of tracer in concentrated recharge [mg]

The concentration of tracer in the epikarst  $c_{epi,tracer}$  [ $mg \ mm^{-1}$ ] is calculated with help of  $Q_{epi,i}$ . If  $Q_{epi,i}$  is zero the concentration is automatically set to zero as well.

$$c_{epi,tracer,i}(t) = \frac{m_{epi,tracer,i}(t)}{Q_{epi,i}}; \quad Q_{epi,i} = 0 \rightarrow c_{epi,tracer,i} = 0 \quad (24)$$

If the sum of  $m_{epi,tracer}$  of all compartments at time step  $t$  is bigger than the injected mass,  $c_{epi,tracer,i}$  of the previous time step ( $t-1$ ) is set to zero. This occurs when very high  $Q_{epi,i}$  are simulated.

Multiplying the concentrations in the epikarst layer by  $R_{diff}$  and  $R_{conc}$  provides  $m_{diff,tracer}$  and  $m_{conc,tracer}$ .

$$m_{diff,tracer,i}(t) = c_{epi,tracer,i}(t) * R_{diff,i}(t) \quad (25)$$

$$m_{conc,tracer,i}(t) = c_{epi,tracer,i}(t) * R_{conc,i}(t) \quad (26)$$



Depending on the recharge type the concentration of tracer in the ground water  $c_{GW,tracer}$  [ $mg\ mm^{-1}$ ] can be determined as followed:

$$c_{GW,tracer,i}(t) = \frac{m_{GW,tracer,i}(t-1) + c_{epi,tracer,i}(t) * R_{diff,i}(t)}{V_{GW,i}(t) + Q_{GW,i}(t) * \Delta t}; \quad i = 1 \dots N - 1 \quad (27)$$

$$c_{GW,tracer,i}(t) = \frac{m_{GW,tracer,i}(t-1) + \sum_{i=1}^N c_{epi,tracer,i}(t) * R_{conc,i}(t)}{V_{GW,i}(t) + Q_{GW,i}(t) * \Delta t}; \quad i = N \quad (28)$$

$\Delta t$ : Modeling time step [d]

The mass of the tracer in the groundwater  $m_{GW,tracer}$  [mg] of each compartment is set by the equation:

$$m_{GW,tracer,i}(t) = c_{GW,tracer,i}(t) * V_{GW,i}(t) \quad (29)$$

The sum of  $c_{GW,tracer,i}(t)$  and  $Q_{GW,i}(t)$  over the compartments is divided by the discharge of the spring, in order to obtain the concentration of tracer at the spring  $c_{Spring,tracer}$  [ $mg\ m^{-3}$ ]. Multiplying the results with the recharge area provides the requested units.

$$c_{Spring,tracer}(t) = A * \frac{\sum_{i=1}^N c_{GW,tracer,i}(t) * Q_{GW,i}(t)}{Q_{main}(t)} \quad (30)$$

Considering the flow of the tracer through the model compartments and the mixing within them, resemble the dispersion of the tracer. Advection processes are not considered in the lumped structure of the model (Mudarra et al., 2019). Therefore, a cross correlation between the simulated and measured tracer concentrations is carried out. By shifting the simulated time series of tracer concentrations by the lag obtained by the cross correlation, advection processes are to be incorporated. The disadvantage of this approach is that the model is using observation data in order to simulate the exacted same data. Therefore, the model cannot be used for predictions. Advection processes are tried to be explained by certain patterns of the observed tracer test, e.g. linear distance between injection point and the springs or the hydrological initial conditions.

### 3.1.3. Model evaluation

A split sample test is performed to validate the productiveness of the VarKarst model. The time series is split into two parts. One of these parts is used to develop the model (calibrate), the other one is estimating the performance of the model (validation). With the 1/3 method of the split sample tests about 67% of the data is used for calibration and 33% for validation. In order to receive model validity with the split sample test, a sufficient large data is required (Steyerberg et al., 2001). Considering the warm up period of the model, the time series of discharge values from the hydrological years 1992 to 2017 is selected and split into three parts. Eight of the nine tracer test are dated in the calibration period (T1-8). Another one (T9) is addressed to the validation period and is to be predicted. This separation is illustrated in Figure 3.4. For the following chapters, it is defined, that validation can be understood as a prediction of the discharge or tracer concentrations. In this study the term simulations is used for the results of the model of the calibration and the validation period. It should not be mistaken with the term prediction.

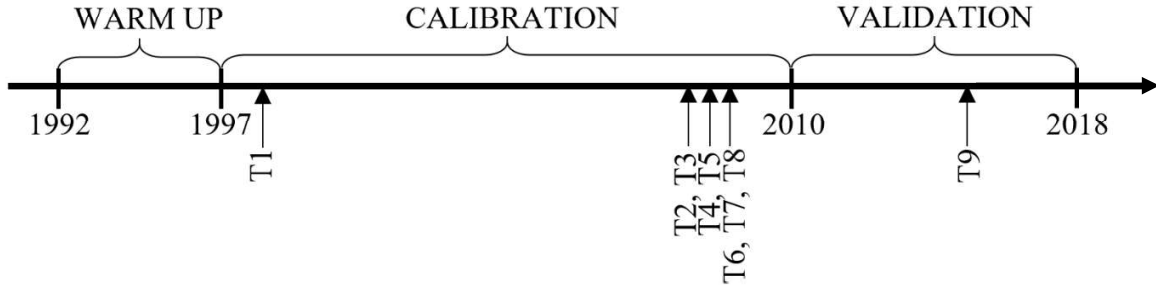


Figure 3.4: Separation of discharge and tracer test data into warm up, calibration and validation period regarding hydrological years.

Table 3.2: Overview of the VarKarst model parameters and their set ranges

Parameter	Unit	Description	Range	
			Lower	Upper
$\alpha_{SE}$	-	Soil/epikarst depth variability constant	Fixed value	
$K_{epi}$	d	Mean epikarst storage coefficient	0.1	50
$V_s$	mm	Mean soil storage capacity	Fixed value	
$V_e$	mm	Mean epikarst storage capacity	0.1	300
$\alpha_{fsep}$	-	Recharge separation variability constant	0.1	10
$\alpha_{GW}$	-	Groundwater variability constant	0.1	10
$A$	$km^2$	Catchment area	Fixed value	
$K_c$	d	Conduit storage coefficient	1	30

A sample of 12500 parameter sets is generated considering a uniform distribution of values chosen within the predefined parameter ranges (see Table 3.2). A uniform Monte-Carlo based estimation sequence is applied. By a certain number of model runs with different parameter combinations model uncertainties and parameter sensitivities can be described. The performance of the model is evaluated by the Kling-Gupta efficiency KGE (Gupta et al., 2009), which compares the simulated and observed values.

$$KGE = 1 - \sqrt{(r - 1)^2 + (\alpha - 1)^2 + (\beta - 1)^2} \quad (31)$$

$$\text{with } \alpha = \frac{\sigma_S}{\sigma_O} \text{ and } \beta = \frac{\mu_S}{\mu_O}$$

Where,  $r$  is the linear correlation coefficient between simulations and observations. The variability  $\alpha$  is described by the standard deviation  $\sigma$  of simulations and observations, while the bias  $\beta$  is described by the mean  $\mu$  of simulation and observations. KGEs can range from minus infinity up to one, with one representing the best possible fit. The KGE are calculated considering discharge and tracer tests data. Parameter sets of the calibration periods with a high KGE are selected to simulate the validation period. By Mudarra et al. (2019) a KGE bigger 0.5 was set as a threshold value to address for satisfying simulations. Different threshold values of the KGE are used in this study in order to find an appropriate way of calibrating the model.

## 4. Results

### 4.1. Developments of VarKarst model

In order to ensure the applicability of the data collected at the weather station in Postojna for the catchment of the Unica springs, a look at the water balance of the system was taken. In Figure 4.1 the compartments of the water balance are shown. The cumulative storage of the system rises from Oct 1991 till Oct 2005. Thereafter it decreases, resulting in 1000 mm of storage at the end of the time period of the simulation. Thus, it was decided that adjusting the observed data at the weather station (precipitation and temperature) were not necessary, in order to be able to describe the discharge of the system. Though, it remains questionable if the catchment can be defined as a closed system.

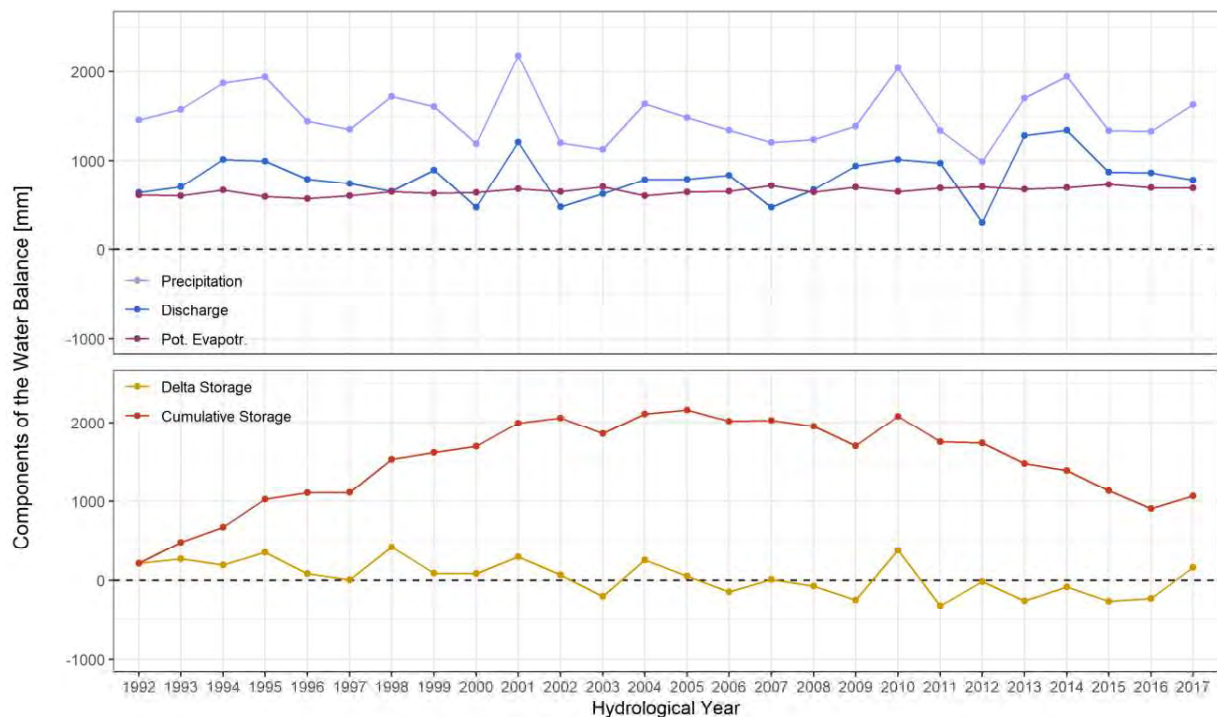
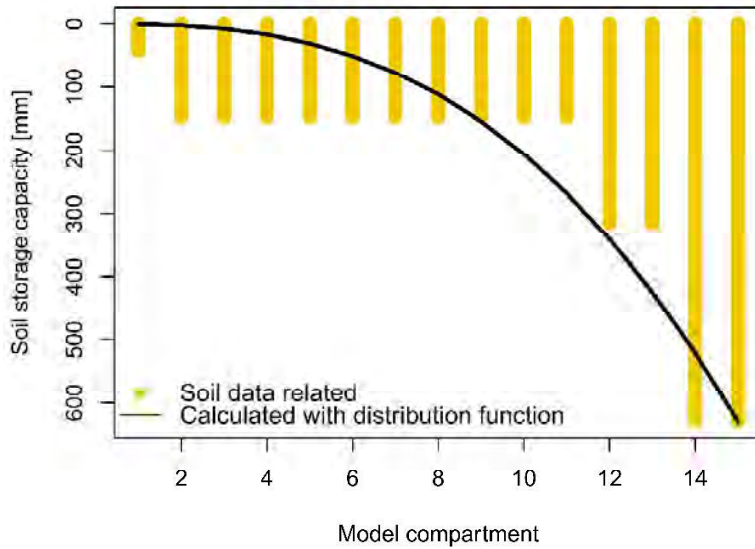


Figure 4.1: Water balance of the catchment of the Unica springs over the simulated time period

As a development of the VarKarst model its sensitivity was to be increased by setting fixed values for the parameters  $V_s$  and  $\alpha_{SE}$  by soil depths and soil textures information of the catchment. The soil depths map, presented in Figure 2.3, contains four different soil depth ranges. In Table 4.1 the percentage coverage of this depth are shown. The VarKarst model was set up with 15 compartments. Therefore, four different depth ranges were distributed over this compartments according their relative coverage. The majority of the soils of the catchment of the Unica springs contained a depth between 200 to 500 mm. Thus, ten of the model compartments were set to have a depth in between this range. For further calculations the mean of this depth ranges were used. In order to get the soil storage capacity for each model compartment, the soil depths were multiplied by the mean effective porosity (0.42). As result the soil storage capacity of each compartment were set as shown in Figure 4.2, varying between 42 and 630 mm.

Table 4.1: Percentage coverage of each soil depth of the catchment of the Unica springs

Depth range [mm]	0 – 200	200 – 500	500 – 1000	1000 – 2000
Mean depth [mm]	100	350	750	1500
Percentage [%]	4.57	70.85	11.71	14.51
Number of Model compartments	1	10	2	2

Figure 4.2: Soil storage capacity of each model compartment and its distribution function with  $\alpha_{SE}=2.756$ 

The distribution function (Equation 2) was fitted to the maximum soil storage capacities resulting in an  $\alpha_{SE}$ -value of 2.756 with a root mean square error of 93.4 mm. Thus, the VarKarst model was run with a set of 12500 different parameter sets of only five varying parameters. Transports of tracers were included considering the calculated recovered mass of tracer observations as injected masses for the simulation (see Table 2.2). In the following chapter the results of these simulations will be presented.

## 4.2. Simulation of time series

The time series of the discharge for the calibration period could be simulated with a KGE up to 0.85 (Table 4.2). In Figure 4.3 a dry hydrological year (2007) and a wet hydrological year (2001) of the simulated time series are presented. In grey the best 5% (95<sup>th</sup> percentile) of the simulations (KGE > 0.75, 625 time series) are shown. A rather good simulation could be achieved for the discharge regarding the dry hydrological year, while high discharge values of the wet hydrological year were tended to be highly over- (February 2001) or underestimated (December 2000). A high variation of simulated discharge values ranging around observed discharge values of 65 m<sup>3</sup>s<sup>-1</sup> can be detected for the wet year in the plot at the bottom right of Figure 4.3. For the dry hydrological year high variations of simulated discharge values seemed to be more likely to appear for observed discharge values of about 10-20 m<sup>3</sup>s<sup>-1</sup>. It might be caused by the fact that those discharge values were appearing especially often during this particular year. Thus, they had to be simulated more often, which led to a higher variation.

Table 4.2: KGEs of the discharge (calibration time period) and of all tracer tests. Best results are marked in green.

KGE	Q <sub>cal</sub>	T1	T2	T3	T4	T5	T6	T7	T8	T9
<b>Maximum</b>	0.85	0.75	0.87	0.81	0.89	0.89	0.76	0.83	0.94	0.94
<b>95<sup>th</sup> Percentile</b>	0.75	0.36	0.19	0.25	0.72	0.54	0.42	0.64	0.35	0.53

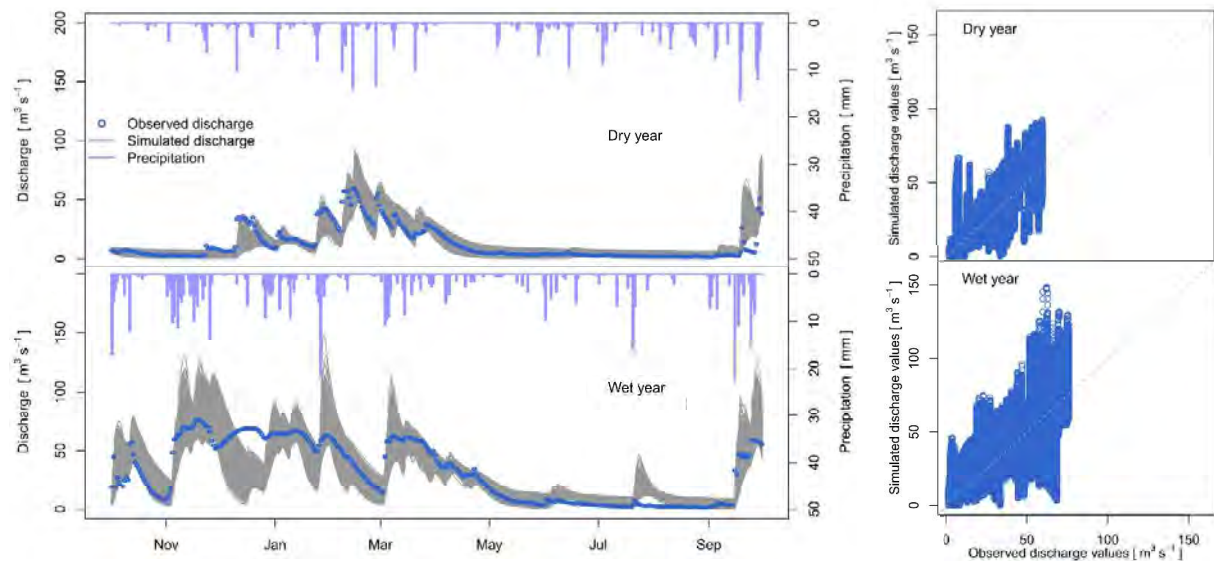


Figure 4.3: Discharge time series of a dry (2007) and wet hydrological year (2001) of the calibration period (left). Simulated discharge values of these time series plotted over their respective observed discharge values (right).

In Figure 4.4 plots of the breakthrough curves of all tracer test T1-T9 are shown. Like for the discharge, the best 5% of each simulation are displayed with gray lines. The maximum KGEs as well as the KGEs of the 95<sup>th</sup> percentiles of these tracer test simulations are listed in Table 4.2. The ability of the model to simulate accurate breakthrough curves varied depending on tracer test. As the tracer tests T4, T5, T7 and T9 not only had good maximum KGEs but also high KGE-values of the 95<sup>th</sup> percentiles, the VarKarst model could simulate their tracer breakthrough curves the best. Though, the model had problems to react appropriately to fast changes of the concentrations. One example is the maximum concentration of the tracer test T4 at the 30<sup>th</sup> of November, which was not simulated by the model at all.

Another example is that the changes of concentration of the tracer test T7 from moment of injection till the 18<sup>th</sup> of June weren't considered by the model. The weakest simulation of the breakthrough curves, regarding the KGE, was observed for tracer test T1. The peak of the concentration was highly overestimated. For the tracer tests T2 and T3, which both showed very narrow tracer breakthrough curves, the maximum concentrations could only be simulated by a small number of model runs. This results in a good maximum KGE, but a rather bad KGE of the 95<sup>th</sup> percentile. The breakthrough curve of tracer test T9 consists of two peaks. The second and smaller peak is within the ratio of the simulation, but could not be simulated as accurate as the first main peak. In general, the efficiency of which the breakthrough curves of the tracer tests were simulated cannot be said to solely depend on the injection point of the tracer, the hydrological condition or the linear distance between the injection point and the springs. The efficiency seemed to depend on how narrow or wide the shape of the breakthrough curve is and not so much on how it fluctuated.

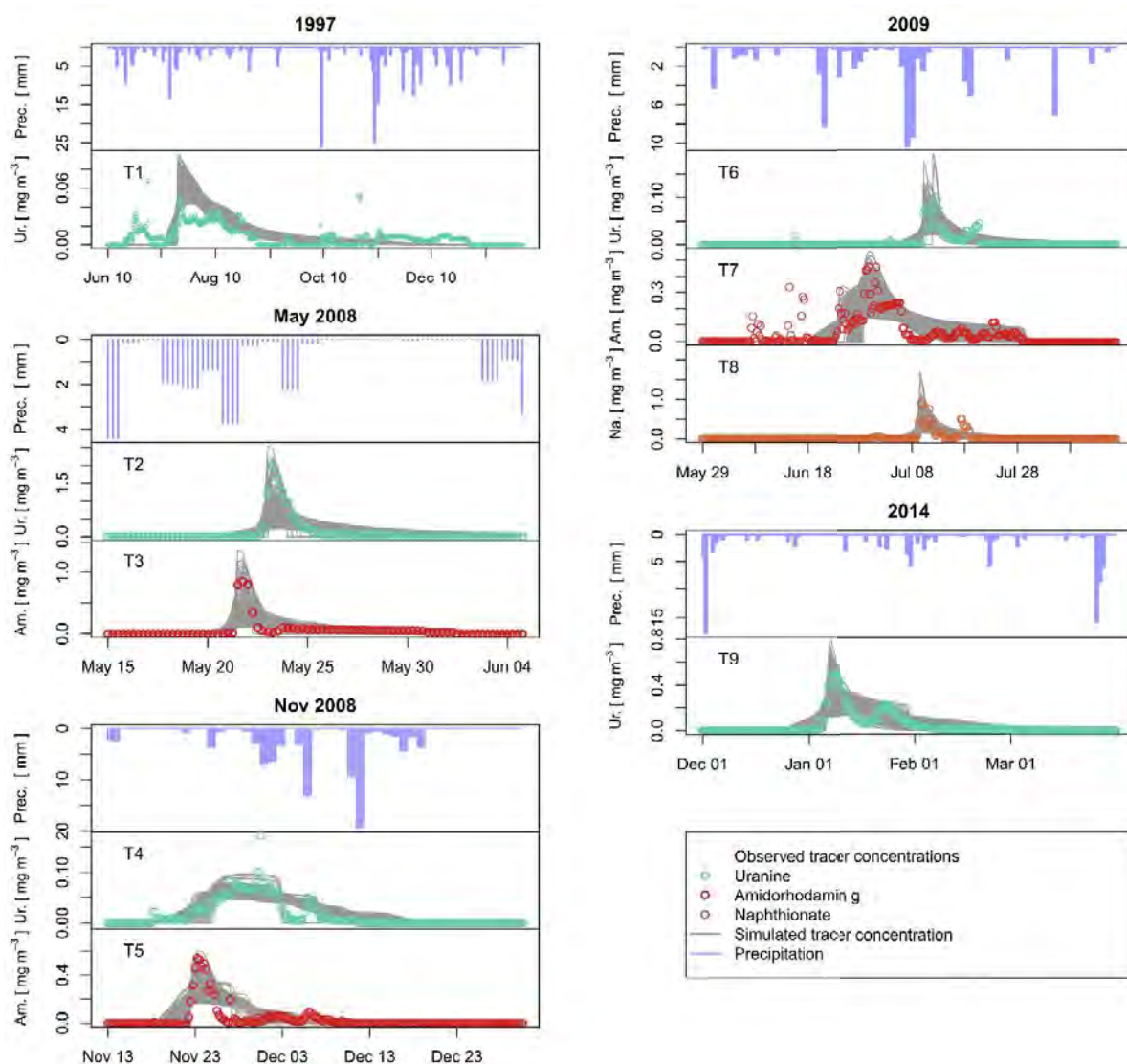


Figure 4.4: The best 5% of simulated tracer breakthrough curves of each tracer test. Note that the magnitudes of the axes differ between the plots.



In order to describe the differences of the characteristics of the tracer tests, the values of the parameters of the best simulations were compared. In Figure 4.5 boxplots of the parameters for each tracer test and the discharge simulations of the calibration and validation period are shown. On the left all parameter sets resulting in a KGE bigger the KGE-threshold of the best 5% were considered. The KGE-threshold values differed for every time series simulated. The values are written at the top left of the figure in purple color. On the right side of the figure the variation of the parameters are shown for parameter sets resulting in a KGE bigger 0.5. The number of parameter sets resulting in a KGE bigger 0.5 is listed at the top right side of the plot in purple color.

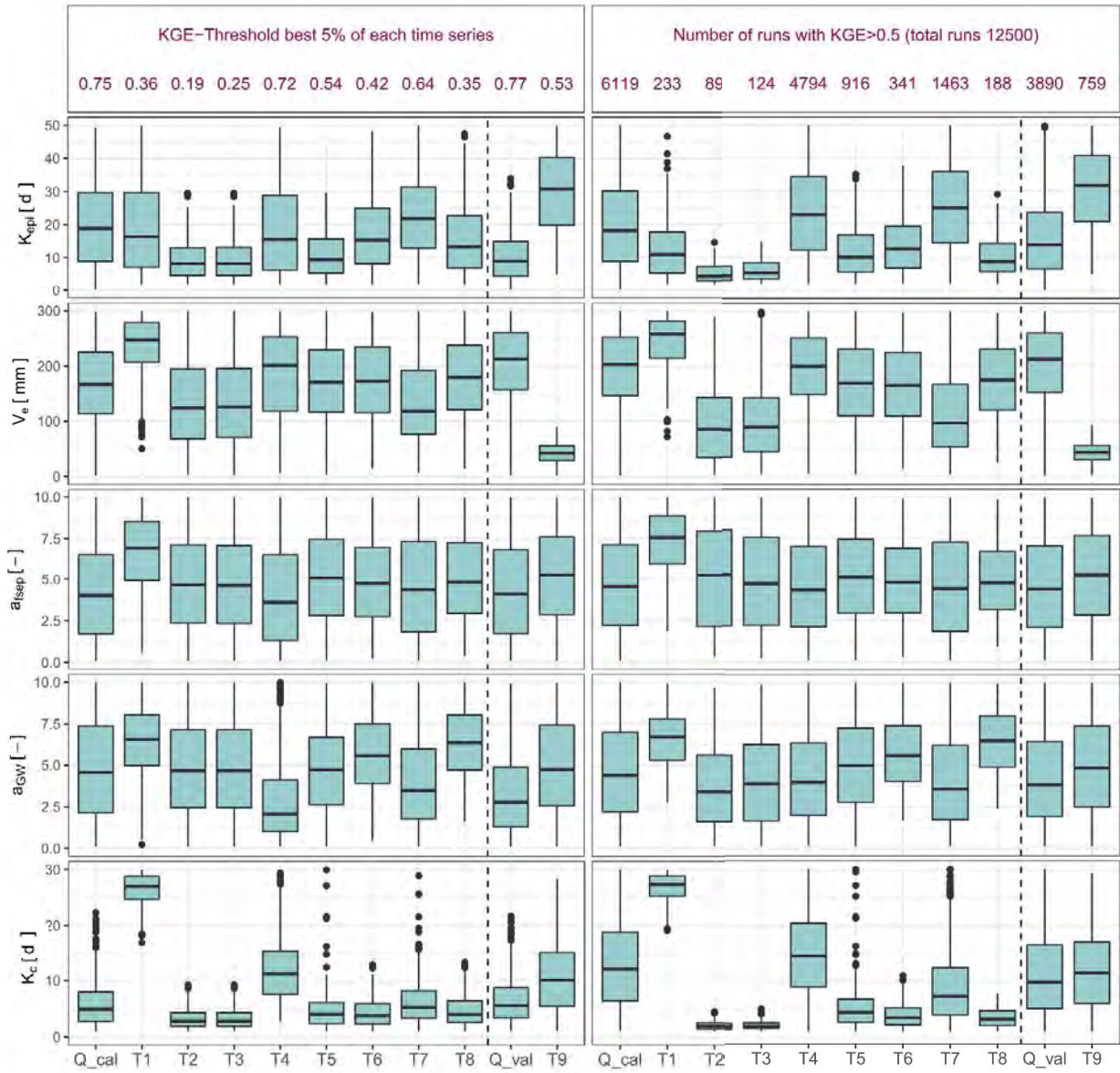


Figure 4.5: Boxplots of parameters for each simulated time series. Left: Best 5% of simulated time series. Right: Simulated time series with KGE>0.5.

A narrow boxplot results in a rather sensitive parameter. Thus,  $K_{epi}$  seemed to be rather sensitive with the best simulations resulting from  $K_{epi}$ -values in the lower region (5-30 d) of the parameter range. Only for the tracer test T9 higher  $K_{epi}$ -values ( $> 20$  d) eventuated in better simulations. Parameter  $V_e$  was providing simulations with good KGEs for rather high values of its set range. A clear exaptation was formed by the range of the tracer test T9, for which a parameter values smaller 50 mm resulted in most accurate simulations. The parameter showing the lowest variation of range regarding the best simulation throughout all simulated time series is the parameter  $\alpha_{fesp}$ . This parameter was not showing a high sensitivity overall. Parameter  $\alpha_{GW}$  was slightly more sensitive, mostly for the tracer tests T1 and T8. Parameter  $K_C$  is showing narrow boxplots and can be considered to be rather sensitive. The majority of the best simulations for all time series resulted in values smaller 10 d. An acceptance needed to be taken for tracer test T1, which showed best results for  $K_C$ -values bigger 25 d. Also tracer tests T4 showed a tendency towards slightly higher values than 10 d. In general there seemed to be a high variation of ranges of selected parameters depending on the simulated time series for the comparison of the best 5% and the  $KGE < 0.5$ . If the variation between selected parameters between the time series wasn't so big, the ranges of the boxplots were covering most of the predefined parameter ranges, which leads to the assumption that those parameters shouldn't be considered to be very sensitivity.

In the following, the tracer tests will be grouped by their initial flow conditions, injection points and shapes of the breakthrough curves, in order to find patterns of the parameter selections to achieve good simulations. The tracer tests T1, T6, T7 and T8 are characterized to be executed under initial low flow conditions. Even though the tracer tests T6, T7 and T8 were applied at the exact same low flow condition, tracer tests T7 was showing different selections of parameter values. Parameter selections of the tracer tests T6 and T8 were similar, although tracers were injected in a sinking stream (T8) and on a karren field (T6). The tracer tests T2 and T3 were applied at medium flow conditions and showed the exact same parameter ranges for their best simulations. For the tracer tests T4, T5 and T9 high flow conditions prevailed. All three tracer tests showed different parameter ranges of their best simulations. The tracer tests T3, T5, T7 and T8 all were injected into a sinking river, tracer tests T1, T2 and T9 into a doline or ponor and the tracer tests T4 and T6 in an oil collector or on a karren field. For this groupings no clear differentiations of tendencies of the parameter selections for good simulations could be made. It could not be said for which conditions the initial hydrological conditions or the injection point of the tracer test was more or less important. Categorizing the widths of the tracer breakthrough curves into narrow (T2 and T3), medium (T4, T5, T7, T9) and wide (T1) finally showed some differences between the groups. The tracer tests with a narrow breakthrough curve were simulated with a good efficiency with different parameter ranges than the other tracer tests. Especial the parameters  $K_{epi}$ ,  $V_e$  and  $K_C$  were selected to be within much smaller ranges



### 4.3. Model predictions

The goal of this thesis was to enable the prediction of tracer breakthrough curves at any time and injection point at the catchment. This goal was expected to be reached by calibrating the model not only with help of discharge but also with tracer test data. Selecting and combining the best parameter sets of the calibration period (discharge from 1997-2009 and tracer tests T1-T8), the discharge of the validation period (2010-2017) and the breakthrough curve of tracer test T9 were meant to be predicted. As mentioned before not all tracer tests could have been described as accurate and compared to each other their parameters for their best simulations did not cover the same ranges. At the right column of Figure 4.5 it is visualized that the boxplots of the discharge of the calibration period and of the breakthrough curves of the tracer tests T1-T8 do not have an area where all of them overlap. Thus, no set of parameters was able to describe all calibration time series, when a KGE of at least 0.5 has to be reached. As a result only tracer tests which had a KGE of the 95<sup>th</sup> percentile bigger 0.5 ( $\rightarrow$  more than 625 of the 12500 simulations had KGEs  $> 0.5$ ) were considered to calibrate the model. Hence, the time series of discharge and the tracer tests T4, T5 and T7 were selected for calibrating the model. Twelve parameter sets could describe these time series with KGEs  $> 0.5$ . In order to get better patterns for the following results, the threshold of the KGE was reduced from 0.5 to 0.475. With this condition 63 parameter sets remained.

#### 4.3.1. Parameter sensitivities

The distribution of the 63 chosen parameter sets along the parameter ranges is shown with help of dot plots and histograms in Figure 4.6. Regarding these dot plots the KGEs of the calibration time series were plotted over each model parameter. The histograms of the figure are showing the frequencies of the parameter values. It attracts attention that the performance of the simulations describing the breakthrough curves of the tracer tests T4 and T5 were reduced from a maximum KGE of 0.89 to a maximum KGE of about 0.6. Discharge and tracer test T7 could still reach KGEs up to about 0.8. While the minimum KGEs for the tracer tests were the set threshold value of 0.475, KGEs of the discharge only reached minimums of 0.59.

The distribution of the by the calibration chosen parameters were displayed with help of histograms and compared to the parameter values of best simulations of the time series which were to be predicted of Figure 4.5. The parameter  $K_{epi}$  was mostly selected to be between 15 and 30 d. The highest frequency for this parameter was 15 out of 63 times for values between 25 and 30 d. The boxplots of tracer test T9 in Figure 4.5 are covering a similar range. Thus, the selected values for parameter  $K_{epi}$  by the calibration suited the characteristics of tracer test T9. The highest frequency of all parameters was reached for the parameter  $V_e$ . Values between 250 and 300 mm were chosen 25 times. It slightly overestimated the parameters selected for the best simulations in Figure 4.5. The range selected by the best simulations of tracer tests T9 was varying around 50 d and is therefore contrary to the range selected by the calibration. The parameter  $\alpha_{fesp}$  was still evenly spread throughout its predefined range, like in Figure 4.5. The highest frequencies of parameter  $\alpha_{GW}$  were at the lower adage of its predefined range between one and two. In Figure 4.5 the medians of this parameter lay between three and five including the parameter chosen by discharge of the validation period and the tracer test T9. All of the 63 selected values of the parameter  $K_C$  were smaller than 11 d. The medians of the parameter sets chosen in Figure 4.5 for the discharge of the validation period and the tracer test T9 were 9 and 11 d.

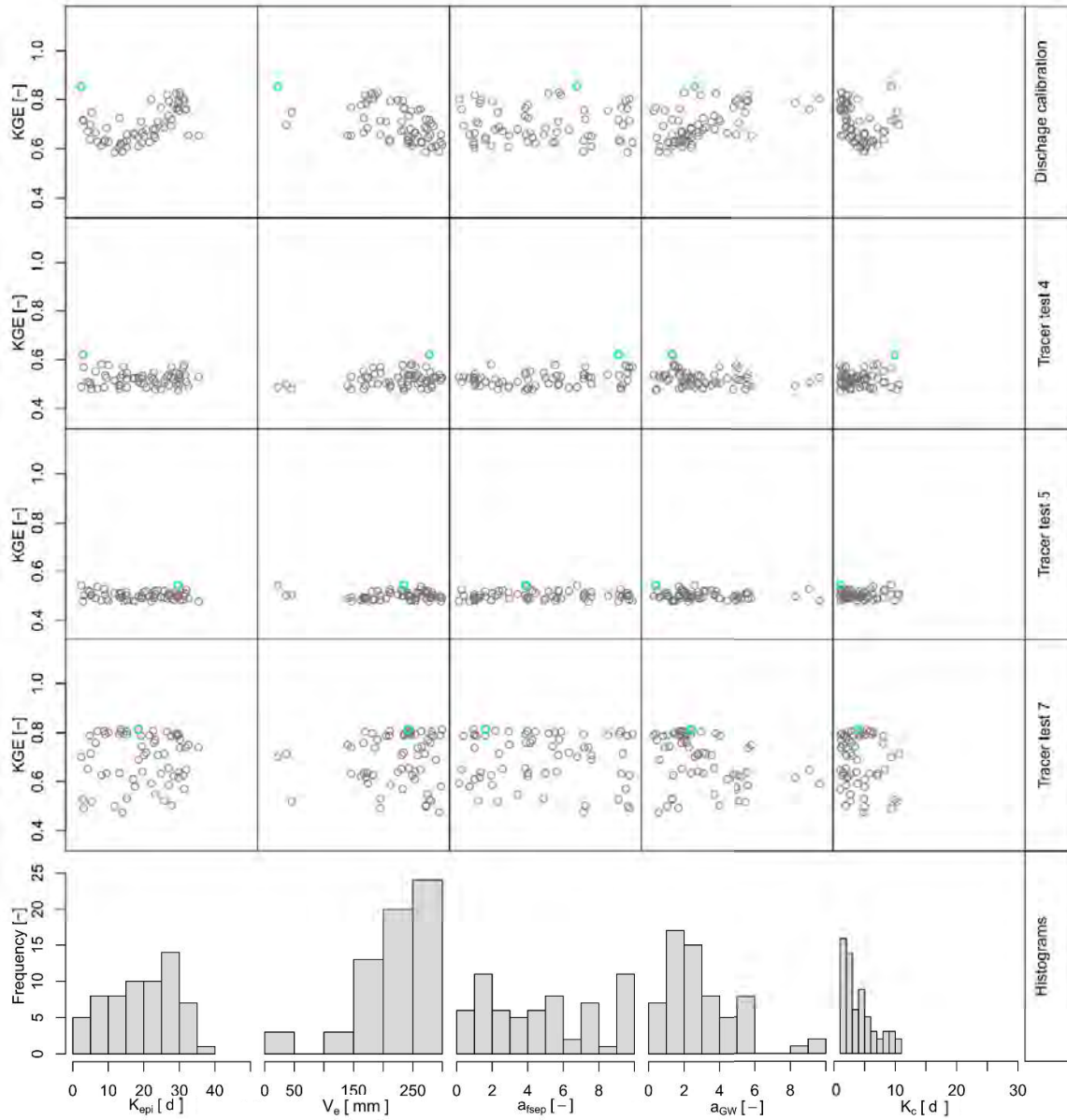


Figure 4.6: Dotty plots and histograms of 63 parameter sets selected by the calibration with discharge and tracer tests T4, T5 and T7 time series simulated with a  $KGE > 0.475$ . The maximum KGE for each time series is marked in blue.

In order to consider the improvement of parameter sensitivities by adding additional information to the calibration period, cumulative parameter distributions of two calibration methods were compared (Figure 4.7). One method is only considering discharge for the calibration, the other is additionally using tracer test data (T4, T5 and T7). Keeping in mind that the more a parameter deviates from the uniform distributions (gray dashed lines) the more it is identifiable, the parameters  $V_e$ ,  $\alpha_{fesp}$  and  $\alpha_{GW}$  had a low identifiability considering only discharge data. In case of the parameters  $V_e$ , and  $\alpha_{GW}$  this changed after applying tracer test data. Though, the parameter  $\alpha_{fesp}$  remained insensitive. The parameter  $K_{epi}$  already showed some amount of identifiability using only discharge data for the calibration. Considering discharge and tracer test data its identifiability only improved slightly. The parameter  $K_C$  showed the highest identifiability for both calibration methods.

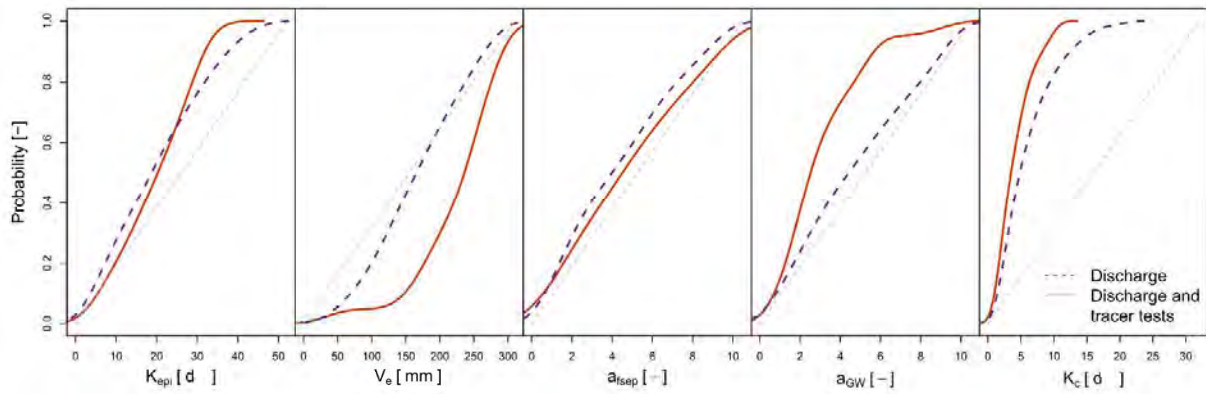


Figure 4.7: Cumulative parameter distributions. The more a parameter deviates from the uniform distributions (gray dashed lines) the more it is identifiable.

#### 4.3.2. Predicted time series

The 63 parameter sets were used to simulate the discharge of the validation time period (2010-2017) and the breakthrough curve of tracer test T9. The results are shown in Figure 4.8 and Figure 4.9. The discharge of a dry hydrological year (2012) was predicted very accurately, while the model had problems to describe the constant high discharge in March of the very wet hydrological year (2013). Thus, the same issues were noticed for the discharge simulations of the calibration period like for the discharge simulations of the validation period. Considering the simulations of the tracer concentrations at the spring, predictions did not seem to be adequately. Compared to the observed tracer concentrations all simulated tracer breakthrough curves showed too small values. The maximum observed tracer concentration was  $0.49 \text{ mg m}^{-3}$  while only values up to  $0.13 \text{ mg m}^{-3}$  were predicted. Additional, the observed breakthrough curve was showing two main peaks and only a single peak was simulated for all 63 parameter sets by the model.

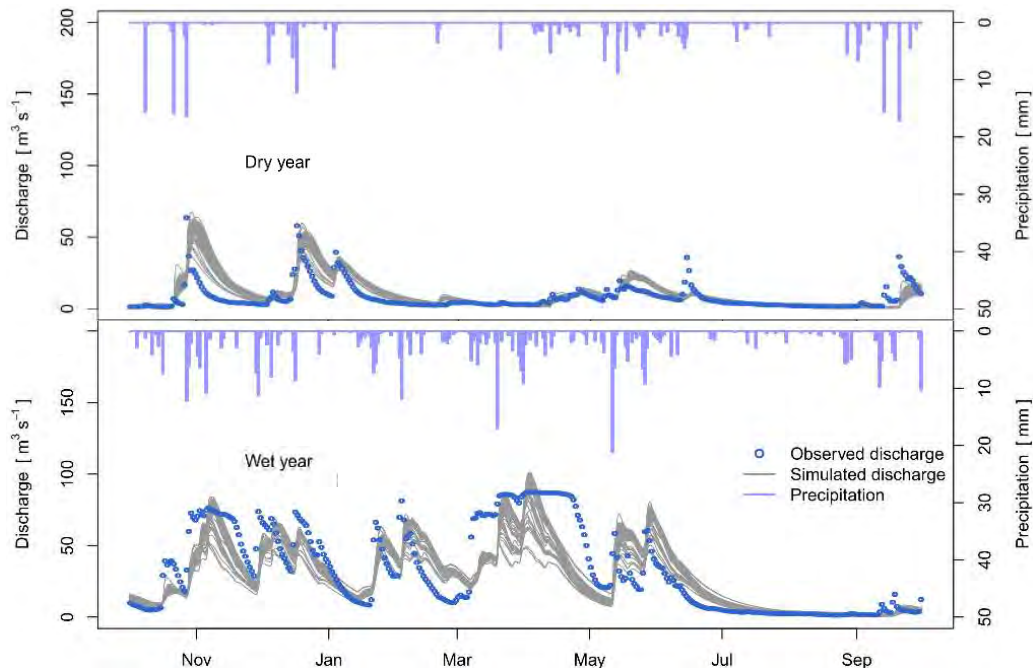


Figure 4.8: Predicted discharge time series of a dry (2012) and wet hydrological year (2013) of the validation period.

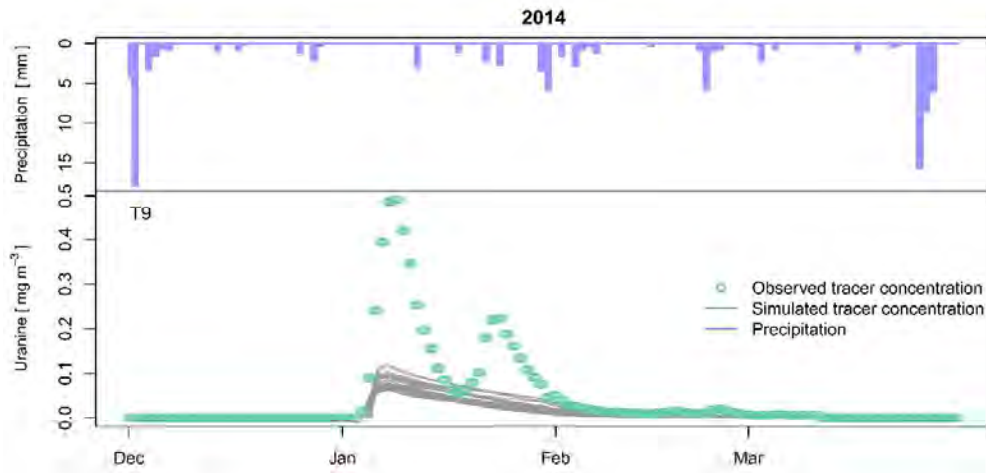


Figure 4.9: Predicted break through curve of the tracer test T9

Describing the goodness of the fit with help of the KGE, the discharge was predicted very well (Figure 4.10). Its KGEs varied between 0.43 and 0.85 and mainly accumulated at values of 0.8. Compared to those efficiencies the tracer test T9 can be set to be described rather poorly. A maximum KGE of only 0.11 was reached and 58 of the 63 simulations had negative KGEs. Thus, only 5 parameter sets were able to describe the tracer breakthrough curve with a KGE bigger than zero. The value of the minimum KGE was -0.16. A reason for the bad model prediction regarding the tracer test T9 could be the different ranges of parameters chosen for good simulation of the tracer test T9 compared to the time series used for the calibration (see Figure 4.5).

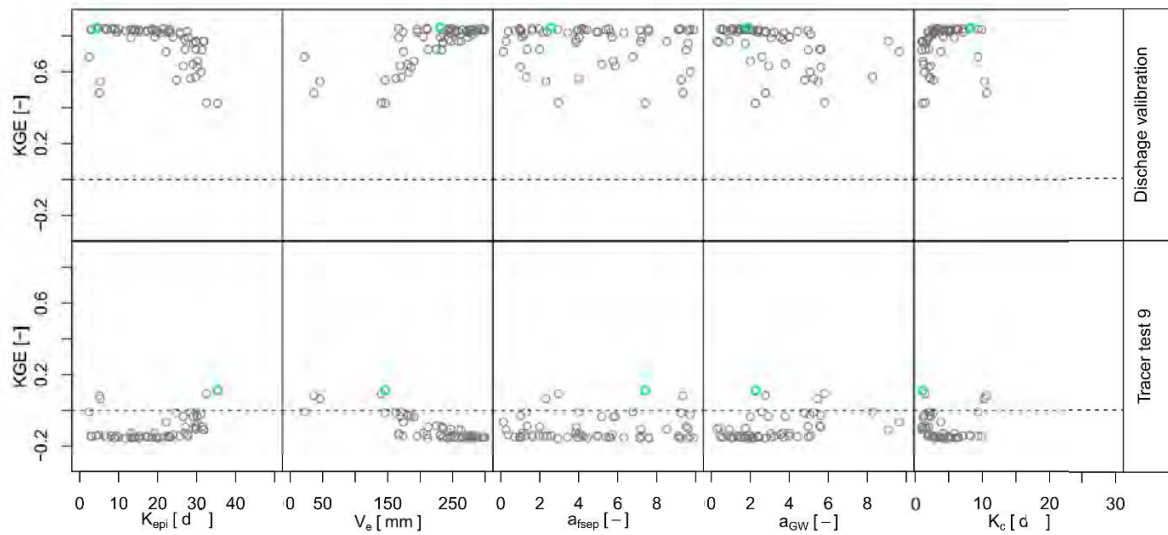


Figure 4.10: Dotty plots of the 63 parameter sets and their KGE regarding the discharge of the validation period (2010-2017) and the tracer test T9. Maximum KGE for each time series is marked in blue.

### 4.3.3. Tracer advection

As described in Chapter 3.1.2, cross correlation was carried out to address for advection processes. Simulated time series were shifted by the lag of the cross correlation. Thus, observation data was used for the cross correlation and a prediction with the model was not possible anymore. In order to enable the prediction of tracer tests, it was of interest to find a way to describe advection processes. Therefore, the lags were tried to be describe with help of the linear distances from the injection point to the springs or the mean simulated discharge 10 d before tracer injection  $Q_{\text{mean}10d}$ . In the following, linear distance from the injection point to the springs will be abbreviated with linear distance. Firstly, the lags were attributed to one of the times describing a tracer breakthrough curve ( $t_{V_{\text{max}}}$ ,  $t_{V_{\text{dom}}}$  or  $t_{V50}$ ). Secondly, velocities of the selected time were tried to be described by the linear distances and the mean discharge 10 d before tracer injection. The lags of the simulations and the times  $t_{V_{\text{max}}}$ ,  $t_{V_{\text{dom}}}$  and  $t_{V50}$  of the observations are compared in Figure 4.11.

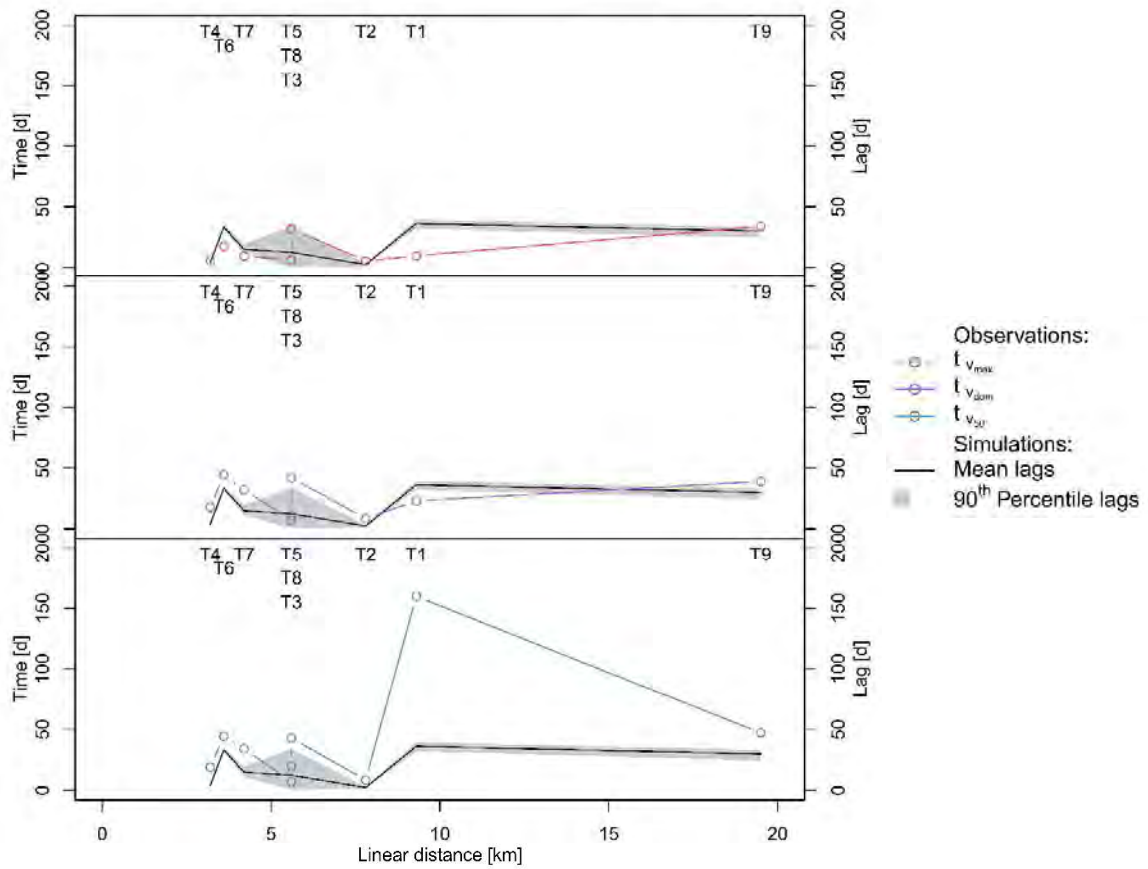


Figure 4.11: Characteristic tracer breakthrough curve times of the observed tracer breakthrough curves compared with the lags (mean and 90<sup>th</sup> percentile) of the cross correlation of the simulated tracer tests

In all three plots the mean and the 90<sup>th</sup> percentiles of the lags of the simulated tracer tests are shown. They are plotted over the linear distances. From top to the bottom the plots are showing  $t_{V_{\text{max}}}$ ,  $t_{V_{\text{dom}}}$  and  $t_{V50}$  calculated by observed tracer tests data. The lags showed a variation of zero to 40 days. The mean lags of tracer tests T1, T6, T7, T8 and T9 were between 22 and 36 days. The other tracer tests showed mean lags from one to three days. Though, a clear tendency throughout the linear distance could not been discovered. The times of  $t_{V_{\text{max}}}$ ,  $t_{V_{\text{dom}}}$  and  $t_{V50}$  have already been mentioned with different names (time till first tracer appears, maximum tracer concentration is reached and 50% of the tracer is recovered) in Chapter 2.1.



For all tracer tests  $t_{Vmax}$  was smaller than  $t_{Vdom}$ , which was smaller than  $t_{V50}$ . The patterns of the three different times over the linear distances were similar, with the exception of  $t_{V50}$  of tracer test T1. Out of the times  $t_{Vmax}$ ,  $t_{Vdom}$  and  $t_{V50}$  the lags were most likely to fit the variation of  $t_{Vdom}$  over the linear distance. Thus, the shift of the simulated time series regarding cross correlation was set to represent the time from tracer injection till the peak of the tracer breakthrough curve. Therefore, only  $t_{Vdom}$  was used for further analyses. The dominant flow velocity, considering different aquifer porosities, is plotted over linear distance and  $Q_{mean10d}$  in Figure 4.12. In the attachments the figures for all three different times and velocities can be found (Figure A.8).

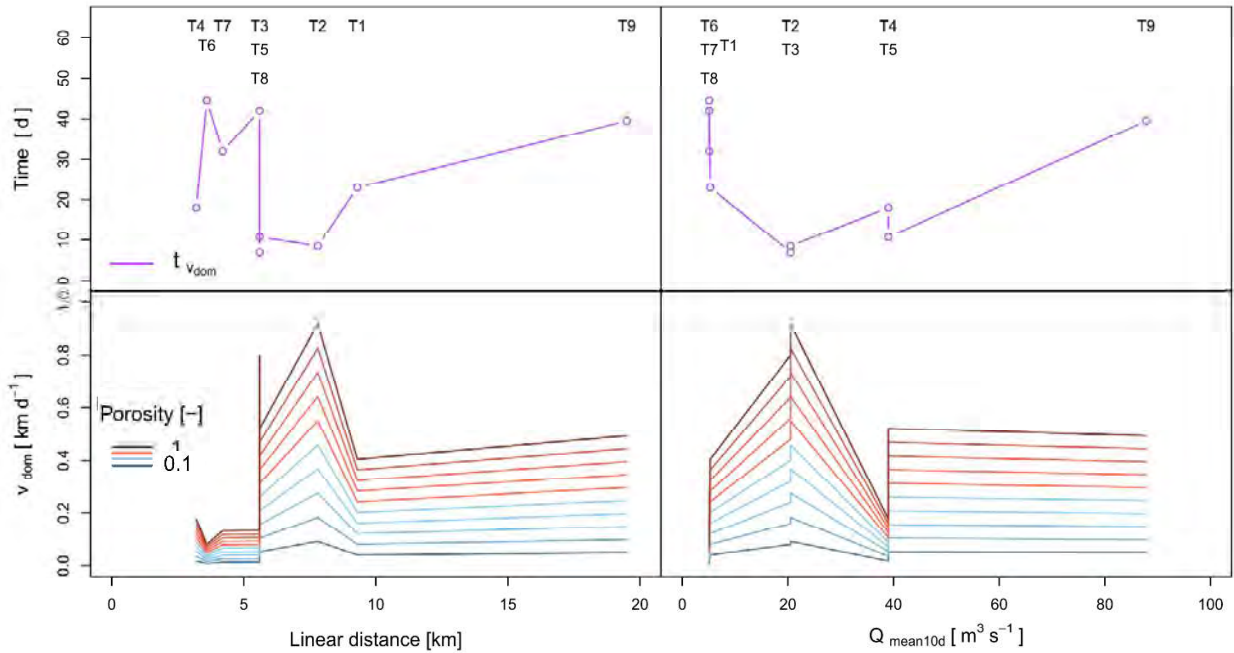


Figure 4.12: Dominant velocities (observed) of all tracer tests plotted over the linear distance and  $Q_{mean10d}$ , considering different aquifer porosities.

First the variation of the dominant velocity regarding an increase of the linear distance will be described (Figure 4.12, left column). Distances smaller 5 km (T4, T6 and T7) provided velocities smaller  $0.2 \text{ km d}^{-1}$ . The tracer tests T4 and T6 were carried out at the oil collector and a karren field. Compared to the other tracer tests those tests can be assumed to show lower aquifer porosity at their injection point. Tracer test T7 was injected into a sinking stream, which leads to a high aquifer porosity. Regarding the velocities of the tracer tests T2, T3 and T5, high values of up to  $0.9 \text{ km d}^{-1}$  were calculated. The linear distances of those tests lay between 5.6 and 7.8 km. The dominant velocity of tracer test T8, with a linear distance of 5.6 km, resulted in maximum velocities of  $0.1 \text{ km d}^{-1}$ . As the tracers of those four tracer tests were injected either into a ponor or a sinking stream, a high aquifer porosity should be assumed for all of them. At a linear distance of 9.3 km (T1) velocities were reduced to a maximum of  $0.4 \text{ km d}^{-1}$ . They slightly increased up to  $0.5 \text{ km d}^{-1}$  for a distance of 19.5 km (T9). Both tracers of the tests T1 and T9 were injected into a doline. Thus, a high aquifer porosity can be assumed. However, because of the sharp increase of the velocities from 4.2 to 5.6 km, the variation of velocities at a distance of 5.6 km and the decrease of velocities from 7.8 to 9.3 km no clear pattern was found for  $v_{dom}$  regarding the linear distance. Assuming different aquifer porosities for the injection points of the tracer tests, did not lead to any further improvements. A high variation of the velocity was observed, even for tracer tests which shared similar linear distance.

Therefore,  $v_{dom}$  was tried to be described by the hydrological condition during the tracer injection.  $V_{dom}$  is plotted over  $Q_{mean10d}$  at the right column of Figure 4.12.  $Q_{mean10d}$  of the traces tests varied from 5.1 to 87.8  $m^3s^{-1}$ . The smallest  $Q_{mean10d}$  value of 5.1  $m^3s^{-1}$  was observed before the tracer tests T6, T7 and T8 were carried out. Velocities only reached values up to 0.1  $km d^{-1}$ . Because of the smaller aquifer porosity of tracer test T6, the velocity of this test should be assumed to be even smaller. The mean discharge of 5.3  $m^3s^{-1}$  before the start of tracer test T1 was only slightly higher than the discharge for tracer tests T6, T7 and T8. A  $v_{dom}$  of 0.4  $km d^{-1}$  was reached. A mean discharge of 20.5  $m^3s^{-1}$  were addressed to the highest velocities 0.8 and 0.9  $km d^{-1}$  of all tests. Velocities of tracer tests with higher initial discharge could not reach such high values. The velocities of mean discharge of 39  $m^3s^{-1}$  (T4 and T5) were with values of 0.2 and 0.5  $km d^{-1}$  similar to those of mean discharges of 5.1 and 5.3  $m^3s^{-1}$ . The maximum velocity 0.2  $km d^{-1}$  of tracer test T4 should set to be smaller, due to the assumed aquifer porosity. This leads to a high variability of the velocity at a constant  $Q_{mean10d}$  of 39  $m^3s^{-1}$ . Not much variation of the dominant velocity occurred for higher mean discharge values. A discharge of 87.8  $m^3s^{-1}$  resulted in maximum velocities of 0.5  $km d^{-1}$  (T9). Even though, different assumed aquifer porosities were considered, there were also no proper patterns found for the dominant velocity regarding the initial hydrological conditions of the tracer tests, expressed by  $Q_{mean10d}$ .

In order to consider the by this figure overlapped information, where either the linear distance or the mean discharge of several tracer tests were the same, these information were plotted again in Figure 4.13. The tracer tests with the same hydrological conditions were plotted separately over the linear distance (Figure 4.13 columns 1-3). Hence, it might be possible to describe  $v_{dom}$  by the linear distance, if the hydrological condition is constant and is not needed to be considered. A tendency of increasing velocity values with increasing linear distances was observed for all tracer tests sharing the same hydrological condition. Though, the ratio of increase was highly differing between the hydrological conditions. For tracer tests T6 to T7, assuming the same aquifer porosity, the velocity increased 0.08  $km d^{-1}$  per kilometer, for tracer test T7 to T8 the ratio was almost sixty times smaller (0.001  $km d^{-1}$  per kilometer).

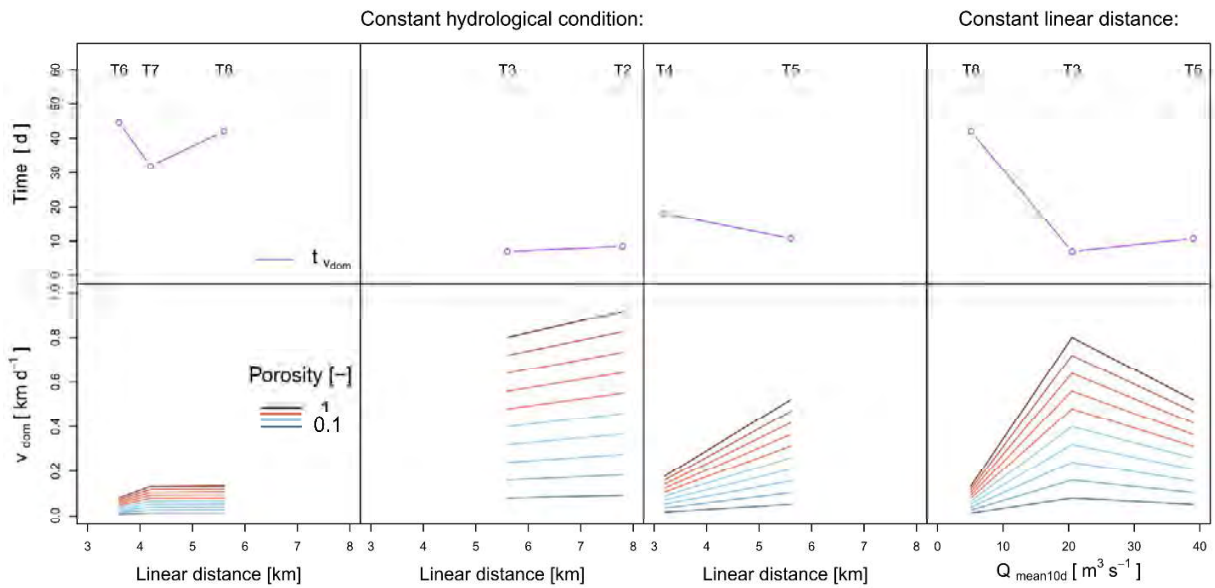


Figure 4.13: Detailed plot of dominant velocities (observed) of all tracer tests plotted over the linear distance and  $Q_{mean10d}$ . Tracer tests are divided into tests with the same hydrological conditions (columns 1-3) and tests with constant linear distances (column 4). With different aquifer porosities considered.

The increase of the velocity from tracer test T3 to T2 was  $0.05 \text{ km d}^{-1}$  per kilometer. The highest ratios was observed for tracer tests T4 and T5. The velocity increased  $0.14 \text{ km d}^{-1}$  per kilometer. If the aquifer porosity is considered, the increase of the velocity for tracer test T6 to T7 and T4 to T5 would be expected to be higher. A change of  $v_{dom}$  considering a constant linear distance and a variable hydrological initial condition of the tracer tests is shown in Figure 4.13 in the right column. As the tracer tests T3, T5 and T8 were all injected at the same point, a constant aquifer porosity can be set. The lowest velocities of  $0.1 \text{ km d}^{-1}$  occurred at the lowest mean discharge values. The velocity increased by  $0.043 \text{ km d}^{-1}$  per  $1 \text{ m}^3 \text{ s}^{-1}$ . The maximum of  $0.8 \text{ km d}^{-1}$  is reached at a discharge of  $20.5 \text{ m}^3 \text{ s}^{-1}$ . From there on the velocity decreases by  $0.015 \text{ km d}^{-1}$  per  $1 \text{ m}^3 \text{ s}^{-1}$  with increasing discharge. Thus, regarding a constant linear distance no clear patterns could be detected. The tracer tests T2 and T3 generally showed a much faster response at the springs than all the other tests, although  $Q_{\text{mean10d}}$  was rather small.

#### 4.3.4. Selection of model compartment for tracer injection

As mentioned in Chapter 3.1.2, the selection of the model compartment to inject the tracer was done by try and error. In order to get the best model results for all tracer tests, results of the model with different points of tracer injection were compared. For this propose the model was run with an iteration of 750. The compartment in which the tracer was injected varied from compartment  $i=1, 5, 10$  and  $15$ . The injected tracer mass was also spread uniformly over all compartments  $i=1-15$  and over the compartments  $i=11-15$ . The maximum and the 3<sup>rd</sup> quantile of KGEs for these scenarios are listed in Table 4.3 for each tracer test. All tracer tests showed their highest maximum KGE for an injection of the tracer in model compartment  $i=15$ , expect for tracer tests T1, T4 and T5. Though, the 3<sup>rd</sup> quantile of the tracer tests T4 and T5 had the maximum KGE for an injection of the tracer in model compartment  $i=15$  as well. Tracer test T1 was not described the best with an injection of the tracer mass in compartment  $i=15$ . However, compartment  $i=15$  was chosen for all tracer tests in order to get comparable results and to simplify the first executions of the model.

Table 4.3: KGEs of different compartments selected for tracer injection. Model was run with 750 parameter sets. Best results are marked in green.

Comp.	KGE	T1	T2	T3	T4	T5	T6	T7	T8	T9
<b>1</b>	Max.	0.197	-0.315	-0.265	0.052	-0.265	0.174	0.214	0.222	-0.129
	3rd Quan.	-0.504	-0.668	-0.663	-0.672	-0.675	-0.606	-0.628	-0.597	-0.658
<b>5</b>	Max.	0.587	-0.146	-0.083	0.432	0.129	0.239	0.648	0.197	0.587
	3rd Quan.	-0.139	-0.424	-0.435	-0.466	-0.474	-0.354	-0.326	-0.345	-0.277
<b>10</b>	Max.	0.753	0.160	0.223	0.817	0.700	0.412	0.662	0.298	0.650
	3rd Quan.	0.380	-0.305	-0.294	0.187	-0.046	0.024	0.109	-0.027	0.077
<b>15</b>	Max.	0.737	0.567	0.646	0.834	0.649	0.842	0.811	0.728	0.907
	3rd Quan.	-0.074	-0.054	-0.012	0.576	0.337	0.222	0.282	0.165	0.142
<b>1 - 15</b>	Max.	0.791	0.052	0.083	0.894	0.537	0.525	0.630	0.425	0.300
	3rd Quan.	0.526	-0.282	-0.269	0.161	-0.039	-0.008	0.021	-0.021	0.019
<b>11 - 15</b>	Max.	0.796	0.383	0.439	0.846	0.743	0.731	0.786	0.604	0.746
	3rd Quan.	0.313	-0.138	-0.109	0.520	0.198	0.157	0.237	0.103	0.131



#### 4.4. Vulnerability

The vulnerability of the catchment was to be described by the ratio of concentrated and diffuse recharge contributing to the groundwater. In Figure 4.14 these 6-hourly resolved ratios are plotted over their particular by the model simulated discharge. Again only the five best percentages of simulations were selected for each tracer tests separately. Tracer breakthrough curves and discharges were calibrated by each tracer test without taking additional information into account. Thus, also tracer tests which were performed simultaneously can describe different patterns of discharge values and ratios.

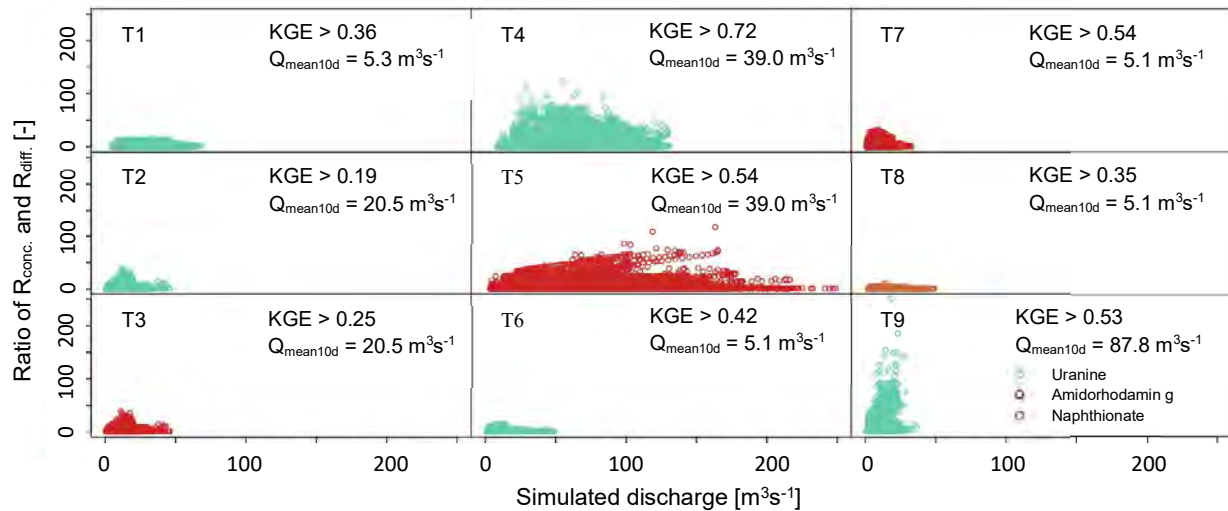


Figure 4.14: Ratios of concentrated and diffuse recharge differentiated for each tracer test. For each tracer test the KGE-threshold value and the  $Q_{mean10d}$  of the observed discharge are added.

In case of the tracer tests T2, T3, T6, T7 and T8 all discharge simulations did not exceed values of  $50 m^3s^{-1}$ . This simulations showed a higher magnitude of maximum discharge values then the observed values. The observed maximum discharges during those tests were 12.8 and  $21.6 m^3s^{-1}$  (see Table 4.4). Tracer tests T1 and T4 simulated maximum discharges lower  $150 m^3s^{-1}$ . During those tests maximum discharges of 68.6 and  $88.6 m^3s^{-1}$  were measured at the springs. Calibrating the discharges only by tracer tests overestimated the discharge values for those tracer tests as well. Observed discharges of the tracer tests T5 are the same like for tracer test T4 as they were applied simultaneously, though discharge values up to  $250 m^3s^{-1}$  were simulated for tracer test T5. Again the discharge was clearly overestimated if the model was only calibrated by the tracer test. In contrast to that, the discharge of the tracer test T9 got highly underestimated. A maximum discharge of  $87.8 m^3s^{-1}$  had been observed, while the highest values simulated could not reach  $50 m^3s^{-1}$ . Calibrating the model with the help of tracer tests like T5 and T9, discharge during the tests were described poorly, while their breakthrough curves were simulated rather well. At the same time using tracer tests like T2 and T3 for the calibration rather low KGEs of the breakthrough curves were reached, while discharge during the tests could be described in a slightly better way. A calibration with the tracer test T7 resulted in good discharge and tracer breakthrough curves simulations. Thus, several tracer tests and discharge data might contain different information of the catchment's characteristics. For the following description of the ratios it should be kept in mind, that the discharges and the tracer breakthrough curves were only calibrated by the respective tracer test in order to be able to compare the different tests.

Table 4.4: 95<sup>th</sup> percentile of the KGE of the simulations of each tracer test. Observed maximum discharge and mean discharge the ten days before the injection of the tracer of each tracer test.

	T1	T2	T3	T4	T5	T6	T7	T8	T9
<b>95<sup>th</sup> Percentile KGE</b>	0.36	0.19	0.25	0.72	0.54	0.42	0.64	0.35	0.53
<b>Q<sub>MAX</sub> (observed)</b>	68.6	21.6	21.6	88.6	88.6	12.8	12.8	12.8	89.0
<b>Q<sub>mean10d</sub> (observed)</b>	5.3	20.5	20.5	39.0	39.0	5.1	5.1	5.1	87.8

Sorting the tracer tests into their different hydrological initial conditions by the observed  $Q_{\text{mean10d}}$ , tracer tests T1, T6, T7 and T8 were set to be started under low flow conditions, tracer tests T2 and T3 under medium flow conditions and tracer tests T4, T5 and T9 under high flow conditions. Lowest ratios of concentrated and diffuse recharges were simulated for tracer tests with low flow initial conditions. For T1, T6 and T8 ratios of up to 30 were reached. Maximum ratios were only slightly higher for the tracer test T7. For this test the tracer was injected directly into the sinking stream and as the model was only calibrated by the breakthrough curve of this test, this model calibration most likely emphasizes fast conduit flows. Though, the tracer of tracer test T8 was injected into a sinking stream as well and at the exacted same hydrological conditions, still only ratios up to 20 were reached. Tracer tests T8 showed ratios comparable to those of tracer test T6. For the tracer test T6 the tracer was applied on a karren field. Thus, the injection point did not seem to have a high influence on the ratios. Higher ratios of up to 50 were reached for the tracer tests T2 and T3. Those tracer tests were carried out simultaneously. Although they were injected at different spots (ponor and sinking stream) they show exactly the same patterns. Though they have pretty narrow breakthrough curves, their simulated ratios are smaller than the ones for the high flow conditions. For the tracer tests applied during high flow ratios of up to 250 were simulated. Thus, 250 times more recharge was originated by concentrated recharge than by diffuse recharge. Even though the tracer of tracer test T4 was not injected into a sinking stream or doline high ratios were simulated. A possible reason might be that the test was carried out during high flow conditions. General, the magnitude of the ratio of concentrated and diffuse recharge could be sorted by the hydrological initial condition of the tracer test but not by the characteristics of the injection point. For none of the tracer tests a clear increase of the ratio with the discharge was identified.

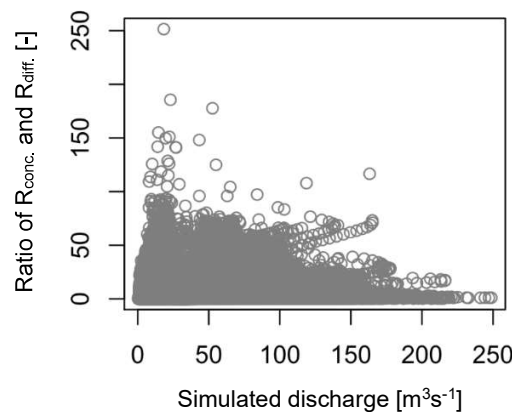


Figure 4.15: Ratios of concentrated and diffuse recharge. Combination of all tracer tests of Figure 4.14.

In Figure 4.15 all ratios simulated for each tracer tests were plotted over their simulated discharge value. This combination is rather suggesting a decrease of the ratio with increasing discharge. Though, the fact that more data points are available for lower than for higher discharge values should not be neglected, while interpreting this figure.

## 5. Discussion

### 5.1. Observation data

Before evaluating the VarKarst model the characteristics and qualities of the observation data, with which the results of the model were compared with, are going to be described. The values of the discharge time series are showing a high variation in order of magnitudes. A huge range of possible discharge values must be enabled to be measured at the gauging station. Analyzing the observed data, it seems like no values bigger  $90 \text{ m}^3\text{s}^{-1}$  could be measured. The data is often showing plateaus at a value around 85 and  $90 \text{ m}^3\text{s}^{-1}$  with no further increase of the discharge although precipitation events were recorded. These plateaus were lasting up to more than one month mainly occurring between November and May. Examples of this plateaus are shown in Figure 4.3 and Figure 4.8. These figures also pointing out that no plateaus were simulated by the model. In case of the model the discharges further increased and exceeded values of  $90 \text{ m}^3\text{s}^{-1}$ . Due to modification at the gauging station Unica Hasberg at the 05.05.2015, the level of the station was changed from 444.98 to 444.88 m.a.s.l. The discharge data was not adjusted to this modification. Though, this modification might have a smaller influence on high discharge values than the inaccuracy of the measurement. Anyway, the observed values of the gauging station of especially high discharge should be handled and interpreted with caution.

Several points need to be mentioned regarding the preprocessing of the observed data of the tracer tests. Regarding those data sets, some issues occurred for the creation of six hourly resolved time series of tracer concentrations at the springs. The concentrations of the two springs should be combined to one value, weighted by their specific discharge values. Four time series with exactly the same time steps were needed in order to create one time series of the tracer concentration. In practice the observed tracer concentrations were measured at different time steps within one tracer test at the two different springs. Some time steps were smaller than six hours and some bigger. The values for the two springs were never measured simultaneously, which complicated the calculation of a weighted mean concentration. Especially the peak of the concentration was impacted by this approach, as the measurements at the peak often were narrower than six hours. If one of the values to calculate the mean weighted tracer concentration of the two springs were missing, no mean weighted tracer concentration could be set. One example can be shown by tracer test T9. For the first week after the injection tracer concentrations but no discharge data were provided. Thus, the concentration data could not been used for that time period and the time of the first appearance of the tracer got effected. In this case the first concentration of the tracer was set much earlier by the original data set than by the temporal rescaled and combined data. By rescaling the temporal resolution of the tracer test data, the recovered mass got effected as well. In order to ensure a good model performance the recovered mass of the tracer tests was calculated with the combined concentration of the two springs and the discharge values of the gauging station after the junction of the two springs (Unica Hasberg). Thus, slightly different values were discovered for the comparison of the masses provided by literature and the masses obtained by the six hourly resolved data. For the tracer tests T1, T2, T6 and T9 the recovered mass calculated and mentioned in literature corresponded, with some small variations probably caused by the adjustments of the data sets, to those calculated by the six hourly resolved data. In the case of tracer tests T3, T4, T5 and T8 no information regarding values of recovered masses were provided by literature. Recovered masses of the tracer tests T4, T5 and T7 were set to be significant higher by the six hourly data than the injected masses. The calculated masses of the simultaneously executed tracer tests T4 and T5 were several times bigger than the injected masses (see Table 2.2). Though, no masses of recovery were found in literature, this overestimations are most likely not only caused by the adjustments of the data sets.

As mentioned in Chapter 2.1, possible explanations were given by the Karst Research Institute ZRC SAZU. First, high discharge values created high masses although only small concentration values, featuring a high uncertainty, were measured. Second, high discharges might have washed out accumulated solids from the aquifer. Due to inaccuracies of the measurement devices these solutes were considered as injected tracers. Ravbar et al. (2012) mentioned a mass of 0.4 kg being recovered with a mass of 0.5 kg being injected for tracer test T8. It is questionable if the high value of recovered mass (1.05 kg) calculated by the six hourly data is only caused by the data adjustments. It might also be caused by other features of the test mentioned for tracer tests T4 and T5. In order to further describe the influence of the temporal rescaling of the data sets, a comparison of  $v_{max}$  calculated by the six hourly resolved data with the one provided by literature will be done. For this comparison the aquifer porosities of all tracer tests were considered to be one for the calculation of  $v_{max}$  of the six hourly resolved data. It is not known if aquifer porosities were considered for the calculations of  $v_{max}$  by literature. Surprisingly, the maximum velocities calculated for tracer tests T9 were the most similar. Though, the first measured tracer concentrations could not have been considered by the six hourly resolved data of this test. Thus, the first small measured tracer concentrations might have also been neglected by Petrič et al. (2018).  $V_{max}$  of the tracer test T1 of both approaches are within the same magnitude. A huge difference of  $v_{max}$  of the two approaches occurred for tracer tests T2 and T4. In literature velocities were set to be three times higher. Especially in case of tracer test T4, where a difference of 4.3 km d<sup>-1</sup> were obtained, this should not only be addressed to the rescaling process but maybe to the differing conditions set by the studies to calculate those velocities. In conclusion, the time series of the tracer tests of this study did show some discrepancies with the data of the tests described in literature. Though, the shapes of the tracer breakthrough curves of this study seemed to be comparable to those of the literatures for all the tracer tests.

## 5.2. Model evaluation

### 5.2.1. Simulation of time series

The VarKarst model was able to simulate time series of discharge and tracer breakthrough curves of different tracer tests. In the results of this study these simulations were presented. The simulations of the discharge and the tracer tests of the calibration period showed very good visual results. The range of selected simulated discharge values of the calibration and validation period covered the observed discharge values most of the time. The shapes of the tracer tests could be described by the VarKarst model very well for the calibration period. For the prediction of the tracer breakthrough curve of the validation period the simulated concentrations seemed to be underestimated. By comparing the efficiencies of time series simulated by the VarKarst model in this study to those of other studies will provide first information about the applicability of the model to the study site and its capability to describe and predict tracer breakthrough curves. In this study a maximum KGE of 0.85 was achieved for the discharge of the calibration period. This value slightly decreased to 0.80 for the discharge of the validation period. The highest KGE of the calibration period of the discharge found in literature is 0.9 (Hartmann et al., 2013a). In the same literature the highest KGE 0.78 of the validation period of the discharge was found. The discharge of a catchment, located in Southern Spain, was simulated with help of the VarKarst model. This catchment was showing comparable hydrogeological characteristics to the catchment of the Unica springs. In the study of Hartmann et al. (2014b) the discharge of another catchment in Southern Spain was simulated with a maximum KGE of 0.89. In Hartmann et al. (2016) the discharge of catchment in Austria was simulated by the VarKarst model. This catchment is located in the “Kalkapfen” and is considered to be not as karstified as the other presented catchments. Only a maximum KGE of 0.41 was reached for the discharge of the calibration period. A maximum KGE of 0.33 was calculated for the validation period.

The KGEs of the previous studies were calculated over time periods of two to four years, while the KGEs of this study were provided by 13 (calibration) or eight years (validation). Calculating the KGE over a longer time period is giving less weight to single outliers. Nevertheless, the discharge of the catchment of the Unica springs can set to be described very well by the VarKarst model.

In the studies Hartmann et al. (2014b), Hartmann et al. (2016) and Mudarra et al. (2019) not only discharge but also solute transports were simulated by the VarKarst model. The KGEs of these simulations will be presented and compared to the KGE of the tracer test simulations of this study. Time series of Chloride (Cl), Nitrate (NO<sub>3</sub>) and Sulfate (SO<sub>4</sub>) concentrations at the discharge of the catchment were modeled in Hartmann et al. (2014b). The simulation of those hydrochemical concentrations had four main differences to the simulation of tracer concentrations. First, the solute was spread evenly throughout the model compartments. Second, the solute was injected on top of the soil layer. Third, an equilibrium concentration of the solute in the matrix had to be considered. Forth, the solute could be injected continuously throughout the time. Hydrochemical and discharge data were used to calibrate the model in order to simulate recharge rates of the catchment. Cl was simulated with a maximum KGE of 0.7 and SO<sub>4</sub> with a KGE of 0.75. NO<sub>3</sub> could only be described with a maximum KGE of 0.45 by the model. The maximum KGEs of each tracer tests of the catchment of the Unica springs for the calibration varied from 0.75 to 0.94. In comparison with the KGEs of the solute concentration of Hartmann et al. (2014b), the tracer tests of this study show very good efficiencies.

Hydrochemical concentrations of dissolved organic carbon (DOC), dissolved inorganic nitrogen (DIN) and SO<sub>4</sub> of the water at the spring were simulated by Hartmann et al. (2016). This time the time series of hydrochemical concentrations were used for the calibration and the validation of the model. The highest KGEs, with a KGE of 0.74 for the calibration and 0.62 for the validation, were reached for SO<sub>4</sub>. KGEs of 0.48 (calibration) and 0.35 (validation) were obtained for DIN. The lowest KGEs of 0.38 (calibration) and 0.35 (validation) were simulated for DOC. For all three solutes only a small decrease of the KGE was observed. The breakthrough curve of the tracer test T9 used for the validation period of the catchment of the Unica springs were simulated with a maximum KGE of 0.11. The KGE was decreased from the calibration to the validation period of about 0.8. Compared to the decrease described by Hartmann et al. (2016), this one is huge. By this information the performance of the model predicting the breakthrough curve of tracer test T9 can be considered to be rather bad.

In the study of Mudarra et al. (2019) a tracer breakthrough curve was simulated by the VarKarst model for the first and so far the only time. The information of the tracer was used for the calibration but not the validation of the model. No tracer breakthrough curves were tried to be predicted. The model was run with 250000 different parameter sets. Out of these parameters sets, sets with a KGE bigger 0.5 regarding discharge and tracer tests were selected. 35 parameter sets remained after this approach. This resulted in a mean KGE of 0.54 with a standard deviation of 0.03 for the discharge of the calibration period and a mean KGE of 0.59 with a standard deviation of 0.21 for the validation period. The mean KGE of the tracer test for the calibration period of the 35 selected parameter sets was 0.6 with a standard deviation of 0.06. A maximum KGE was not provided by the study. Considering the given data, the maximum KGE could be between 0.61 and 0.895. This covers the range of the maximum KGEs of the tracer tests simulated for the catchment of the Unica springs (see Table 4.2). The means and the standard deviations of the discharge and the tracer test from Mudarra et al. (2019) can be compared to the ones of the discharge and the tracer tests T4, T5 and T7 of the catchment of the Unica springs after selecting the 63 parameter sets with KGE>0.475. The KGE of the discharge regarding the calibration period was 0.70±0.07 and 0.76±0.11 for the validation period.

Like in the study of Mudarra et al. (2019), the mean KGE increases from calibration to validation, which indicates a better simulation in average. Though, the standard deviation is increasing as well, which describes a higher variation and inaccuracy of the model performance. Considering only the KGEs, the discharge was simulated well for the calibration and the validation period. The mean KGE and the standard deviation of the tracer tests are  $0.53 \pm 0.03$  (T4),  $0.50 \pm 0.02$  (T5) and  $0.69 \pm 0.10$  (T7). The values of these means and standard deviations are comparable in terms of magnitude with those obtained by Mudarra et al. (2019). Whereas, the mean KGE and standard deviation of the tracer test T9 with  $-0.11 \pm 0.07$  is suggestion a bad model performance regarding a prediction of this time series. Comparing the KGEs of the VarKarst model from different studies, it should be considered that they were carried out at different study sites and with different model settings. In summary, it can be captured that regarding the KGE of this study in comparison with KGEs of other studies, the discharge and the tracer breakthrough curves of the calibration period and the discharge of the validation period were simulated very well. Whereas, the tracer breakthrough curve of the validation period was predicted rather poorly.

### 5.2.2. Current limitations of tracer breakthrough curve predictions

The issues, which prevent a good prediction of the tracer breakthrough curve, will be discussed hereinafter. Firstly, it was not possible to describe the high variability of all the tracer tests within the same parameter selections, while considering a certain efficiency. The ranges of parameters chosen for a good simulation of each tracer test were not congruent throughout the tracer tests. Every tracer tests showed his own range of parameter values after selecting its best simulations. After reducing the number of tracer tests to be considered for the calibration of the model, parameter combinations were able to be provided. Therefore, the tracer tests which showed the best simulations were selected. This are the tracer tests T4, T5 and T7, they all share similar characteristics. They have a not too narrow or too wide tracer breakthrough curve and they only have one main peak. The fact that those tests can be considered to be comparable, might have been the reason why parameter combinations of those three tracer tests and the discharge were found. Nevertheless, all time series can contain different information of the catchment's characteristics. Thus, a reduction of the number of tracer tests considered for the calibration, is minimizing the variability which is actually needed, in order to cover all possible conditions at which tracer tests could be carried out.

This is leading to the second issue: The high variability of the catchment of the Unica springs was not able to be described by only a few tracer tests. The tracer tests T4, T5 and T7 couldn't cover all of the characteristics of the tracer test T9. Tracer tests T9 is not within the calibration range set by the discharge and tracer tests T4, T5 and T9. For example, tracer test T9 was showing two main peaks in the shape of the tracer breakthrough curve, while none of the three tracer tests of the calibration were featuring this characteristic. As a result, the shape of the tracer breakthrough curve of tracer tests T9 was predicted with only one instead of two peaks. Even if all tracer tests would have been able to be considered for the calibration, it is highly possible that this calibration still wouldn't be able to describe the shape of the tracer test T9 properly. One exemplary reason for this statement is that good simulations of the tracer T9 showed significant small values of the parameter  $V_e$ . This range was not covered by any other tracer test or the discharge time series. Considering to which extent the tracer tests T4, T5 and T7 and the discharge were able to describe the tracer tests T1, T2, T6 and T8, it gets obviously that tracer tests (T6 and T8) which show a high similarity to the tracer tests used for the calibration could be predicted in a better way. A simulation of a tracer test which was carried out at the top of a thick soil layer and describes slow flow ways through the system would most likely not be described well with the current calibration of the model. The tracer tests of this study all highly emphasize fast flow ways through the conduit system. Not all possible injection points through the catchment can be predicted by the model yet.

It was already mentioned that if the predictability regarding the KGE of the tracer tests and the discharge time series are compared, the discharge time series was predicted very well and the tracer tests rather bad. The main difference between the discharge and the tracer tests is the number of simulations with a KGE bigger than 0.5 and not necessarily the ranges of parameters chosen for good simulations. It has to be kept in mind that the KGE of the discharge was calculated for a time period of several years, while the KGE of the tracer tests could only be calculated for several weeks or months, as the concentrations weren't recorded any longer at the springs. An increase of the efficiency of all tracer tests might lead to an inclusion of more tracer tests for the calibration and therefore to a higher variability of possible predictions of the model. This might also lead to better efficiency of tracer test predictions. Thus, the third current issues of predicting tracer tests is that a higher amount of good efficiencies of the tracer test simulations is needed. The question is, how to increase the number of good efficiencies of the model describing tracer breakthrough curves. A simple increase of the number of model runs (number of parameter sets) might do the trick. So far no exchange between the tracers in the conduit and in the matrix systems are considered by the model. Including those exchanges might improve the model performances. For the distribution of the tracers through the layers and compartments complete and instantaneous mixing is assumed. In a real system the tracer would not be distributed immediately within one storage. Describing those mixing processes in more detail might also increase the models' efficiency. Currently, the compartment of tracers injection is set to be the compartment which emphasizes fast flow ways ( $i=15$ ). But for some tracer tests presented in this study tendencies of better simulations were found for tracers applied at a different compartment, e.g. tracer test T1. If the model would be enabled to choose the injection compartment automatically, some tracer tests might have been described in a better way by the model. One way to automate this selection might be by a spatial resolved recharge rate map like presented in Hartmann et al. (2014b). Every recharge rate is linked to a model compartment. A map showing areas addressed to different model compartments is generated. The compartment of the area the tracer test was injected can easily be defined. This approach was already tested, but led to contradictory results. Further work would will be needed.

The forth and most grave issues of predicting tracer tests is that advection processes are not described by the current version of the VarKarst model. So far, the advection was considered by a cross correlation between the observed and simulated time series of concentrations. This prevents a prediction of the tracer tests. By shifting the tracer concentrations over time, the mass balance of the tracer cannot be solved anymore. In order to avoid using observation data, it was tried to describe the advection by statistical patterns of the velocities of the executed tracer tests over the linear distance or the mean discharge ten days before the injection. As no precise values of the porosities were known, it was not possible to find any patterns. It just can be said that all shifts of the tracer curves by the cross correlation were found to be smaller than 50 d. A number of only nine tracer tests was not a high enough number to provide statistical significant results for a recharge area of 820 km<sup>2</sup> with highly variable hydrological conditions. But maybe considering additional characteristics of the recharge area to the linear discharge and the mean discharge ten days before the injection of the tracer could improve the results. A higher number of executed tracer tests would also help to enable an indication of a possible pattern. Another way might be to further extent the VarKarst model to consider advection processes by adding a delay function for the tracer tests. Therefore, an additional parameter would be appended to the model.

### 5.2.3. Model precision and accuracy

As a first step of this thesis the VarKarst model was set up with only discharge information and seven varying parameters for the catchment of the Unica springs. The model instantly showed good efficiency of discharge simulations. Also when varying the ranges of parameters most of the parameter sets always resulted in good discharge simulations. Thus, the precision and accuracy of the model had to be increased. Soil information was added to reduce the number of model parameters from seven to five and to reduce the possibilities of overparameterization and equifinality of the model and the parameter sets. Not only discharge but also tracer tests information were used to calibrate the model and to increase the sensitivity of the model parameters. Including tracer tests information to the calibration clearly increased the sensitivities of all parameters but especial those of  $V_e$  and  $\alpha_{GW}$ . Only the parameter  $\alpha_{sep}$  remained insensitive.

In the following, a comparison of the selected parameter ranges of this studies and previous studies will be done to enable a better classifications of the model results, their accuracies and the resulting catchment characteristics. The comparison is visually displayed in Figure 5.1. The figure is showing the set ranges for the model parameters (grey), the fixed parameter values (orange), the best parameter sets chosen by only discharge (blue) or discharge and solute information (pink) and the mean and standard deviation of parameter sets selected by discharge and tracer test information (black). The mean and standard deviation of 63 parameter sets of this study and 35 parameter sets of the study of Mudarra et al. (2019) were calculated.

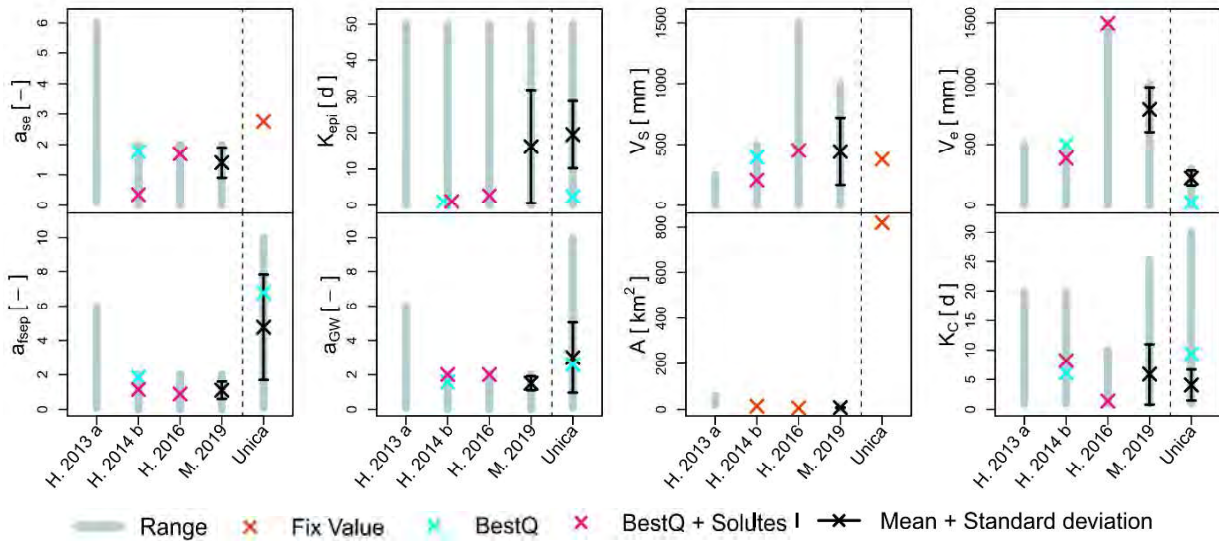


Figure 5.1: Comparison of selected parameter ranges and values of best model performances by different approaches. This study (Unica) is faced off to different studies of Hartmann et al. (H.) and Mudarra et al. (M.).

The parameter  $\alpha_{SE}$  describes the variation of  $V_{S,i}$ ,  $V_{e,i}$  and  $K_{epi,i}$ . A bigger  $\alpha_{SE}$  value leads to a steeper increase of the soil storage capacity, the epikarst storage capacity and the epikarst storage coefficient over the model compartments one to fifteen. Smaller minimum and bigger maximum values will be reached, while the mean values of those capacities and efficiencies remain constant. The ranges chosen by previous studies mostly were set between zero and two. Though, in many cases the best model performance was found to be at the upper range chosen. By this study the parameter  $\alpha_{SE}$  was set to the fixed value 2.756 by soil information of the catchment of the Unica springs. Thereby, bigger variations of  $V_{e,i}$  and  $K_{epi,i}$  values were defined than for the studies of Hartmann et al. (2014b), Hartmann et al. (2016) and Mudarra et al. (2019). In Hartmann et al. (2013a) the range was set from zero to six. Though, it was not mentioned in the study which parameter values provided the best simulations.



The mean soil storage capacity  $V_s$  for all studies was set to be smaller than 0.5 m by the performances of the VarKarst model. This goes along quite well with the fact that karst regions are known to have a thin soil layer. In dependency of the effective porosity of the soil, the amount of water being able to be stored in this layer is rather small. This has the effect that less water can evaporate and higher recharge and discharge values are reached. The calculated  $V_s$  of this study seems to have a comparable magnitude regarding the ranges and values of the parameter of previous studies. It stands out that the parameter range selected by Hartmann et al. (2016) is significantly bigger than the one from all other studies. As the catchment is showing less karstification a slightly different approach was used to describe the soil layer of this catchment.

The range of the mean epikarst storage capacity  $V_e$  was set to be at least 500 mm by literature. This parameter describes how much water can be stored in the epikarst layer. In this study the maximum of this range was chosen to be 300 mm. For every single time series of the discharge and tracer tests the mean of the parameter for the best simulations was about 150 mm. Thus, the range was thought to be set appropriately for this study site. However, when combining discharge and tracer tests information for the validation the parameter value for the best simulation was set at the upper limit of the range. The standard deviation of the parameter selected by tracer test and discharge information was rather small compared to the study of Mudarra et al. (2019). The parameter selection for the catchment of the Unica springs is very precise, but it is questionable if it is also accurate. As the best parameter range is chosen at the upper limit of the range, an adjustment of this range might lead to very different parameter selections. The upper limit of the parameter range of  $V_e$  for the study Hartmann et al. (2016) was set to be up to three times higher compared to other literatures. The best model performance was chosen to be with a mean epikarst storage capacity of 1495 mm. Thus, a huge amount of water can be stored in the epikarst layer at this study site. This has an influence on the magnitude of the epikarst layer discharge. Though, this discharge is also highly influenced by the parameter  $K_{epi}$  and it is not assigned to be originated from the matrix or the conduit system. A high value of the parameter  $V_e$  should not be considered to signify a highly karstified study site.

This is leading to the characteristics of the parameter  $K_{epi}$ . A high value of this parameter reduces the discharge of the epikarst layer and a higher amount of water will be enabled to be stored. The range set for this parameter by all studies was from 0-50 d. All best parameter values selected by discharge or discharge and hydrochemical information suggest a value smaller 3 d. The mean and standard deviation for the parameter chosen by discharge and tracer tests by the study of the catchment of the Unica springs and the study of Mudarra et al. (2019) both show a tendency towards higher  $K_{epi}$  values. Though, a higher precision was reached for the study of the catchment of the Unica springs than for the study of Mudarra et al. (2019). This might be achieved by the consideration of three tracer tests instead of only one tracer test. As the tracer tests of both studies highly represent fast flow ways through the epikarst system, the results of high  $K_{epi}$  values were surprisingly. One possible reason in case of the study of the catchment of the Unica springs might be that the upper range of the parameter  $V_e$  was set to small. In order to compensate this and to describe the storage of the epikarst layer appropriately, a high  $K_{epi}$  value might be chosen by the model.

The parameter  $\alpha_{sep}$  describes the distribution of concentrated and diffuse recharge. A higher value leads to less concentrated recharge from the model compartments  $i = 1$  to  $N-1$ . The concentrated recharge of the model compartment  $i = N$  is not influenced by this parameter. The complete discharge of the epikarst layer will be generated into concentrated recharge in case of this compartment ( $i = N$ ). Nevertheless, a higher  $\alpha_{sep}$  value describes less concentrated recharge in total. The range of this parameter chosen by this study was significant higher than the ones chosen by previous studies. The chosen values for the best model performances were significantly higher as well.

A comparison of the values of the standard deviation between this study and the study of Mudarra et al. (2019) showed low precisions for the parameter  $\alpha_{fsep}$  of this study. As mentioned earlier, this parameter seemed to be insensitive throughout all model developments and adjustments done so far. In comparison with all other studies the range of the parameter  $\alpha_{fsep}$  should maybe be adjusted. Interpreting the current results, the high  $\alpha_{fsep}$  for the catchment of the Unica springs could mean that less concentrated recharge was generated in this catchment compared to the catchments of the other studies. However, this statement doesn't suit the characteristics of the catchment of the Unica springs presented in Chapter 2. At least, a lower  $\alpha_{fsep}$  value would have been expected in comparison with the study site of Hartmann et al. (2016), which was described with a lower karstification. However, it is not known if parameter ranges would have been of more similar sizes, different patterns might showed up.

The higher the parameter  $\alpha_{GW}$  is, the smaller is the amount of diffuse recharge contributed to the discharge of the spring. The contributions of the concentrated recharge to the discharge of the spring is not influenced by this parameter. The ranges of this parameter are the same like the parameter ranges of  $\alpha_{SE}$  for all studies. Though, this time all the parameter values which led to the best simulations were placed at the upper limit of the set ranges in case of all studies of previous literature. The upper limit of the range of the catchment of the Unica springs was chosen to be much higher. Selecting the parameter by discharge and tracer test information resulted in high standard deviations and therefore in a low precision. Because of the high standard deviation the range chosen by discharge and tracer tests could be assumed to be rather accurate. The standard deviation of the study of Mudarra et al. (2019) is much smaller. But it is questionable if the selection of the parameters of both studies are comparable, because of their different ranges of the parameter  $\alpha_{GW}$ . The upper limits of the ranges of the parameter  $\alpha_{GW}$  of the previous studies could maybe be adjusted.

The ranges chosen for the parameter  $K_C$  varied from 1-10 and 1-30 d. Though, this parameter is called conduit storage coefficient, the value of this parameter will not only influencing the storage coefficient of the conduits but also the one from the matrix system. The higher  $K_C$  is, the more water of the groundwater will be contributed to the spring. In the study of Hartmann et al. (2016) a good simulation was provided by a small  $K_C$  value of 1.37 d. This indicates that more water was stored in the groundwater layer like in other studies. For all other studies including the study of the catchment of the Unica springs the  $K_C$  values were set beneath 10 d. The study of the catchment of the Unica springs and the study of Mudarra et al. (2019) have almost the same parameter ranges of  $K_C$ . The values of  $K_C$  chosen by the discharge and the three tracer tests in the study of the catchment of the Unica springs show less deviation and a higher precision as the values of the study of Mudarra et al. (2019) chosen by only one tracer tests and the discharge. It was found that a variation of this parameter highly effects the peaks of the discharge.

Finally, the recharge area of the study sites are going to be discussed. A higher recharge area results in a higher discharge value at the spring. For some of the studies carried out in the past the value of this area was set to be variable (Hartmann et al., 2013c; Hartmann et al., 2013a; Mudarra et al., 2019). For some other studies the recharge areas were set to a fixed value (Hartmann et al., 2014b; Hartmann et al., 2016). Overall the recharge areas of the presented studies varied between 5 and 60 km<sup>2</sup>. Whereas, the recharge area of the catchment of the Unica springs with approximately 820 km<sup>2</sup> is of magnitudes bigger. This significant difference might have an effect on the selection of the other parameter values, which provide good simulations.

### 5.3. Improvements of the conceptual model

In Chapter 2.2 a preliminary conceptual model of the catchment of the Unica springs was developed by information of observations. The findings of the modeling part of this thesis can now be used to further improve the understanding and quantification of the catchment side. Comparing the findings of the VarKarst model of the catchment of the Unica spring with those of previous studies, showed a low but highly variable storage capacity in the epikarst layer of the catchment of the Unica springs. This highly variable storage capacity in the epikarst layer goes a long quiet well with the characteristics assumed for a highly karstified aquifer. Surprisingly the model showed big epikarst storage efficiencies and low contributions to concentrated recharges from the epikarst to the groundwater layer. At the same time high ratios of groundwater emerged at the spring. It seems like that the values of the parameters for the best simulations at some cases were contrary and compensated each other. Though, the number of parameters was reduced the possibility of equifinality should not be neglected. Nevertheless, according to the results of the VarKarst model the importance of the conduit system might have been overestimated by the conceptual model. Changes of the parameter sets of this study and the previous studies might lead to other conclusions for the comparison of them. With the help of the VarKarst model not only the recharge behaviors of the catchment could be quantified but also the ratio of concentrated and diffuse recharge contributions. Higher ratios were simulated for tracer tests applied during high flow than low flow conditions, suggesting higher recharge contributions from concentrated flow ways for high flow conditions. This result goes along well with the preliminary conceptual model.

The VarKarst model was chosen to describe the catchment of the Unica springs because it is accounting for diffuse and concentrated flow ways and shows a semi-distributed structure. But is the model actually considering all the characteristics described by the preliminary conceptual model? Formations of vertical conduits in the unsaturated and epiphreatic zones and formations of horizontal conduits in the saturated zones were described by literature and were assumed for the catchment of the Unica springs. This orientations of the conduits are also taken into account by the VarKarst model. But the exchanges between the conduit system and matrix system were not considered by the model. Though, they have been described in the preliminary conceptual model. Additionally, a closed catchment had to be assumed for the VarKarst model. It is known that for the tracer test T1 a huge amount of the injected tracer was measured at a spring outside the set boundaries of the catchment of the Unica springs. The catchment is not providing the conditions of a closed system. However, the results of the water balance allowed an application of the VarKarst model for the catchment of the Unica springs. The setup of the model is not taking any tracer losses into account. Nevertheless, those have been known to occur during all nine tracer tests. As a next step the VarKarst model could be set up with a varying recharge area like in the studies of Hartmann et al. (2013a), Hartmann et al. (2013b) and Mudarra et al. (2019). Thereby, the VarKarst model might reproduce the characteristics of the conceptual model in an improved way.

#### 5.4. Classification as vulnerability method

The state of the art of karst vulnerability methods was presented in Chapter 1.1.2. The methods were categorized in qualitative, semi-quantitative and quantitative, intrinsic and specific and resource and source vulnerability methods. The evolved VarKarst model of this study will be classified into a vulnerability method and its advantages and disadvantage compared to other vulnerability methods will be discussed. As the VarKarst model is designed as a process-based model, it can be assigned as a quantitative vulnerability method. Although solute transports of tracers were simulated by the model, only intrinsic vulnerabilities were described. The reason for this is that the properties of the tracers were set to be highly conservative, so they would behave similar to water. The structure of the VarKarst model allows to account for resource and source vulnerabilities. The high advantage of this method compared to all other presented methods is that temporal and spatial resolved information were provided without a too high number of model parameters and too much required input data. Recharge and discharge formations could be described for varying hydrological conditions. A proper calibration was able to be executed to consider model uncertainties and to increase the reliability of the model. For almost all other karst vulnerability methods no model uncertainties were found to be described in literatures. Predicting future behaviors of the catchment of the Unica springs remained challenging within the framework of this thesis. Nevertheless, it seems most likely that a solution can be found for the issues occurred for the validation. Regarding the results of the VarKarst model, like for most of the quantitative methods, there is no categorization into vulnerabilities yet. The VULK method resulted into transit time distributions and the  $VI$  and  $C_v$  method described the ratio of spring discharge originating from the conduit system and from the matrix system and the concentrations of a standard contaminant in the spring water. In case of the VarKarst model no transit time distributions can be simulated at the current state of the research. Nevertheless, the concentrations of a possible contaminant (tracer) and the ratios of concentrated and diffuse recharge can be compared to those of Butscher and Huggenberger (2008). Before the characteristics of the study sites of Butscher and Huggenberger (2008) will be described. This study site covered an area of only one square meter showing high porosities. A time period of 461 d with maximum discharge values of  $9.3 \cdot 10^{-3} \text{ m}^3 \text{ s}^{-1}$  was simulated. Maximum concentrations of a possible contaminant at the spring reached values up to  $2000 \text{ mg m}^{-3}$ . The maximum ratio of concentrated and diffuse recharge emerging at the spring was 15. In comparison the catchment of the Unica springs is 820 times bigger and the simulated time period 10 times longer. The catchment of the Unica springs also showed high porosities. Maximum discharge values were  $10^4$  times bigger than those of the study site of Butscher and Huggenberger (2008). The maximum tracer concentration at the Unica springs was  $2 \text{ mg m}^{-3}$ . With the consideration of maximum discharge values the concentration of possible contaminations of Butscher and Huggenberger (2008) was ten times bigger than those of the catchment of the Unica springs. The ratio of concentrated and diffuse recharge of the catchment of the Unica springs were calculated for the recharge and not for the discharge. This ratio is influenced by the value of the parameter  $\alpha_{GW}$ , if the ratio for the discharge wants to be described. As all the water which is entering the VarKarst model is eventually exiting it, the mean of the ratios for the recharge and the discharge will be the same, only the ratios of single time steps are not equal. The ranges of ratios varied throughout the tracer tests but all of them showed higher values than 15. If this is because by the characteristics of the catchments or by the structure of the models cannot be said yet. An application of the VarKarst to the study site of Butscher and Huggenberger (2008) could tell whether or not the results of the models are comparable.

## 6. Conclusion and Outlook

The main goal of this thesis was to predict transit time distributions of virtual tracer tests for a karst catchment in order to be able to describe spatiotemporal resolved karst vulnerabilities for changing climate conditions. The presented developments of the semi-distributed numerical model designed for karst regions, enabled the simulation of several tracer breakthrough curves for a highly karstified catchment. Those tests were all injected at different points of the catchment and executed during different hydrological conditions. The linkage between the model and the spatial distributed soil information seemed to account for spatiotemporal variabilities of the catchment of the Unica springs. The particular influences of the injected tracer test at different points of the catchment on the spring were characterized for all hydrological conditions of the tracer tests. Shapes of tracer breakthrough curves which lasted two to three months could be described the most accurate by the model.

If overparameterization and equifinality of the model are omitted by the reduction of the number of parameters could not be clarified. It is most likely that they at least got reduced by this approach. Using not only discharge but discharge data and data of three tracer tests improved the precision of the model. The more tracer tests are added to the calibration the higher the accuracy of the VarKarst model will become. A way how to further increase the number of tracer tests used for the calibration is to be worthwhile. The problem when trying to use more than three tracer tests was that no parameter sets were found which could predict all tracer tests and the discharge with a certain minimum efficiency. This could be caused by too few parameter sets or not a high enough number of good simulations of the tracer tests or too different ranges of parameters of good simulations.

This causations might also be the reasons for the low efficiencies of the predictions of the tracer test. Another reason for the low performance of the model regarding the prediction of a tracer breakthrough curve is that the tracer test to be predicted was not within the range the model was calibrated. The calibration of the model presented in this study is not showing a sufficient amount of variability yet. Additionally, advection processes of the tracer test could not be described by any pattern regarding the linear distance between the injection point or the springs or the mean discharge ten days before the injection. So far, observation data still had to be used for the model simulations, which is preventing any predictions.

By the combination of observation data and modeling results some of the characteristics of the preliminary conceptual model were approved and some were disapproved. The highly variable characteristics of the soil and epikarst have been supported by the results of the model. Whereas, the model results suggest that the importance of the conduit system are set to be overestimated by the preliminary conceptual model. As soon as predictions of tracer breakthrough curves are enabled, additional information of the catchment can be obtained. This will further improve the understanding of the characteristics of the catchment.

Values like transit time distributions and ratios of concentrated and diffuse recharge of the recharge and the discharge can be used as vulnerability indices. If they are resolved over space and time spatiotemporal vulnerability can be described. At the present status of the study spatiotemporal karst vulnerability can only be describe with some limitations. With the enabling of tracer breakthrough curve predictions, information about the vulnerability of the catchment regarding climate changes can be provided. Thus, adequate water management could be proposed in order to sustain good water qualities for springs in karst regions.

This thesis can be presumed as first step of the evolution of the VarKarst model towards a spatiotemporal resolved and properly validated karst vulnerability method.

## List of References

- Andreo, B., Goldscheider, N., Vadillo, I., Vías, J.M., Neukum, C., Sinreich, M., Jiménez, P., Brechenmacher, J., Carrasco, F., Hötzl, H., Perles, M.J., Zwahlen, F., 2006. Karst groundwater protection: First application of a Pan-European Approach to vulnerability, hazard and risk mapping in the Sierra de Lívar (Southern Spain). *The Science of the total environment* 357 (1-3), 54–73.
- Andreo, B., Ravbar, N., Vías, J.M., 2009. Source vulnerability mapping in carbonate (karst) aquifers by extension of the COP method: application to pilot sites. *Hydrogeology Journal* 17 (3), 749–758.
- Ballabio, C., Panagos, P., Monatanarella, L., 2016. Mapping topsoil physical properties at European scale using the LUCAS database. *Geoderma* 261, 110–123.
- Beven, K., 2006. A manifesto for the equifinality thesis. *Journal of Hydrology* 320 (1-2), 18–36.
- Butscher, C., Huggenberger, P., 2007. Implications for karst hydrology from 3D geological modeling using the aquifer base gradient approach. *Journal of Hydrology* 342 (1-2), 184–198.
- Butscher, C., Huggenberger, P., 2008. Intrinsic vulnerability assessment in karst areas: A numerical modeling approach. *Water Resour. Res.* 44 (3), 161.
- Butscher, C., Huggenberger, P., 2009a. Enhanced vulnerability assessment in karst areas by combining mapping with modeling approaches. *The Science of the total environment* 407 (3), 1153–1163.
- Butscher, C., Huggenberger, P., 2009b. Modeling the temporal variability of karst groundwater vulnerability, with implications for climate change. *Environmental science & technology* 43 (6), 1665–1669.
- Chen, Z., Goldscheider, N., Auler, A., Bakalowicz, M., Broda, S., Drew, D., Hartmann, J., Jiang, G., Moosdorf, N., Richts, A., Stevanovic, Z., Veni, G., Dumont, A., Aureli, A., Clos, P., Krombholz, M., 2017. World Karst Aquifer Map (WHYMAP WOKAM). BGR, IAH, KIT, UNESCO.
- Clemens, T., Hückinghaus, D., Liedl, R., Sauter, M., 1999. Simulation of the development of karst aquifers: role of the epikarst. *International Journal of Earth Sciences* 88 (1), 157–162.
- Cooperation in Science and Technology, 1995. COST 65: Hydrogeological aspects of groundwater protection in karstic areas, Final report (COST action 65) Rep. Brussels, Luxemburg, 446 pp.
- Daly, D., Dassargues, A., Drew, D., Dunne, S., Goldscheider, N., Neale, S., Popescu, I., Zwahlen, F., 2002. Main concepts of the "European approach" to karst-groundwater-vulnerability assessment and mapping. *Hydrogeol J* 10 (2), 340–345.
- Davis, A.L.M.W.A., 2002. KARSTIC: a sensitivity method for carbonate aquifers in karst terrain. *Environmental Geology* 42 (1), 65–72.
- Doerfliger, N., 1996. Advances in karst groundwater protection strategy using artificial tracer tests analysis and multiattribute vulnerability mapping (EPIK method): thesis. N. Doerfliger.
- Filipponi, M., Jeannin, P.-Y., Tacher, L., 2009. Evidence of inception horizons in karst conduit networks. *Geomorphology* 106 (1-2), 86–99.

- Focazio, M.J., 2002. Assessing Ground-water Vulnerability to Contamination. Providing Scientifically Defensible Information for Decision Makers. U.S. Department of the Interior, U.S. Geological Survey.
- Gabrovšek, F., Kogovšek, J., Kovačič, G., Petrič, M., Ravbar, N., Turk, J., 2010. Recent results of tracer tests in the catchment of the Unica River (SW Slovenia). *Acta carsologica* 39 (1), 27–37.
- Goldscheider, N., 2002. Hydrogeology and vulnerability of karst systems - examples from the Northern Alps and the Swabian Alb [online].
- Goldscheider, N., 2005. Karst groundwater vulnerability mapping: application of a new method in the Swabian Alb, Germany. *Hydrogeology Journal* 13 (4), 555–564. <https://doi.org/10.1007/s10040-003-0291-3>.
- Goldscheider, N., Drew, D.P., 2007. *Methods in karst hydrogeology*. Taylor & Francis, London.
- Goldscheider, N., Klute, M., Sturm, S., Hötzl, H., 2000. The PI method - A GIS-based approach to mapping groundwater vulnerability with special consideration of karst aquifers. *Zeitschrift für angewandte Geologie* 46 (3), 157–166.
- Gregor Kovačič, 2010. Hydrogeological study of the Malenščica karst spring (SW Slovenia) by means of a time series analysis. *Acta carsologica* 39 (2), 201–215.
- Gupta, H.V., Kling, H., Yilmaz, K.K., Martinez, G.F., 2009. Decomposition of the mean squared error and NSE performance criteria: Implications for improving hydrological modelling. *Journal of Hydrology* 377 (1-2), 80–91.
- Hartmann, A., Barberá, J.A., Lange, J., Andreo, B., Weiler, M., 2013a. Progress in the hydrologic simulation of time variant recharge areas of karst systems – Exemplified at a karst spring in Southern Spain. *Advances in Water Resources* 54, 149–160.
- Hartmann, A., Goldscheider, N., Wagener, T., Lange, J., Weiler, M., 2014a. Karst water resources in a changing world: Review of hydrological modeling approaches. *Rev. Geophys.* 52 (3), 218–242.
- Hartmann, A., Kobler, J., Kralik, M., Dirnböck, T., Humer, F., Weiler, M., 2016. Model-aided quantification of dissolved carbon and nitrogen release after windthrow disturbance in an Austrian karst system. *Biogeosciences* 13 (1), 159–174.
- Hartmann, A., Lange, J., Weiler, M., Arbel, Y., Greenbaum, N., 2012. A new approach to model the spatial and temporal variability of recharge to karst aquifers. *Hydrol. Earth Syst. Sci.* 16 (7), 2219–2231.
- Hartmann, A., Mudarra, M., Andreo, B., Marín, A., Wagener, T., Lange, J., 2014b. Modeling spatiotemporal impacts of hydroclimatic extremes on groundwater recharge at a Mediterranean karst aquifer. *Water Resour. Res.* 50 (8), 6507–6521.
- Hartmann, A., Mudarra, M., Marín, A., Andreo, B., Wagener, T., 2015. Relating Land Surface Information and Model Parameters for a Karst System in Southern Spain, *Hydrogeological and Environmental Investigations in Karst Systems*. Springer, Berlin, Heidelberg, pp. 345–352.
- Hartmann, A., Wagener, T., Rimmer, A., Lange, J., Brielmann, H., Weiler, M., 2013b. Testing the realism of model structures to identify karst system processes using water quality and quantity signatures. *Water Resources Research* 49 (6), 3345–3358. <https://agupubs.onlinelibrary.wiley.com/doi/pdf/10.1002/wrcr.20229>.

- Hartmann, A., Weiler, M., Wagener, T., Lange, J., Kralik, M., Humer, F., Mizyed, N., Rimmer, A., Barbera, J.A., Andreo, B., Butscher, C., Huggenberger, P., 2013c. Process-based karst modelling to relate hydrodynamic and hydrochemical characteristics to system properties. *Hydrology and earth system sciences* Vol. 17, H. 8, 3305–3321. <https://edoc.unibas.ch/30800/1/hess-17-3305-2013.pdf>.
- Iván, V., Mádl-Szőnyi, J., 2017. State of the art of karst vulnerability assessment: overview, evaluation and outlook. *Environmental Earth Sciences* 76 (3), 112. <https://doi.org/10.1007/s12665-017-6422-2>.
- Jeannin, P.-Y., CORNATON, F., ZWAHLEN, F., PERROCHET, P., 2001. VULK: a tool for intrinsic vulnerability assessment and validation. *Sciences et techniques de l'environnement. Mémoire hors-série*.
- Jiménez-Madrid, A., Carrasco-Cantos, F., Martínez-Navarrete, C., 2012. Protection of groundwater intended for human consumption: a proposed methodology for defining safeguard zones. *Environmental Earth Sciences* 65 (8), 2391–2406.
- Kattaa, B., Al-Fares, W., Al Charideh, A.R., 2010. Groundwater vulnerability assessment for the Banyas Catchment of the Syrian coastal area using GIS and the RISKE method. *Journal of environmental management* 91 (5), 1103–1110.
- Kogovšek, J., Knez, M., Mihevc, A., Petrič, M., Slabe, T., Šebela, S., 1999. Military training area in Kras (Slovenia). *Environmental Geology* 38 (1), 69–76.
- Koutsis, R., Stournaras, G., 2011. Groundwater vulnerability assessment in the Loussi polje area, N Peloponnessus: the PRESK method. In: N. Lambrakis, G.K. Stournaras, K. Katsanou (Editors), *Advances in the research of aquatic environment. Voume 2*. Springer, Berlin, pp. 335–342.
- Kralik, M., Keimel, T., 2003. Time-input, an innovative groundwater-vulnerability assessment scheme: application to an alpine test site. *Environmental Geology* 44 (6), 679–686.
- Laimer, H.J., 2005. Die Erfassung der Karstgrundwasser-Vulnerabilität mit der Methode „VURAAS“. *Grundwasser* 10 (3), 167–176.
- Malik, P., Jaromir, S., 1999. REKS: an alternative method of Karst groundwater vulnerability estimation. *Hydrogeology and Land Use Management (XXIX Congress of IAH, Bratislava)*, 79–85.
- Metka Petrič, J.K., 2005. Hydrogeological characteristics of the area of intermittent karst lakes of Pivka. *Acta carsologica* 34 (3), 599–618.
- Mudarra, M., Hartmann, A., Andreo, B., 2019. Combining Experimental Methods and Modeling to Quantify the Complex Recharge Behavior of Karst Aquifers. *Water Resour. Res.* 55 (2), 1384–1404.
- Nguyet, V.T.M., Goldscheider, N., 2006. A simplified methodology for mapping groundwater vulnerability and contamination risk, and its first application in a tropical karst area, Vietnam. *Hydrogeology Journal* 14 (8), 1666–1675.
- Petrič, M., Kogovšek, J., 2005. Hydrogeological characteristics of the area of intermittent karst lakes of Pivka. *AC* 34 (3), 599–618.
- Petrič, M., Kogovšek, J., Ravbar, N., 2018. Effects of the vadose zone on groundwater flow and solute transport characteristics in mountainous karst aquifers – the case of the Javorniki–Snežnik massif (SW Slovenia). *Acta carsologica* 47 (1).



- Plagnes, V., Kavouri, K., Huneau, F., Fournier, M., Jaunat, J., Pinto-Ferreira, C., Leroy, B., Marchet, P., Dörfliker, N., 2010. PaPRIKa, the French Multicriteria Method for Mapping the Intrinsic Vulnerability of Karst Water Resource and Source – Two Examples (Pyrenees, Normandy). In: B. Andreo, F. Carrasco, J.J. Durán, J.W. LaMoreaux (Editors), *Advances in Research in Karst Media*. Springer, Heidelberg, pp. 323–328.
- Prelovšek, M., 2014. The Hydrogeological Setting of Križna jama. *Verlag der Österreichischen Akademie der Wissenschaft* 21, 27–33.
- Ravbar, N., 2013. Variability of groundwater flow and transport processes in karst under different hydrologic conditions. *AC* 42 (2-3).
- Ravbar, N., Barberá, J.A., Petrič, M., Kogovšek, J., Andreo, B., 2012. The study of hydrodynamic behaviour of a complex karst system under low-flow conditions using natural and artificial tracers (the catchment of the Unica River, SW Slovenia). *Environmental Earth Sciences* 65 (8), 2259–2272.
- Ravbar, N., Goldscheider, N., 2007. Proposed Methodology of Vulnerability and Contamination Risk Mapping for the Protection of Karst Aquifers in Slovenia. *AC* 36 (3), 397–422.
- Rawls, W.J., Brakensiek, D.L., Miller, N., 1983. Green-ampt Infiltration Parameters from Soils Data. *Journal of Hydraulic Engineering* 109 (1), 62–70.
- Schoups, G., van de Giesen, N.C., Savenije, H.H.G., 2008. Model complexity control for hydrologic prediction. *Water Resour. Res.* 44 (12), 203.
- Schoups, G., Vrugt, J.A., Fenicia, F., van de Giesen, N.C., 2010. Corruption of accuracy and efficiency of Markov chain Monte Carlo simulation by inaccurate numerical implementation of conceptual hydrologic models. *Water Resour. Res.* 46 (10), 83.
- Sinreich, M., Cornaton, F., Zwahlen, F., 2014. Evaluation of reactive transport parameters to assess specific vulnerability in karst systems. *Groundwater Vulnerability Assessment and Mapping: IAH-Selected Papers* 11 (Chapter 2), 21–32.
- Stevanović, Z., 2019. Karst waters in potable water supply: a global scale overview. *Environmental Earth Sciences* 78 (23), 771.
- Steyerberg, E.W., Harrell, F.E., Borsboom, G.J.J.M., Eijkemans, M.J.C., Vergouwe, Y., Habbema, J.D.F., 2001. Internal validation of predictive models. *Journal of Clinical Epidemiology* 54 (8), 774–781.
- Thorntwaite, C.W., 1948. An Approach toward a Rational Classification of Climate. *Geographical Review* 38 (1), 55.
- Vías, J.M., Andreo, B., Perles, M.J., Carrasco, F., Vadillo, I., Jiménez, P., 2006. Proposed method for groundwater vulnerability mapping in carbonate (karstic) aquifers: the COP method. *Hydrogeology Journal* 14 (6), 912–925.
- Vrba, J., Zaporozec, A., 1994. *Guidebook on mapping groundwater vulnerability*. H. Heise, Hannover.
- Whittaker, G., Confesor, R., [No last name!], JR., Di Luzio, M., Arnold, J.G., 2010. Detection of Overparameterization and Overfitting in an Automatic Calibration of SWAT. *Transactions of the ASABE* 53 (5), 1487–1499.

- 
- Williams, P., 2008. The role of the epikarst in karst and cave hydrogeology: a review. *IJS* 37 (1), 1–10.
- Williams, P.W., 1983. The role of the subcutaneous zone in karst hydrology. *Journal of Hydrology* 61 (1-3), 45–67.
- Zupan Hajna, N., 2019. Dinaric karst—Geography and geology. In: W.B. White, D.C. Culver, T. Pipan (Editors), *Encyclopedia of caves*. Academic Press, London, pp. 353–362.

## Appendix

### A. Figures

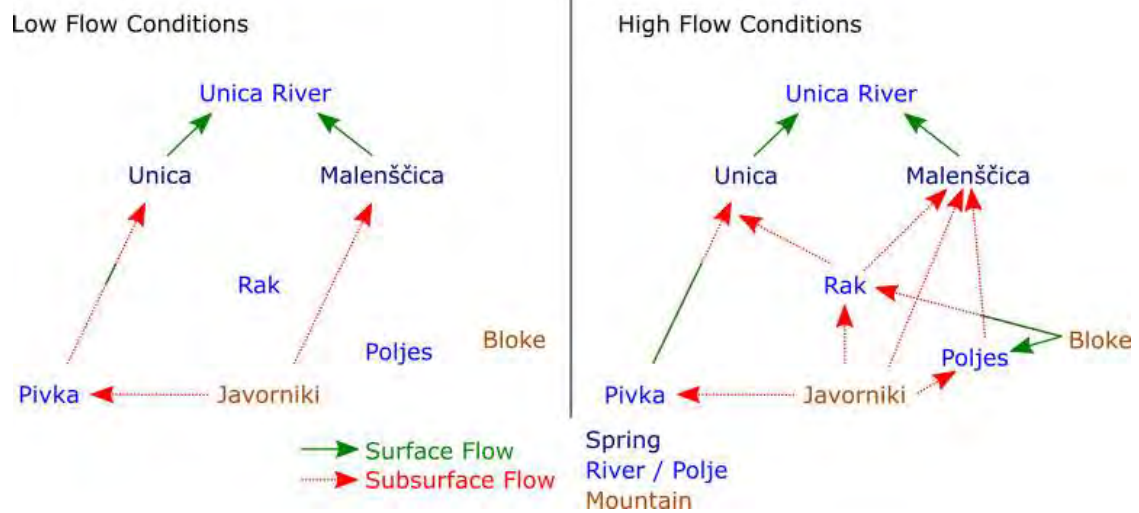


Figure A.1: Sketch of flow directions at low and high flow conditions



Figure A.2: Pictures of the injection point of tracer test T4 (Oil collector) (photo taken by Nataša Ravbar)

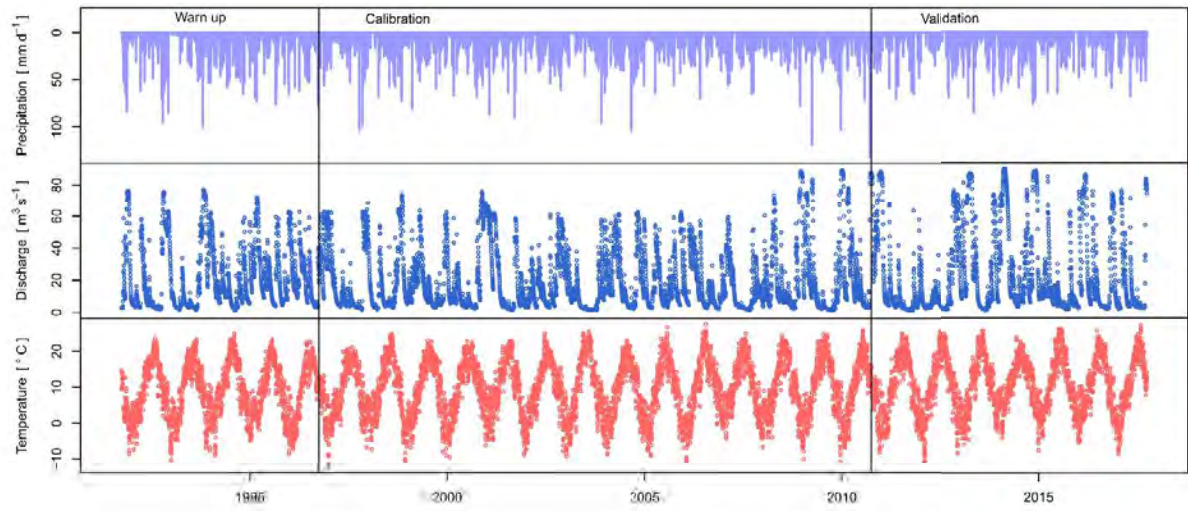


Figure A.3: Input data of the VarKarst model subdivided into warm up, calibration and validation periods.

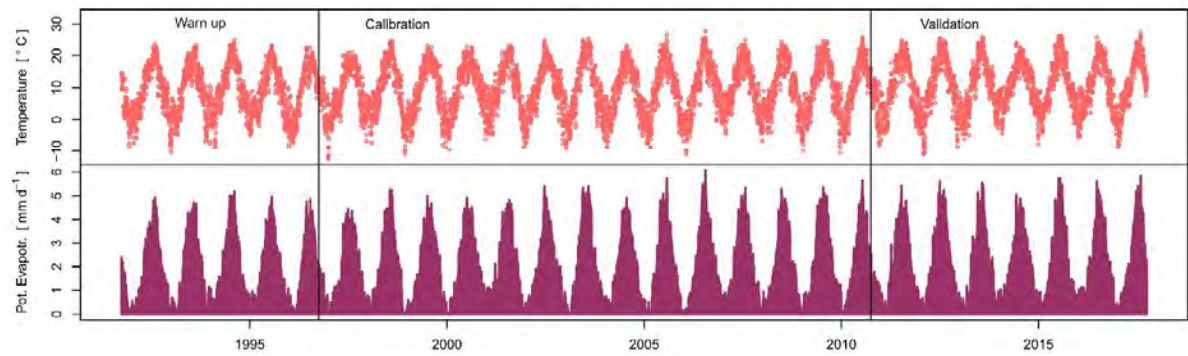


Figure A.4: Calculated potential evapotranspiration for the warm up, calibration and validation periods.

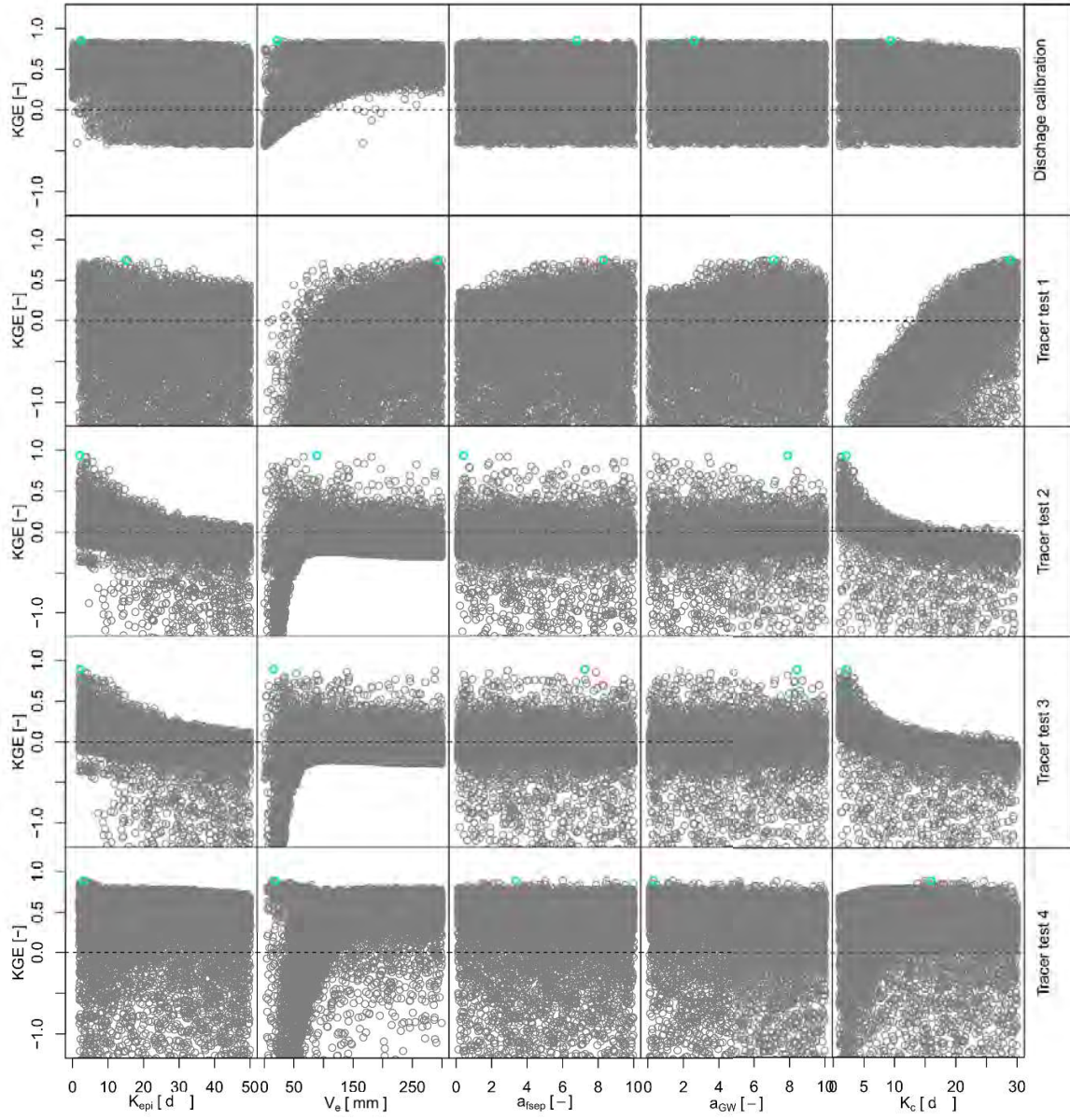


Figure A.5: Dot plots of all simulations. Maximum KGE colored in blue (Part 1)



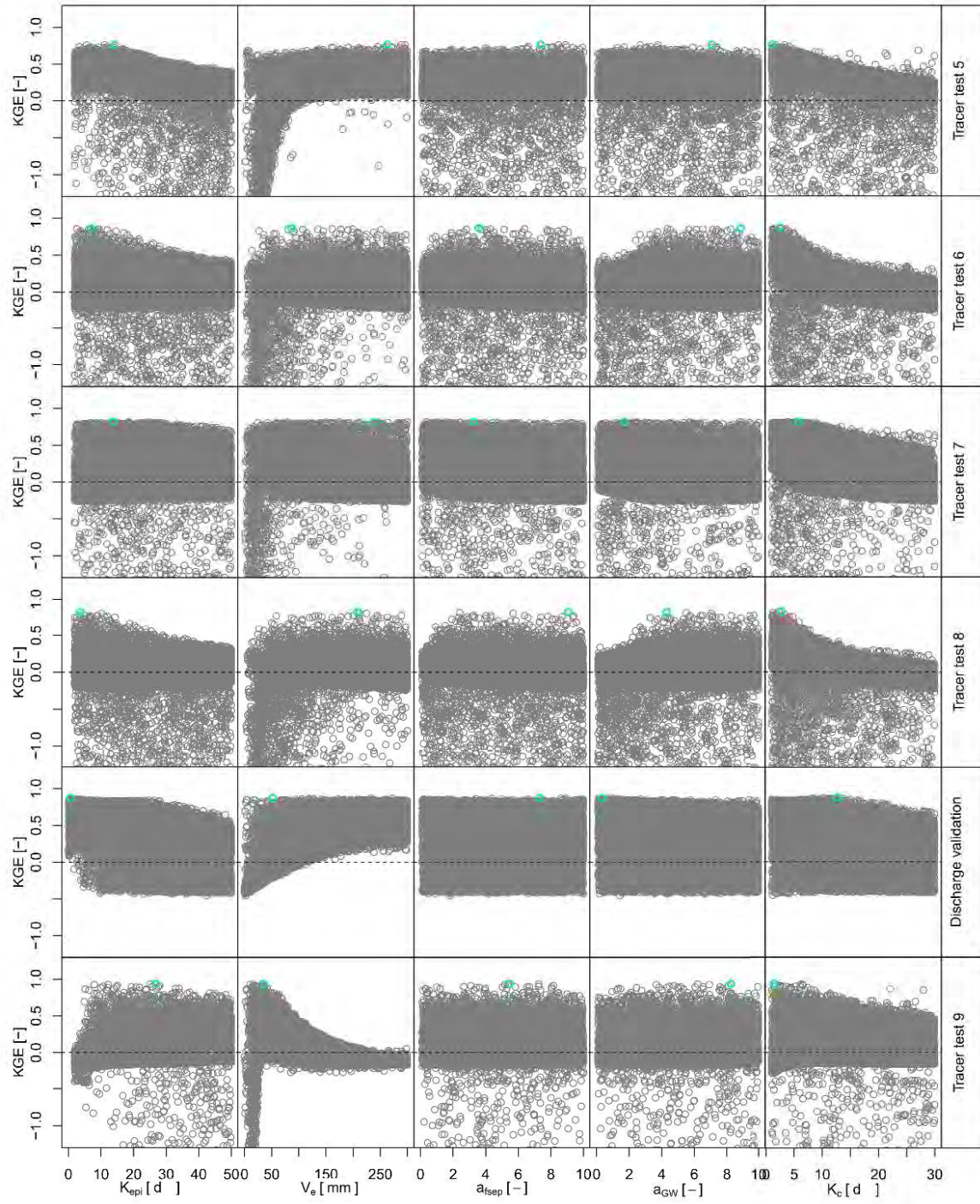


Figure A.6: Dot plots of all simulations. Maximum KGE colored in blue (Part 2)

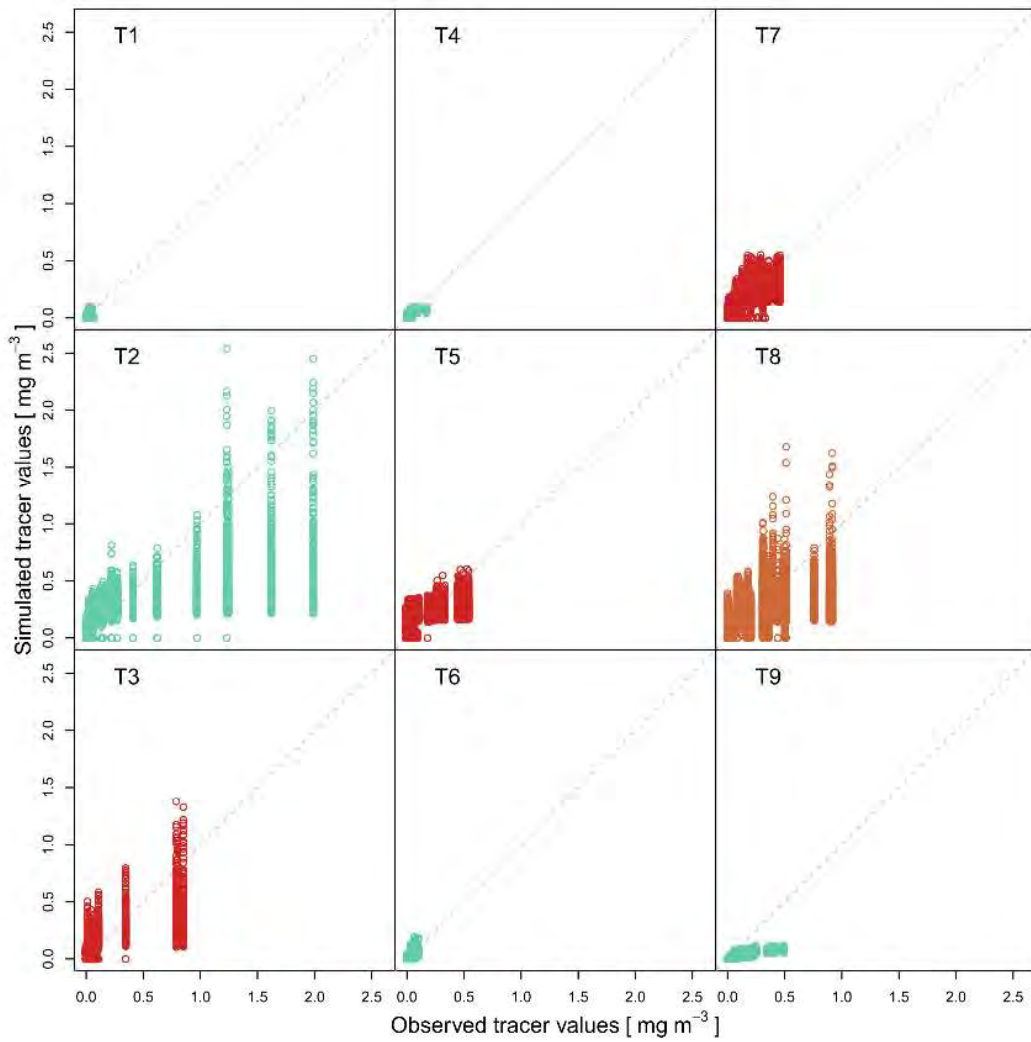


Figure A.7: Comparison of simulated and observed tracer concentrations

Table A.1: Comparison between different numbers of varying parameters

	KGE	$Q_{cal}$	$Q_{val}$	T1	T2	T3	T4	T5	T6	T7	T8	T9
<b>5 varying parameters</b>	Max.	0.82	0.85	0.74	0.57	0.65	0.83	0.65	0.84	0.81	0.73	0.91
	3rd Quan.	0.64	0.54	-0.07	-0.05	-0.01	0.58	0.34	0.22	0.28	0.17	0.14
<b>7 varying parameters</b>	Max.	0.73	0.79	0.78	0.44	0.47	0.86	0.74	0.85	0.79	0.82	0.90
	3rd Quan.	0.49	0.54	0.49	-0.06	-0.01	0.60	0.30	0.28	0.22	0.26	0.15

Table A.2: Comparison of different numbers of parameter sets

Sets	KGE	$Q_{cal}$	$Q_{val}$	T1	T2	T3	T4	T5	T6	T7	T8	T9
<b>750</b>	Max.	0.82	0.85	0.74	0.57	0.65	0.83	0.65	0.84	0.81	0.73	0.91
	3rd Quan.	0.64	0.54	-0.07	-0.05	-0.01	0.58	0.34	0.22	0.28	0.17	0.14
<b>12500</b>	max	0.85	0.87	0.75	0.87	0.81	0.89	0.89	0.76	0.83	0.94	0.94
	3rd Quan.	0.64	0.55	-0.06	0.21	0.28	0.00	0.58	0.34	0.16	0.13	-0.05

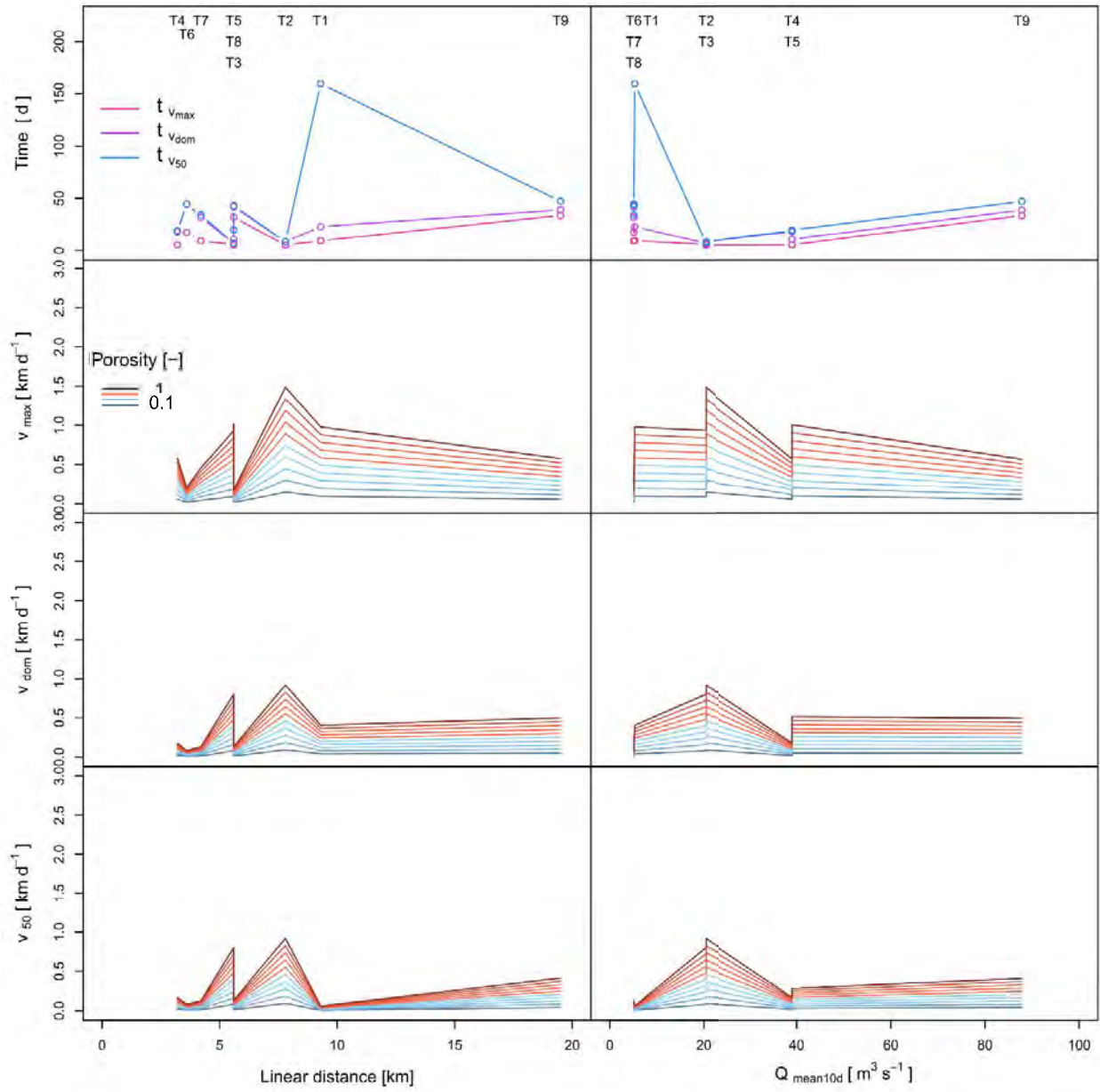


Figure A.8: Maximum and dominant velocities and velocity of 50% of tracer recovered of all tracer tests plotted over the linear distance and  $Q_{mean10d}$



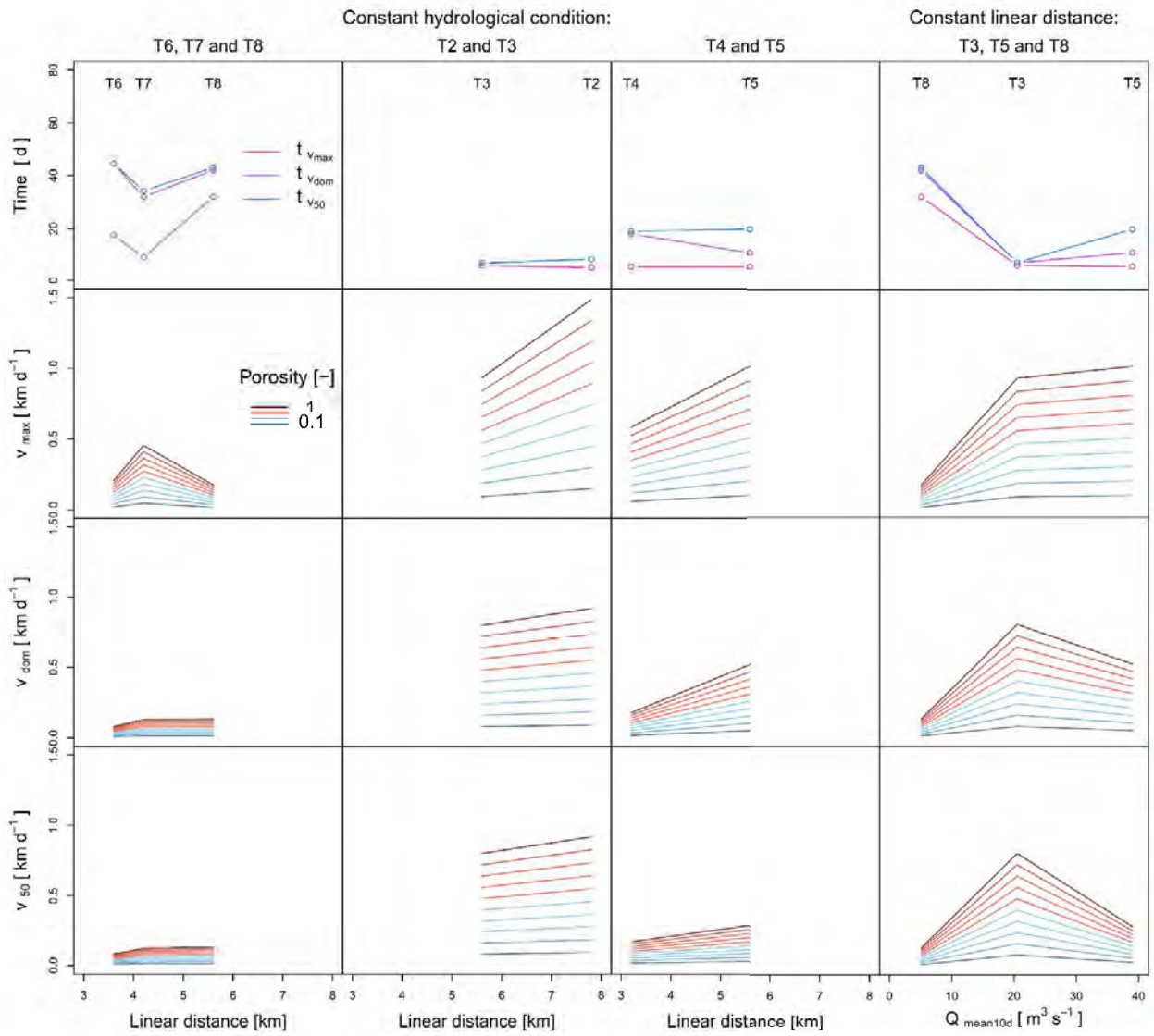


Figure A.9: Detailed plot of maximum and dominant velocities and velocity of 50% of tracer recovered of all tracer tests plotted over the linear distance and  $Q_{mean10d}$

## B. Equations

### Thornthwaite equation

$$E_{pot} = \left( \frac{0.533 * L}{12} \right) * \left( 10 * \frac{T}{I} \right)^{\alpha} \quad (32)$$

$E_{pot}$ : Potential Evapotranspiration after Thornthwaite [mm]

$L$ : Mean day length [h]

$T$ : Daily mean temperature [ $^{\circ}\text{C}$ ]

$I$ : Warmth index [-]

$\alpha$ : Equation parameter [-]

Where warmth index is describe by:

$$I = \sum_{i=1}^{12} \left( \frac{T_{mon}}{5} \right)^{1.514} \quad (33)$$

$T_{mon}$ : Monthly mean temperature [ $^{\circ}\text{C}$ ]

The equation parameter is defined by:

$$\alpha = (6.75 * 10^{-7}) * I^3 - (7.71 * 10^{-5}) * I^2 + (1.792 * 10^{-2}) * I + 0.49239 \quad (34)$$

Mean daily length can be calculated according Equation 33.

$$L = 24 * \frac{\arccos \left( 1 - \left( 1 - \tan \left( \frac{Lat}{180 * \pi} \right) * \tan \left( \frac{Obl}{180 * \pi} * \cos \left( \pi * \left( \frac{t}{PerSol} \right) \right) \right) \right) \right)}{\pi} \quad (35)$$

$Lat$ : Mean latitude of site

$Obl$ : Obliquity of the ecliptic

$PerSol$ : period between solstices [d]

$t$ : time steps (regarding astronomic year) [d]